

**A TRIP AROUND THE TRANSPORT CYCLE: THE STRUCTURAL BASIS OF
GLUTAMATE TRANSPORTER FUNCTION**

by

Jie Jiang

B.S. Zhejiang University, P.R. China, 2001

M.S. Zhejiang University, P.R. China, 2004

Submitted to the Graduate Faculty of
The School of Medicine in partial fulfillment
of the requirements for the degree of
Doctor of Philosophy

University of Pittsburgh

2011

UNIVERSITY OF PITTSBURGH

SCHOOL OF MEDICINE

This dissertation was presented

by

Jie Jiang

It was defended on

September 20, 2011

and approved by

Michael Cascio, Associate Professor, Dept. of Chemistry and Biochemistry,
Duquesne University

Christof T. Grewer, Associate Professor, Dept. of Chemistry,
State University of New York at Binghamton

Jon W. Johnson, Professor, Dept. of Neuroscience, University of Pittsburgh

Judith Klein-Seetharaman, Associate Professor, Dept. of Structural Biology,
University of Pittsburgh

Gonzalo E. Torres, Associate Professor, Dept. of Neurobiology, University of Pittsburgh

Dissertation Advisor:

Susan G. Amara, Detre Professor and Chair, Dept. of Neurobiology, University of Pittsburgh

Copyright © by Jie Jiang

2011

A TRIP AROUND THE TRANSPORT CYCLE: THE STRUCTURAL BASIS OF GLUTAMATE TRANSPORTER FUNCTION

Jie Jiang, PhD

University of Pittsburgh, 2011

Neuronal and glial glutamate transporters function to clear synaptically released glutamate from the extracellular space. This process not only ensures the spatial and temporal fidelity of excitatory signaling, but also prevents neuronal death triggered by excess glutamate. In addition, glutamate transporters possess a substrate-gated anion channel function, which may play an important role in shaping synaptic transmission. Although much progress has been made on the topology, structure, and function of these carriers, our knowledge of the conformational dynamics that drive glutamate transporter functions is far from complete.

Using biochemical, electrophysiological and functional assays in combination with computational simulations, we identified several large-scale collective motions that are intrinsic to glutamate transporter trimers. These collective motions are functionally important for substrate transport, but not for the substrate-gated anion conductance. Furthermore, we showed that these collective motions are coupled to the inward movement of the transport domain, and thus serve a critical function in the transport cycle. Next, we identified a conserved arginine residue, R388 in human EAAT1, that is involved in both substrate transport and anion conduction. Mutants reversing the positive charge (R388D and R388E) predominantly exist in the anion leak state and abolish the substrate-activated anion current. We also demonstrated that the transport domain in the negatively-charged mutant R388D spends a longer time in the

inward-facing orientation in the absence of substrate compared to the wild type transporter. These results not only suggest the characterized arginine residue is an important element in the functional coupling between substrate transport and the anion channel activity, but also indicate the role of the inward transport domain movement in anion permeation. Finally, we constructed a functional glutamate transporter concatemer. Our preliminary results suggested that glutamate transporters are functional as trimers and the individual subunits transport substrate independently.

The work presented in this dissertation provides a greater understanding of the structural determinants of the dual functions of glutamate transporters. Furthermore, it provides a powerful tool to further study contributions of subunit interactions and the inward piston-like movement of the transport domain to channel gating and anion permeation.

TABLE OF CONTENTS

PREFACE.....	XVI
1.0 INTRODUCTION.....	1
1.1 GLUTAMATE TRANSPORTERS AND EXCITATORY SYNAPTIC TRANSMISSION	1
1.1.1 Extracellular glutamate is mainly removed by glutamate transporters and reused in the cell	2
1.1.2 Glutamate transporters and diseases	2
1.2 FUNCTIONAL PROPERTIES OF GLUTAMATE TRANSPORTERS.....	3
1.2.1 Glutamate transporter subtypes.....	3
1.2.2 Glutamate transport cycle.....	4
1.2.3 Transporter associated anion conductance	5
1.3 MOLECULAR STRUCTURES OF GLUTAMATE TRANSPORTERS.....	8
1.3.1 Membrane topology of glutamate transporters	8
1.3.2 Glutamate transporters form trimers.....	15
1.4 BINDING SITES FOR GLUTAMATE AND COUPLED IONS.....	17
1.4.1 Substrate binding site	17
1.4.2 Na⁺ binding sites.....	21

1.4.3	K⁺ binding site	23
1.4.4	H⁺ binding site	24
1.5	MECHANISMS OF SUBSTRATE TRANSPORT	26
1.6	THE STRUCTURAL BASIS FOR THE TRANSPORTER-ASSOCIATED ANION CONDUCTANCE	30
1.7	THESIS GOALS	33
2.0	LARGE COLLECTIVE MOTIONS REGULATE THE FUNCTIONAL PROPERTIES OF GLUTAMATE TRANSPORTER TRIMERS	34
2.1	INTRODUCTION	34
2.2	RESULTS	36
2.2.1	Inhibition of substrate transport by CuPh and cadmium ions in mutants V449C and I453C	36
2.2.2	Single cysteine substitutions at the N-terminal end of helix HP2b are more reactive to CuPh and form spontaneous crosslinks	40
2.2.3	The formation of disulfide bonds in V449C and I453C as confirmed by biochemical assays	42
2.2.4	Crosslinks in the mutant carrier V449C take place between two transporter subunits in the same trimer	45
2.2.5	Molecular dynamics (MD) simulations show spontaneous opening of the HP2 loop	51
2.2.6	ANM analysis suggests that large collective motions of glutamate transporter trimers significantly alter intersubunit distances	54

2.2.7	Crosslinking cysteine substituted mutants of several residues at the N-terminal end of TM8	57
2.2.8	Residue V449C in the uncrosslinked subunit is inaccessible for modification after crosslinking	59
2.2.9	Residue L376C in the uncrosslinked subunit is exposed intracellularly after crosslinking of V449C.....	62
2.2.10	Glutamate transporters favor stepwise transitions between outward-facing and inward-facing states	65
2.2.11	Impact of crosslinking on the substrate-gated anion flux.....	68
2.3	DISCUSSION.....	70
3.0	A CONSERVED POSITIVE CHARGE IN TM7: A KEY PLAYER IN GLUTAMATE TRANSPORTER DUAL FUNCTIONS	77
3.1	INTRODUCTION	77
3.2	RESULTS	80
3.2.1	Residue R388 plays an important role in substrate transport.....	80
3.2.2	Residue R388 is critical for the anion channel function.....	84
3.2.3	The mutant carrier R388D predominantly exists in the anion leak state..	88
3.2.4	The corresponding mutant carrier R410E of rat EAAT4 predominantly exists in the anion leak state	90
3.2.5	The mutant carriers R388A and R388D have dramatically increased anion leak currents.....	92

3.2.6	The mutant carrier R388D spends more time in the inward-facing conformation in the absence of substrate	93
3.3	DISCUSSION.....	99
4.0	SUBUNIT INTERACTIONS OF GLUTAMATE TRANSPORTERS.....	106
4.1	INTRODUCTION	106
4.2	RESULTS	108
4.2.1	Characterization of a concatenated glutamate transporter trimer.....	108
4.2.2	The mutant carrier R479C in human EAAT1 changes its substrate specificity.....	111
4.2.3	A single subunit of glutamate transporter trimer is capable of transporting substrate	113
4.2.4	Each subunit of the glutamate transporter trimer uptakes substrate independently from each other	114
4.3	DISCUSSION.....	114
5.0	CONCLUSIONS, GENERAL DISCUSSIONS AND FUTURE DIRECTIONS	116
5.1	LARGE COLLECTIVE MOVEMENTS PROVIDE A DIFFERENT VIEW TO UNDERSTAND THE ALTERNATING ACCESS MECHANISM OF GLUTAMATE TRANSPORTERS	118
5.2	DETERMINATION OF THE FREQUENCY OF THE LARGE COLLECTIVE MOVEMENTS AS A MEANS TO ESTABLISH THEIR PHYSIOLOGICAL RELEVANCE.....	120

5.3	ADDITIONAL CROSSLINKING STUDIES TO ADDRESS THE RELATIONSHIP BETWEEN LARGE COLLECTIVE MOTIONS AND THE PISTON-LIKE MOVEMENT OF THE TRANSPORT DOMAIN.....	122
5.4	LARGE COLLECTIVE MOVEMENTS AND THE GLUTAMATE BUFFERING THEORY	123
5.5	EXPLORING THE ANION PERMEATION PATHWAY.....	125
5.6	LINKING THE INWARD MOVEMENT OF THE TRANSPORT DOMAIN TO THE ANION CHANNEL ACTIVITY.....	125
6.0	MATERIALS AND METHODS	127
6.1	MATERIALS	127
6.2	MUTAGENESIS.....	127
6.3	CELL CULTURE AND TRANSFECTION	127
6.4	XENOPUS OOCYTE PREPARATION.....	128
6.5	RNA PREPARATION AND OOCYTE INJECTION	128
6.6	CUPH-CATALYZED DISULFIDE BRIDGE FORMATION AND DTT APPLICATION	129
6.7	UPTAKE ASSAYS AND TRANSPORT KINETIC MEASUREMENTS .	130
6.8	CALCULATION OF THE REACTION RATE CONSTANTS	130
6.9	CELL SURFACE BIOTINYLATION	131
6.10	OOCYTE MEMBRANE PREPARATION	132
6.11	BLUE NATIVE POLYACRYLAMIDE GEL ANALYSIS	132
6.12	WESTERN BLOTTING	133
6.13	ELECTROPHYSIOLOGY.....	133

6.14	MOLECULAR DYNAMICS SIMULATIONS	134
6.15	ANISOTROPIC NETWORK MODEL (ANM) ANALYSIS	134
6.16	MODELING THE STRUCTURE AND DYNAMICS OF INTERMEDIATE STATES	135
6.17	DATA ANALYSES.....	136
APPENDIX A	138
BIBLIOGRAPHY	139

LIST OF TABLES

Table 1. Residues contributing to substrate and coupled ion binding as suggested by Glt_{Ph} crystal structures, computational simulations and by mutagenesis studies in the mammalian EAATs	25
---	-----------

LIST OF FIGURES

Figure 1. Transport cycle and stoichiometry of EAATs	7
Figure 2. Structural features of Glt_{ph} and the mammalian EAATs.....	10
Figure 3. Mammalian EAATs and Glt_{ph} share similar structure features.....	13
Figure 4. Binding sites for substrate and coupled sodium ions	20
Figure 5. Mechanisms of substrate transport.....	29
Figure 6. Inhibition of substrate transport by CuPh and cadmium ions in mutants V449C and I453C.....	38
Figure 7. The effect of prolonged incubation of CuPh or additional incubation with MTSET on uptake activity of the I453C mutant carrier	39
Figure 8. Single cysteine substitutions at the N-terminal end of the helix HP2b are more reactive to CuPh and form spontaneous crosslinks.....	41
Figure 9. CuPh catalyzes the formation of disulfide bonds in V449C and I453C as confirmed by biochemical assays.....	43
Figure 10. The effect of a bifunctional crosslinking reagent, M8M, on the mutant V449C.	44
Figure 11. CuPh-catalyzed V449C crosslinks take place between two transporter subunits	46
Figure 12. human EAAT1 forms trimers	46

Figure 13. CuPh induced crosslinks occur within the trimeric structure	48
Figure 14. Sequence alignment of Glt_{ph} and human EAAT1	50
Figure 15. Molecular dynamics (MD) simulations show spontaneous opening of the HP2 loop.....	53
Figure 16. Large collective motions of glutamate transporter trimers predicted by ANM analysis.....	56
Figure 17. Crosslinking cysteine substituted mutants of several residues at the N-terminal end of TM8.....	58
Figure 18. Residue V449C in the uncrosslinked subunit is inaccessible for modification after crosslinking.....	61
Figure 19. Residue L376C in the uncrosslinked subunit is exposed intracellularly after crosslinking of V449C.....	64
Figure 20. Cumulative overlap of ANM modes and transitions between pairs of conformations.....	67
Figure 21. V449C retains substrate-activated anion conductance after crosslinking	69
Figure 22. Neutralizing the charge of residue R388 with amino acid alanine impairs substrate transport.....	81
Figure 23. The mutant carriers R388D and R388E accumulate substrate through an electroneutral process.....	83
Figure 24. Neutralizing the charge of Residue R388 alters the anion channel function of EAAT1	85
Figure 25. Substrate no longer elicits additional currents in the negatively-charged R388 mutants.....	87

Figure 26. The mutant carrier R388D predominantly exists in the anion leak state	89
Figure 27. The mutant carrier rEAAT4 R410E predominantly exists in the anion leak state	91
Figure 28. The mutant carriers R388A and R388D have dramatically increased anion leak currents	94
Figure 29. The mutant carrier R388D spends more time in the inward-facing conformation in the absence of substrate compared to the wild type transporter	97
Figure 30. Characterization of a concatenated glutamate transporter trimer	110
Figure 31. The mutant carrier R479C in human EAAT1 changes its substrate specificity	112
Figure 32. A single subunit of the glutamate transporter trimer is capable of transporting substrate	113
Figure 33. Each subunit of the glutamate transporter trimer uptakes substrate independently from each other	115

PREFACE

ACKNOWLEDGMENTS

The work presented in this dissertation would not have been possible without academic and personal support from a number of people. I would like to first express my heartfelt thanks to my mentor, Dr. Susan Amara, for her professional guidance, constant encouragement, and tremendous support. From the first day I joined the lab, Susan has provided me with an ideal balance between freedom and guidance in pursuing research ideas. She offered everything possible to ensure the success of my graduate study and to help my future career. Her enthusiasm, broad knowledge and critical scientific thoughts also set up a model for me to be a great scientist. I feel really lucky to have the opportunity to work with her.

I owe thanks to my dissertation committee, consisting of Dr. Michael Cascio (chair), Dr. Jon Johnson, Dr. Judith Klein-Seetharaman, and Dr. Gonzalo Torres. They dedicated significant time and efforts during my graduate training, and offered new perspectives and insightful suggestions on my projects. They challenged me to interpret the data from un-biased angles, which has shaped my work along the way. I would also like to thank my outside examiner Dr. Christof Grewer for giving his input. I have greatly enjoyed following the work that has come from his lab, and it is an honor to discuss my thesis work with him.

I enjoyed the exciting collaboration with Dr. Ivet Bahar's group in the Department of Computational and Systems Biology. In particular, I would thank Dr. Inidra Shrivastava and Dr. Ivet Bahar, who performed and analyzed the computational simulations presented in the part 2 of this dissertation (Figure 15, 16 and 20). The continuous interactions with members of Dr.

Bahar's group have taken my research to a new level, combining computational modeling with biochemistry, molecular biology and physiology.

I also thank all of the past and current members of the Amara lab, who have not only contributed to this work, but also made a home-like environment: Ethan Block, Christopher Divito, Andreia Fontana, Conrad Hong, Bozena Kutymba-Brooks, Mads Larsen, Gal Levin, Yong-Jian Liu, Megan Miller, Ole Mortensen, Delany Torres-Salazar, Suzanne Underhill, and Spencer Watts. I owe an extra thank to Dr. Spencer Watts and Dr. Delany Torres-Salazar. Spencer taught me many hands-on skills, and he has been willing to share his expertise and advice. Delany brought a lot of expertise in electrophysiology to the lab and we had a great time working together in part 3 of this dissertation.

I would like to extend my immense gratitude to my family and friends. My wife, Huafei Zou, is my constant source of love and support. She shares the ups and downs of my research and her understanding keeps me moving forward. My parents and my in-laws give me every opportunity to succeed. They are so proud of me and they always believed that I will achieve my goals. My daughter, Sophia Yanchen Jiang filled my life with joy in the last two years. My friends have also been wonderful and their support has been extremely important during my journey in the USA.

As I reach this milestone, I am so grateful to all of those who have helped me to make it here. To them, I dedicate this dissertation.

ABBREVIATIONS

ANM	Anisotropic network model
BN-PAGE	Blue native polyacrylamide gel electrophoresis
CSLS	Highly functional cysteineless version of human EAAT1
CuPh	Copper phenanthroline
DTT	Dithiothreitol
EAAT	Excitatory amino acid transporter
FRET	Fluorescence/Förster resonance energy transfer
HP	Helical hairpins
M8M	1,8-Octadiyl Bismethanethiosulfonate
MD	Molecular dynamics
MTSEA	2-Aminoethyl methanethiosulfonate, hydrobromide
MTSES	Sodium (2-sulfonatoethyl) methanethiosulfonate
MTSET	[2-(Trimethylammonium) ethyl] methanethiosulfonate bromide
NEM	N-ethylmaleimide
PDB	Protein data bank
SDS	Sodium dodecyl sulfate
TBOA	DL- <i>threo</i> -benzyloxyaspartate
TM	Transmembrane

1.0 INTRODUCTION

1.1 GLUTAMATE TRANSPORTERS AND EXCITATORY SYNAPTIC TRANSMISSION

The amino acid L-glutamate is the major excitatory neurotransmitter in the mammalian central nervous system. It is released from presynaptic neurons in response to electrical impulses (*e.g.* action potentials). Within less than a millisecond, glutamate diffuses across the synaptic cleft and transmits information to postsynaptic neurons by acting on both synaptic and extrasynaptic glutamate receptors. The glutamate concentration in the extracellular environment determines the extent and duration of receptor activation and thus glutamate clearance plays an essential role in the maintenance of precise communication between neurons. In addition, excessive activation of glutamate receptors is neurotoxic and the rapid clearance of glutamate limits the neuronal death that can be caused by high extracellular glutamate concentrations (1).

1.1.1 Extracellular glutamate is mainly removed by glutamate transporters and reused in the cell

Unlike the neurotransmitter acetylcholine, glutamate is not inactivated by specific extracellular enzymes. Although simple diffusion plays an important role in reducing glutamate concentrations in the synaptic cleft at a submillisecond timescale, the maintenance of low extracellular glutamate concentrations relies on the active uptake into cells by glutamate transporters (2). These carriers transport L-glutamate, L-aspartate and D-aspartate with high affinity (K_m in low micromolar range). Once it enters the neuronal cytoplasm, glutamate can be used subsequently for protein synthesis in cellular metabolism, or packaged in vesicles for re-release during neurotransmission. By contrast, glutamate transported into glial cells is initially converted to glutamine by glutamine synthetase. Glutamine is then actively transported back from glial cells into presynaptic neurons to serve as a source for new glutamate synthesis. This trafficking of glutamate and glutamine between neurons and glial cells is referred to as the glutamine-glutamate cycle, and has been proposed to be a major pathway by which glutamate is recycled (3).

1.1.2 Glutamate transporters and diseases

As the major excitatory signaling molecule, glutamate contributes to nearly all aspects of normal brain development and function. Altered clearance of glutamate as a consequence of glutamate transporter malfunction is associated with a variety of neurological diseases and psychiatric disorders (4). Sustained elevation of extracellular glutamate, either due to the downregulation of transporter activity or by glutamate release through a direct reversal of the transporter, leads to

severe excitotoxic damage to surrounding neurons. This mechanism is implicated in both acute brain injuries (*e.g.* epilepsy and ischemia), and chronic pathological conditions, including amyotrophic lateral sclerosis, Huntington's disease and Alzheimer's disease (4). On the other hand, glutamate hypoactivity, which could result from the upregulation of transporter functions, has been reported to occur in schizophrenia patients (1, 4). Glutamate transporters thus represent potential therapeutic targets for treating these neuropsychiatric and neurodegenerative diseases, and understanding the structural determinants of transporter functions will help in the design of allosteric transport regulators and inhibitors of reverse transport.

1.2 FUNCTIONAL PROPERTIES OF GLUTAMATE TRANSPORTERS

Over the last three decades, the study of the structure and function of glutamate transporters has spanned from initial investigations of transport system in brain slices, synaptosomes and plasma membrane vesicles to extensive explorations of individual transporter subtypes exogenously expressed in cultured cells, greatly expanding our knowledge of this protein family.

1.2.1 Glutamate transporter subtypes

Early studies showed that glutamate transport activities in different brain regions have distinct pharmacological profiles, suggesting the existence of more than one subtypes of glutamate transporters (5-6). This diversity was confirmed by the cloning of the first three genes encoding different subtypes of glutamate transporters in 1992: rat GLAST, rat GLT-1 and rabbit EAAC1 (7-9). To date, five members of glutamate transporter family have been characterized from

human (10-12) and a variety of other eukaryotic species (for a review, see (13)). The human transporters were named using the acronym EAAT (Excitatory Amino Acid Transporter) (12). Based on sequence similarity, EAAT1 is homologous to GLAST, EAAT2 to GLT-1 and EAAT3 to EAAC1. Several prokaryotic genes have also been isolated, including proton dependent glutamate transporters from *Escherichia coli*, (GltP_{Ec}), *Bacillus stearothermophilus* (GltT_{Bs}) and *Bacillus caldotenax* (GltT_{Bc}), as well as a dicarboxylic acid transporter from *Rhizobium meliloti* (DctA) (14-16). Other glutamate transporter family members include two related neutral amino acid transporters ASCT1 and ASCT2, which transport L-alanine, L-serine and L-cysteine (17-18). The primary sequences of the five mammalian carriers share ~50% identity and ~60% similarity, while the identity with the prokaryotic carriers is around 20-30%. It is therefore reasonable to assume that the mammalian EAATs will have many structural and mechanistic features in common with their prokaryotic counterparts. However, considerable variations in structure, ion requirements and substrate selectivity exist between different subtypes, which sometimes makes it difficult to compare structure-function data obtained from different family members.

1.2.2 Glutamate transport cycle

Glutamate transporters belong to a secondary active transporter family that uses free energy stored in ion/solute gradients to enable the uphill translocation of their substrates. Studies in brain slices, synaptosomes and brain-derived cell lines revealed that glutamate transport is thermodynamically coupled to the inward movement of multiple sodium ions (19-20) and a proton ion (or an OH⁻ is ejected) (21), and to the outward movement of a potassium ion (22). The

detailed coupling stoichiometry has been further explored using the cloned human EAAT1 expressed in *Xenopus* oocytes (23), as well as GLT-1 expressed in CHO cells (24). It is now generally accepted that for mammalian carriers the transport cycle involves two sequential half-cycles (**Figure 1A**): i) co-transport of 1 glutamate with 3 sodium ions and 1 proton ion into the cell cytosol, and ii) counter-transport of 1 potassium ion to return transporters to their externally-facing, unoccupied state. Based on the Goldman-Hodgkin-Katz equation and physiological ion gradients, such stoichiometry enables the generation of up to a 10^6 -fold gradient of glutamate across the cell membrane, which could bring the extracellular glutamate concentration down to approximately 10 nM (23). Glutamate transport is therefore electrogenic, as two net positive charges move into the cell with each transport cycle. The resulting current is referred to as transport current, and is sometimes termed coupled transport current or uptake current because it represents the stoichiometric charge movements associated with glutamate transport.

1.2.3 Transporter associated anion conductance

Glutamate transporters also function as anion channels (**Figure 1B**). Before the cloning of glutamate transporters, Attwell's group observed a glutamate-activated chloride conductance in retina photoreceptors (25). These currents displayed properties in common with glutamate transporters: they were Na^+ -dependent, and could be inhibited by transporter inhibitors. Several groups made similar observations (26-27), but the direct association of an anion current with a glutamate transporter remained unclear until the identification and characterization of a human EAAT4 (11). Application of glutamate to *Xenopus* oocytes expressing recombinant EAAT4 generates a current that is predominantly due to chloride ions and is not blocked by compounds that inhibit endogenous chloride channels. The chloride current through the transporter is

thermodynamically uncoupled from the substrate transport process because the rate of uptake is independent of the presence of Cl^- or the direction of Cl^- flux (11). Subsequent studies of other transporter subtypes confirmed that mammalian EAATs as well as structurally related neutral amino acid transporters, known as ASCTs, have intrinsic anion channel activities (10, 28-31). More recently, Ryan *et al.* used proteoliposomes to identify an uncoupled chloride conductance in a glutamate transporter homolog Glt_{ph} from the archaeal species *Pyrococcus horikoshii*, suggesting that chloride permeation is a feature conserved in both prokaryotic and eukaryotic carriers (32). In addition to the anion conductance activated by glutamate, mammalian EAATs also possess an anion leak conductance in the absence of substrate (33-35). The anion leak currents are activated by extracellular Na^+ and can be blocked by transporter inhibitors. Thus, there are two distinct anion currents associated with EAATs, and they are referred to as the Na^+ -activated anion leak current and the substrate-activated anion current.

Although the physiological function of the Na^+ -activated leak chloride current associated with glutamate transporters is not yet clear, the substrate-activated chloride current can influence synaptic transmission in several ways. First, coupled glutamate transport generates a net transfer of two positive charges per transport cycle. The influx of Cl^- counteracts the accumulation of positive charges during transport, which otherwise will depolarize the cell and inhibit voltage-dependent glutamate transport. Consistent with this idea, the rate of transport slows rapidly in Glt_{ph} -containing liposomes if Cl^- or other permeant anions are not present in the uptake media (32). Second, the influx of Cl^- may serve as a feedback sensor of extracellular glutamate concentration to dampen neuron excitability and prevent further glutamate release. This mechanism is elegantly demonstrated in rat rod bipolar cells which express a transporter that has relatively large Cl^- conductance compared to the coupled transport current (36).

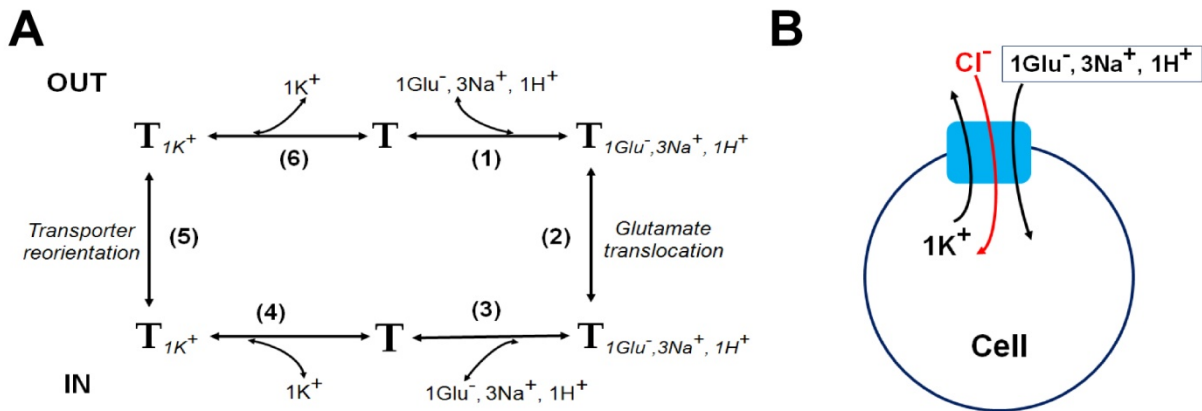


Figure 1. Transport cycle and stoichiometry of EAATs

(A) Simplified state diagram of the EAAT transport cycle. After glutamate and coupled ions (step 1) bind to the transporter (T), they are translocated (step 2) and released into the cell cytosol (step 3). Next K^+ binds from the intracellular side (step 4) and reorients the substrate-free transporter (step 5). K^+ is released outside the cell (step 6).

(B) Cartoon illustrating the ion coupling stoichiometry of an EAAT (blue). The uptake of 1 glutamate molecule is coupled with the influx of 3 Na^+ , 1 H^+ and the efflux of 1 K^+ (black). In addition, EAATs have a glutamate-activated Cl^- conductance (red), which results in the influx of chloride ions under physiological conditions.

1.3 MOLECULAR STRUCTURES OF GLUTAMATE TRANSPORTERS

An appreciation of the molecular structures of glutamate transporters has been a crucial first step towards understanding how structural elements contribute to different aspects of transporter function. This section will focus on the current knowledge of the general membrane topology and the subunit stoichiometry of glutamate transporters.

1.3.1 Membrane topology of glutamate transporters

Hydropathy analyses of GLAST-1, GLT-1 and EAAC-1, as well as direct experimental evidence provided support for the presence of six transmembrane (TM) α -helices in the N-terminal part of glutamate transporters with two N-glycosylation sites located in the extracellular loop between TM domain 3 & 4 (**Figure 2**) (37-38). However, structural predictions were ambiguous for the C-terminus, in part because of many charged residues present within the otherwise hydrophobic domains. Early studies attempted to assess the membrane orientation of a reporter epitope fused with sequential C-terminal deletions of glutamate transporters, resulting in several different models for the C-terminal domains (37, 39-40). Despite the the information gathered, these studies were criticized for being based on data using truncated non-functional transporters, which might not reflect the organization of full-length native carriers.

As an alternative approach, several laboratories used cysteine substitutions combined with thiol-modifications to determine the membrane topology of the C-terminal domains. In these strategies, single cysteine residues are introduced into regions of interest and their accessibility probed with various sulfhydryl-reactive reagents. Residues that can be modified by

both membrane permeable and impermeable agents are designated as extracellular, whereas residues that can only be modified by membrane permeant agents are intracellular. Finally, residues that do not react with either permeable or impermeable agents are presumed to reside within TM domains (41). Two models were developed for human EAAT1 (42-43) and GLT-1 (44-45) respectively using this kind of approach, and the results for GLT-1 generally agreed with the predicted topology of the bacterial transporter Glt_{T_{Bs}} (46-47). Both mammalian carrier models (**Figure 2A and 2B**) proposed the existence of re-entrant loops, but differed in the number and location of the TM domains and re-entrant loops. The major basis for the differences in the two models is the accessibility of a single substituted residue, A395C in human EAAT1 (A393C in GLT-1) (43, 45). Although A395C in human EAAT1 could be readily modified by small impermeant methanethiosulfonate reagents (MTSET and MTSES), implying an extracellular location, Kanner and colleagues showed that the corresponding residue in GLT-1, A393C, is inaccessible by these reagents and placed it at the end of a large intracellular loop.

A breakthrough in understanding the membrane topology of glutamate transporters came with the first crystallization of the archaeal transporter Glt_{ph} [Protein data bank (PDB) ID: 1XFH] (48). Glt_{ph} exists as a trimer comprised of three identical subunits in the crystal. Each protomer contains eight TM domains and two re-entrant loops. The first six TM domains form a scaffold surrounding a C-terminal transport domain that contains structural elements required for the transport mechanism. The C-terminal transport domain includes two opposite-facing helical hairpins (HP1 and HP2), a seventh TM helix interrupted by a β -linker and an amphipathic helix, TM8 (**Figure 2C and 2D**). A non-protein electron density nestled between HP1 and HP2 was also observed in the crystal and was later confirmed to be the bound substrate (49).

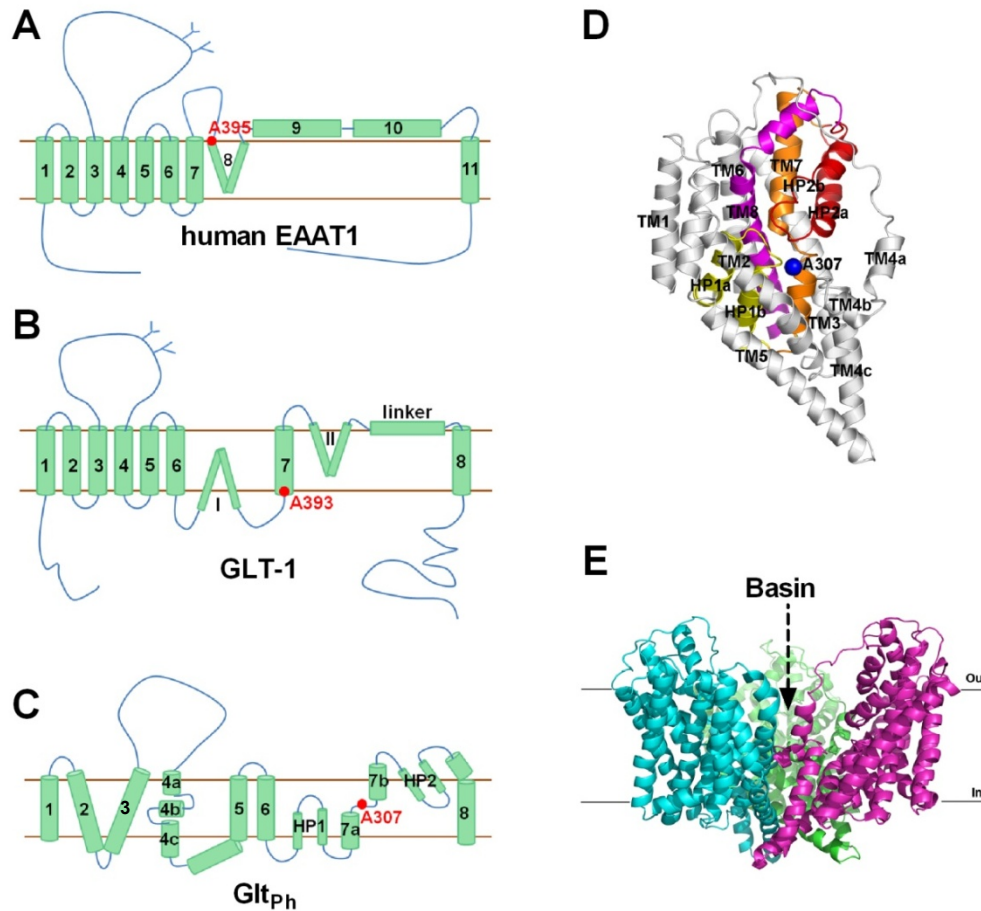


Figure 2. Structural features of Glt_{Ph} and the mammalian EAATs

Three different membrane topology models are illustrated in panels A-C. Two were suggested based on the results obtained in substituted cysteine modification studies using human EAAT1 (A) and GLT-1 (B), and the third (C) was revealed by the crystallization of an archaeal homolog from *Pyrococcus horikoshii*, Glt_{Ph}. (D) Cartoon representation of the Glt_{Ph} protomer viewed in the plane of the membrane. Transmembrane domains 1-6 colored in grey form a scaffold that holds the transport domain comprised of HP1 (yellow), TM7 (orange), HP2 (red) and TM8 (magenta). Residue A395 in human EAAT1 referred to in the text (equivalent to A393 in GLT-1 and A307 in Glt_{Ph}) is shown as red dots in the topology models (A-C) and is also illustrated as a blue sphere in the Glt_{Ph} protomer (D). (E) View of a Glt_{Ph} trimer parallel to the membrane. Subunits in the trimer are colored green, magenta or cyan. The protomer and the trimer structure are based on the Glt_{Ph} crystal structure 1XFH (48), and are made using the software Pymol (Schrödinger, LLC).

Therefore, this Glt_{ph} structure is referred to as the substrate-bound conformation. One striking feature of Glt_{ph} is that it forms a large bowl-shaped basin that extends halfway through the membrane and thus, several regions in the C-terminal part are solvent accessible despite their location within the plane of the membrane (**Figure 2E**).

Although many structural features of glutamate transporters, including the existence of two re-entrant loops, were predicted by the substituted cysteine modification studies, the exact locations of the TM domains and the re-entrant loops in Glt_{ph} differ from the proposed mammalian models (**Figure 2C**). How well does the membrane topology of Glt_{ph} represent that of the mammalian EAATs?

To address this question, it is useful to revisit data obtained from substituted cysteine modification studies in light of not only the substrate-bound Glt_{ph} structure, but also the two other available 3-dimensional Glt_{ph} structures. A second structure (PDB ID: 2NWW), referred to as the TBOA-bound conformation, was crystallized in the presence of a competitive inhibitor, *DL-threo*-benzyloxyaspartate (TBOA) (**Figure 3A**). The overall structural features of the TBOA-bound Glt_{ph} are very similar to those of the substrate-bound carrier (PDB ID: 1XFH) except that the HP2 region is displaced away from the substrate binding site (49). A third Glt_{ph} structure (PDB ID: 3KBC) was recently resolved by crosslinking two cysteines introduced into TM2 and HP2 (**Figure 3B**). This structure is referred to as the inward-facing conformation, in which the C-terminal transport domain moves inward approximately 18Å toward the cytoplasm (50).

Each crystal structure of Glt_{ph} may represent a single snapshot of one of many conformational states that occur during the transport cycle, and the carrier dynamics are likely to affect the solvent accessibility of certain protein domains. When residues characterized in

substituted cysteine modification studies using mammalian carriers were mapped onto the three reported Glt_{ph} structures based on their sequence alignment, the thiol-modification behavior of many of these residues can be explained by at least one of these Glt_{ph} structures. For example, the residue A395C in human EAAT1 noted above is located in the vicinity of the unwound segment “NMDGT” in TM7 and is occluded by the HP2 region in the substrate-bound Glt_{ph} structure (**Figure 2D**). At first glance, this residue seems to be inaccessible from either the intracellular or extracellular side of the cell. However, the displacement of HP2 in the TBOA-bound Glt_{ph} structure exposes this residue to the extracellular environment (**Figure 3A**) and the inward movement of the transport domain in the inward-facing Glt_{ph} structure exposes it intracellularly (**Figure 3B**). Therefore, A395C can be accessed from both sides of the cell, which reconciles differences in the modification of this residue observed experimentally in human EAAT1 and GLT-1 (43, 45). Indeed, the modification of the residue A395C by another thiol-reactive methanethiosulfonate reagent, MTSEA, was protected by L-glutamate only when MTSEA was applied at low concentrations but not at high concentrations. As MTSEA can permeate the cell membrane under some conditions, this observation suggests that at high concentrations MTSEA can modify A395C from the cytoplasm and supports the idea that this residue is alternatively accessed from either side of the membrane (43).

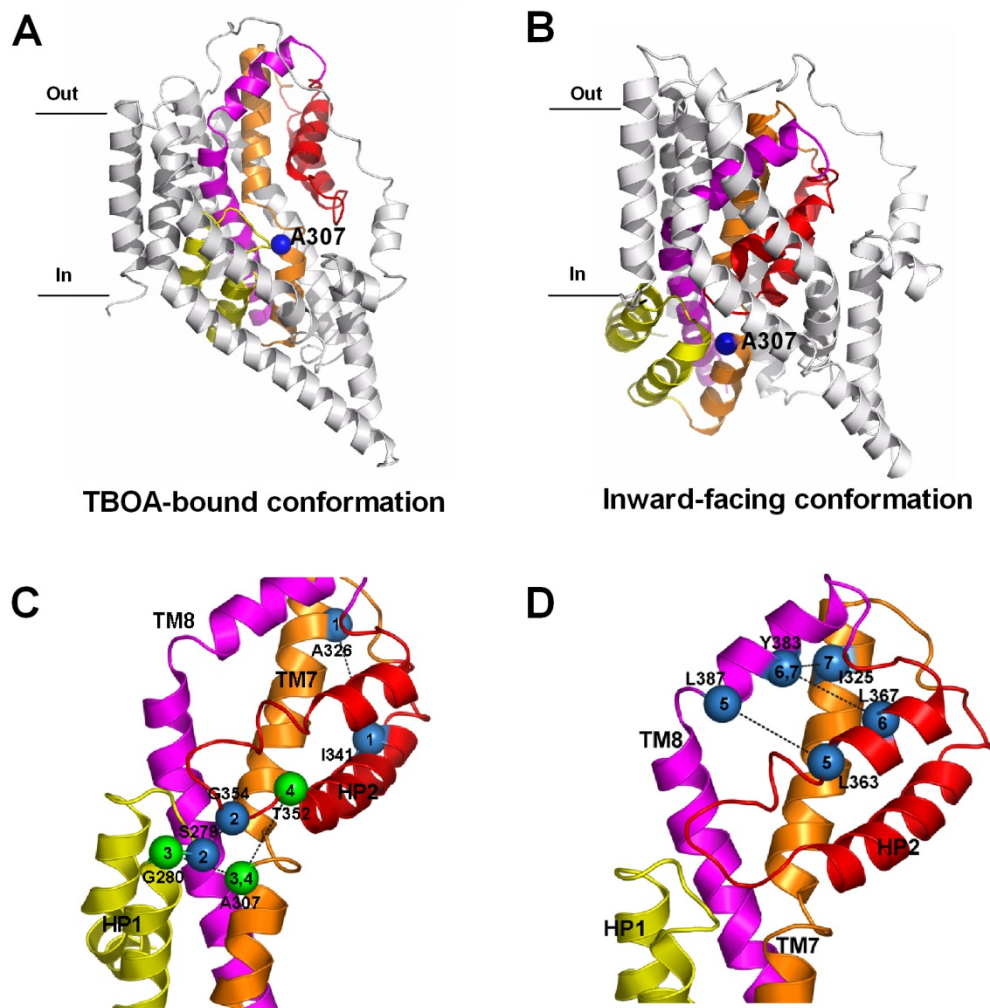


Figure 3. Mammalian EAATs and Glt_{ph} share similar structure features

Residue A307 shown as a blue sphere (equivalent to residue A395 in human EAAT1 and A393 in GLT-1, refer to the main text), is accessible from either the extracellular space in the TBOA-bound conformation (A) or the intracellular space in the inward-facing conformation (B). Note that TBOA in (A) is removed from the structure for clarity. The spatial relationships among C-terminal transmembrane domains are conserved between Glt_{ph} and EAATs, as shown in C and D. (C) Residue pairs in the mammalian EAATs that were characterized to form copper phenanthroline (CuPh)-induced disulfide crosslinks when substituted with cysteines are illustrated on the Glt_{ph} structure. Shown in blue are two pairs identified in GLT-1, A412C/V427C (pair 1, TM7/HP2) and A364C/S440C (pair 2, HP1/HP2), corresponding to A326/I341 and S279/G354 in Glt_{ph}, respectively. Shown in green are two pairs

identified in human EAAT1, A395C/A367C (pair 3, TM7/HP1) and A395C/A440C (pair 4, TM7/HP2), corresponding to G280/A307 and A307/T352 in Glt_{ph}, respectively. **(D)** Residue pairs that are spatially close in the Glt_{ph} structure were confirmed by substituted cysteine crosslinking studies in the mammalian EAATs. These include pairs of L363/L387 (pair 5, HP2/TM8), L367/Y383 (pair 6, HP2/TM8) and I325/Y383 (pair 7, TM7/TM8) in Glt_{ph}, corresponding to M449C/L466C, L453C/I463, I411C/I463C in GLT-1, respectively. The illustrations are based the Glt_{ph} crystal structures 2NWW, 2NWX and 3KBC, and are made using the software Pymol (Schrödinger, LLC).

Cysteine crosslinking studies have provided even stronger evidence supporting the structural similarities between Glt_{ph} and the mammalian EAATs. These studies aimed to look for residue pairs that are close in space and when mutated to cysteines could be crosslinked by oxidizing reagents such as copper phenanthroline (CuPh). The rationale for the original studies was simply based on similarities of residue pairs in thiol accessibility and modification rate, and in the ability of substrates, coupled ions and non-transportable analogs to prevent or enhance modification. These studies identified residue pairs of A412C/V427C (TM7/HP2) and A364C/S440C (HP1/HP2) in GLT-1 (51), and pairs of A395C/A440C (TM7/HP2) and A395C/A367C (TM7/HP1) in human EAAT1 (52). When these residue pairs are mapped onto the substrate-bound Glt_{ph} structure, they are also sufficiently close in space to allow the formation of disulfide bonds when substituted with cysteines (**Figure 3C**). The structure of Glt_{ph} was also used as a model to look for additional pairs, which led to the identification of residue pairs of M449C/L466C (HP2/TM8), L453C/I463C (HP2/TM8), I411C/I463C (TM7/TM8) in GLT-1 (**Figure 3D**) (53). These results clearly demonstrate that the relative positions of TM7, TM8, HP1 and HP2 are conserved in Glt_{ph} and the mammalian EAATs.

1.3.2 Glutamate transporters form trimers

It has long been proposed that EAATs form multimers (54) and the quaternary stoichiometry was explored with various biochemical approaches, including the use of chemical crosslinking reagents. Early studies showed that GLT-1 migrates as a trimer in SDS polyacrylamide gels after crosslinking, whereas GLAST may exist as both trimers and dimers (54). Similar crosslinked

trimer species were observed for two bacterial transporters, Glt_{Bc} and Glt_{Bs} (55) and for the mammalian transporter EAAC1 (56). The trimeric structure was further confirmed for human EAAT2 and the bacterial transporter GltP_{Ec} using blue native polyacrylamide gel analysis (57). In addition, by applying a coupled chromatographic and spectroscopic technique that accurately measures the native molecular masses of membrane proteins, Yernool *et al.* have shown that Glt_{T_{Bc}} and Glt_{T_{Bs}} have molecular weights of 140 kDa and 154 kDa respectively under non-denaturing conditions, approximately three times the size of their corresponding protomers (55). Although one study reported a pentameric assembly of human EAAT3 (58), with the crystallization of Glt_{ph} as a symmetric trimer, it is generally accepted that glutamate transporters are comprised of three identical subunits, and this stoichiometry appears conserved in both prokaryotic and eukaryotic carriers (48). In addition, recent studies demonstrated that EAAT3 and EAAT4, but neither EAAT1 and EAAT2 nor EAAT2 and EAAT3, coassemble into stable heterotrimers in *in vitro* expression systems (59). Although the biological significance of the hetero-oligomerization of EAAT3 and EAAT4 is currently unknown, it has been shown that EAAT3 and EAAT4 are coexpressed in several cell types in the mammalian brain (60-61), suggesting that heterotrimers might represent a significant portion of the native transporters.

Thus, Glt_{ph} and the mammalian EAATs form trimers and also share similar 3-dimensional membrane topology, at least for the C-terminal part of the proteins. In addition to these shared features, the mammalian EAATs have a segment of more than 50 amino acids between TM4b and TM4c containing N-linked glycosylation sites, which is absent in Glt_{ph}. It has been postulated that these extra residues form a loop that extends from the center of the trimer basin and is accommodated in the large vestibule formed by the assembly of three subunits (62). Further studies are needed to reveal the membrane topology of the N-terminal part

of the mammalian EAATs in three dimensions, particularly the structure of the additional residues not present in Glt_{ph}.

1.4 BINDING SITES FOR GLUTAMATE AND COUPLED IONS

Structural analyses, including mutagenesis studies and crystallography, have also examined potential binding sites for substrates and for the various coupled ions, Na⁺, H⁺ and K⁺, providing data that have facilitated our understanding of transport mechanisms. Mutagenesis studies have generally focused on conserved polar or charged amino acid residues because of their potential for interacting with charged substrates and coupled ions. However, these studies have limitations because changes in substrate binding or ion dependence can arise from structural changes that indirectly alter the binding sites. In this section, we will consider the residues critical for the binding of glutamate and coupled ions, comparing results from mutagenesis studies with the binding sites resolved in the Glt_{ph} structures (49).

1.4.1 Substrate binding site

Elements of the substrate binding site were resolved at the atomic level for Glt_{ph} by exploiting the fact that L-cysteine sulphinic acid (L-CS) binds tightly to Glt_{ph} and produces a clear anomalous scattering from its sulfur atom (49). Because Glt_{ph} prefers L-aspartate over L-glutamate as a substrate, the structure of L-aspartate was superimposed on the electron density of L-CS assuming that the γ -carboxyl group of L-aspartate occupies the same position as the

sulphinic acid group of L-CS. This strategy revealed a substrate binding site formed by the tips of HP1 and HP2, the unwound region of TM7 (NMDGT motif) and the polar residues of amphipathic TM8 (**Figure 4A**), which is very similar to the previously observed non-protein electron density in the substrate-bound Glt_{ph} (48). Several key interactions important for substrate binding were also suggested for Glt_{ph}. These include interactions between the amino and α -carboxyl groups of L-aspartate with R276/S278 (HP1), V355 (HP2), D394/N401 (TM8), as well as interactions between the γ -carboxyl group with T314 (TM7), G359 (HP2) and R397 (TM8).

The importance of the charged residues D394 and R397 for substrate binding is compatible with data obtained in the mammalian EAATs. Without any available high resolution structural information, these studies were based on the comparison of amino acid sequence variations between subtypes displaying different substrate specificities. Conradt *et al.* noticed that R479 in GLAST-1 (R397 in Glt_{ph}) is conserved in acidic amino acid transporters, but a threonine residue sits in the corresponding position in the neutral amino acid transporter, ASCT1. Mutation of the arginine in GLAST-1 to threonine abolishes glutamate uptake, suggesting that R479 is essential for substrate transport (63). Evidence directly linking this residue to glutamate binding came from a mutagenesis study of the equivalent residue in EAAC-1, R447 (64). Wild type EAAC-1 transports L-cysteine in addition to acidic amino acids. Mutated carriers with uncharged or negatively-charged substitutions at R447 no longer transport acidic amino acids, but are still able to accumulate L-cysteine. In addition, these mutated carriers transport L-serine, which is not a substrate for wild type EAAC-1. Acidic amino acids do not compete with L-cysteine, indicating that they no longer bind to the R447 mutant carriers. Thus, it was proposed that R447 (EAAC-1 numbering) interacts with the γ -carboxyl group of glutamate.

Studies using a similar strategy identified another conserved aspartate residue D444 in EAAC-1 (D394 in Glt_{ph}) that is also important for the productive interaction with acidic amino acid substrates (65). The bacterial dicarboxylic acid transporter DctA has a serine residue in place of the aspartate corresponding to D444 in EAAC-1. Wild type EAAC-1 does not bind the dicarboxylic acid succinate, but DctA can. When D444 in EAAC-1 is mutated to neutral residues, succinate can bind to the mutant carriers and inhibit Na⁺-induced transient currents, which are thought to represent charge-moving conformational changes following binding/unbinding of sodium ions. Unlike the R447 mutant carriers, D444 mutant carriers still bind acidic amino acids, but no longer transport substrates. Instead, acidic amino acids function as non-transportable inhibitors that block the Na⁺-induced transient currents as well as Na⁺-activated anion leak currents. The authors proposed that the interaction of D444 with the amino group of substrates is an obligate step for the translocation of acidic amino acids (65).

The role of other residues proposed to comprise the substrate binding site in Glt_{ph}, such as R276, T314 and N401, has not been thoroughly investigated in the mammalian EAATs (**Table I**). Mutations of these corresponding residues in human EAAT1 generally abolishes or significantly impairs glutamate uptake (42). Further experiments are necessary to clarify whether the reduced transport activity of these mutants reflects their inability to bind substrates correctly.

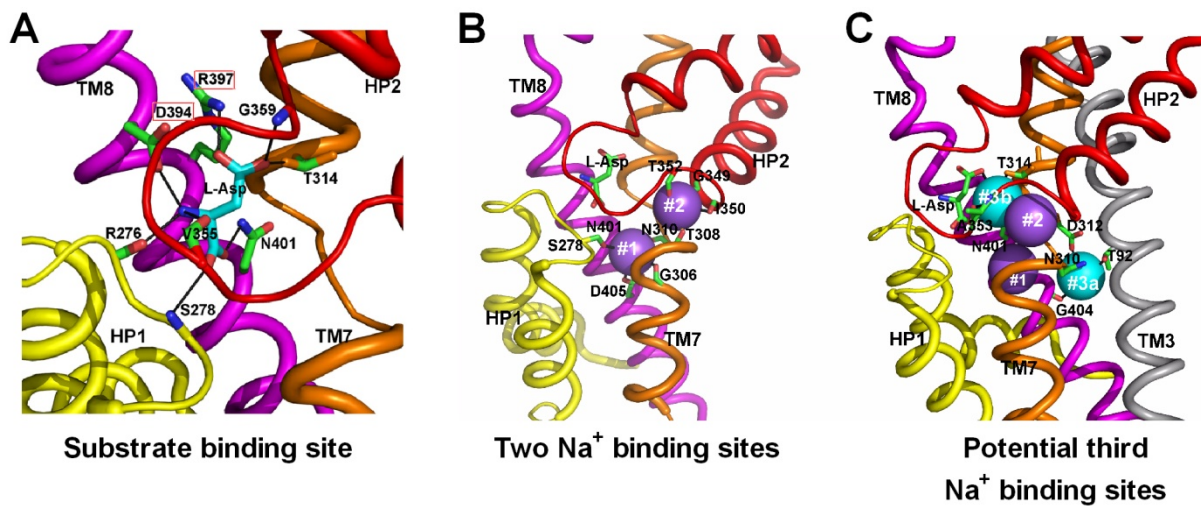


Figure 4. Binding sites for substrate and coupled sodium ions

(A) The substrate binding site revealed in the Glt_{ph} structure is comprised of residues from HP1 (yellow), TM7 (orange), HP2 (red) and TM8 (magenta). Residues highlighted in red boxes represent those also proposed from the results of mutagenesis studies in the mammalian EAATs. (B) Two sodium binding sites revealed in the Glt_{ph} structure. The two sodium ions are shown as purple spheres. Residues S278 (HP1), G306/N310 (TM7), and N401/D405 (TM8) form the Na⁺ binding site #1, whereas residues T308 (TM7) and S349/I350/T352 (HP2) form the Na⁺ binding site #2. (C) Potential third Na⁺ binding sites, shown as cyan spheres. The site #3a is proposed to be a transient Na⁺ binding site that is comprised of T92 (TM3), N310/D312 (TM7), and G404 (TM8), whereas the newly suggested site #3b is formed by residues T314 (TM7), A353 (HP2), and N401 (TM8) as well as the substrate itself. When a sodium ion binds to the site #1, the sodium ion at the site #3a moves quickly over to the site #3b (see text). The illustrations are based the Glt_{ph} crystal structure 2NWX, and are made using the software Pymol (Schrödinger, LLC).

1.4.2 Na⁺ binding sites

The coupling of sodium ions to the movement of substrate is a mechanistic feature shared by the mammalian EAATs and their prokaryotic ancestors. Y403 in GLT-1 was the first residue to be implicated in Na⁺ binding. The mutant carrier Y403F not only exhibits an approximately 8-fold increase in the apparent Na⁺ affinity, but also allows glutamate transport when Na⁺ is replaced by lithium or cesium ions (66). Efforts to identify residues near Y403 that influence Na⁺ binding revealed two additional amino acids within the loop structure of HP2 (S440 and S443 in GLT-1). It has been demonstrated that Li⁺ can replace at least one sodium ion, but not all three, to support transport activity in GLT-1 (67), whereas all three sodium ions can be replaced by lithium ions to support substrate transport by EAAC-1 (68). Mutation of S440 in GLT-1 to glycine, the residue found at this position in EAAC-1, allows Li⁺ to drive substrate uptake. Transport by this mutant carrier also depends on the nature of amino acid at position S443 (69). The reciprocal mutation of glycine to serine in EAAC-1 disrupts the ability of Li⁺ to support substrate transport (68). These results suggest that S440 and S443 in GLT-1 play a role in sodium ion discrimination. Further studies (**Table I**) have focused mainly on conserved, negatively charged or polar residues that have the potential to interact with cations. The mutant carrier T370S of EAAC-1, which is near the equivalent residue of Y403 (GLT-1 numbering), also disrupts Li⁺ dependent substrate transport (68). Moreover, Tao *et al.* showed that residue T101 and D367 in EAAC-1 are involved in the binding of Na⁺ to the substrate-free form of transporters (70-71). The substrate itself, in cooperation with a conserved aspartate residue D439 in EAAC-1, helps determine the affinity for binding of additional sodium ions (72).

Residues that form the Na⁺ binding sites in Glt_{ph} were also suggested by the crystallization of the transporter with two thallium ions, which have stronger anomalous

scattering properties than sodium ions (49). The Na⁺ binding site #1 is buried deeply in the protein and is comprised of residues (Glt_{ph} numbering) S278 (HP1), G306/N310 (TM7), and N401/D405 (TM8). Residues T308 (TM7) and S349/I350/T352 (HP2) form the Na⁺ binding site #2 (**Figure 4B**). Interestingly, although they are nearby to the two proposed sites, most of the residues characterized in mutagenesis studies do not agree precisely with the ones proposed for Glt_{ph} (**Table I**). These observations illustrate some of the limitations inherent in using mutagenesis studies to predict binding sites for substrates and coupled ions. In addition, concerns have also been raised as to whether the anomalous difference map seen in TI⁺-soaked Glt_{ph} accurately represents the Na⁺ binding sites because TI⁺ does not support substrate transport in Glt_{ph} (49).

Computational approaches, such as molecular dynamics simulations and electrostatic mapping, have also been used to model the Na⁺ binding sites (73-75). These studies revealed two putative Na⁺ binding sites in the vicinity of those suggested by the Glt_{ph} structure. In addition, molecular dynamics simulations suggest that one sodium ion is stabilized by interacting with N310 and D312 in the “NMDGT” motif of TM7, and G404/N401 in TM8 of Glt_{ph} (74-76). The aspartate D312 is equivalent to D367 in EAAC-1, a residue that has been suggested to bind sodium ions prior to glutamate binding (70) and also to form a β-bridge with the residue N310 (77). T101 of EAAC1 (equivalent to T92 in Glt_{ph}) protrudes into a hydrophilic cavity occupied by the D367 side chain and is also involved in the initial Na⁺ binding (78). These results suggest a previously uncharacterized Na⁺ binding site comprised of T92 (TM3), N310/D312 (TM7), and G404 (TM8) in Glt_{ph} (site #3a in **Figure 4C**). Larsson *et al.* further proposed that this Na⁺ binding site is transient (75). When a sodium ion binds to the site #1, the sodium ion at the site #3a moves quickly over to a new place that is formed by the substrate itself and residues T314

(TM7), A353 (HP2), and N401 (TM8) (site #3b in **Figure 4C**). The Na⁺ binding site #3b is also suggested by the electrostatic mapping study (73) and agrees with the proposal that the bound substrate controls the rate and the extent of Na⁺ interactions with the transporter (72).

1.4.3 K⁺ binding site

In addition to its proposed contribution to Na⁺ binding, Y403 in GLT-1 has been implicated in the K⁺-induced reorientation of the substrate-free carriers. Mutation of this residue locks the transporter in a Na⁺-dependent exchange mode and renders the transporter insensitive to K⁺ (66). A similar phenotype has been reported for mutations of the residue E404 in GLT-1, which is also involved in H⁺ binding and will be discussed later in section 1.4.4, and the residue R447 in EAAC-1, which interacts with the γ -carboxyl group of glutamate (64, 79). Although Tl⁺ is traditionally viewed as a K⁺ congener, the thallium binding sites in Glt_{ph} are thought to be genuine Na⁺ binding sites because only Na⁺, but not K⁺ diminishes the thallium anomalous density peaks during crystallization (49). However, Glt_{ph} does not require K⁺ to support substrate transport (80) and it is intriguing that the Na⁺ binding sites analogous to those identified in the Glt_{ph} structure may bind K⁺ in the mammalian EAATs. In support of this idea, Tl⁺ can replace intracellular K⁺ to mediate glutamate transport in EAAC-1 (81) and residue D455 in GLT-1, which corresponds to D405 in the Na⁺ binding site #1 of Glt_{ph}, is required for the interaction of the transporter with K⁺ (81-82). In addition, a 3-dimensional representation of the K⁺ binding site was generated using electrostatic mapping based on a homology model of EAAC-1 (73). The proposed site overlaps substantially with the glutamate binding site and is mutually exclusive with glutamate binding. These results suggest that the K⁺ binding site overlaps with the binding sites for glutamate, H⁺ and Na⁺, and may explain why the K⁺-induced orientation step is

vulnerable to mutations in various regions. It is conceivable that as EAATs reorient to the outward-facing state, K^+ interacts with regions that were previously occupied by glutamate and coupled ions. Recently, a compound present in spider venom, Parawixin1, has been isolated and characterized to specifically speed the K^+ -induced reorientation step of the transport cycle (83). Further studies using Parawixin1 and related compounds may help delineate how K^+ binds and drives the reorientation of substrate-free transporters.

1.4.4 H^+ binding site

It was originally proposed that a proton ion is transported by EAATs along with the protonated form of glutamate (23). Because the γ -carboxyl group of glutamate appears to interact with residue R447 in EAAC-1, this mechanism requires that H^+ binds to the negatively charged glutamate which has bound to the transporter. By contrast, work by Watzke *et al.* (84) demonstrated that EAAC-1 must be protonated before glutamate binds at the extracellular side and implied the existence of an ionizable residue in the transporter with apparent pKa of 8. In addition, the pKa of this residue shifts by at least 1.5 units after glutamate translocation (84). The residue has been identified as E373 in EAAC-1, because amino acid substitutions at E373 render substrate transport by the carriers pH-independent (85). E373 is equivalent to E404 in GLT-1, which has also been proposed to be crucial for the K^+ -induced reorientation step (79). Taken together, these data support a general mechanism in which E373 in EAAC1 functions as a proton acceptor at the extracellular side before glutamate binding, as a proton donor at the intracellular side, and once deprotonated, as a binding site for K^+ which triggers the reorientation of transporters.

Table 1. Residues contributing to substrate and coupled ion binding as suggested by Glt_{Ph} crystal structures, computational simulations and by mutagenesis studies in the mammalian EAATs

Residues suggested by computational simulations are marked with asterisks and residues highlighted in red are equivalent between two subtypes.

	Residues in Glt _{Ph}	Residues explored in the mammalian EAATs	Proposed role in the mammalian EAATs	References
Substrate binding site	R276, HP1 S278, HP1 T314, TM7 V355, HP2 G359, HP2		D444 in EAAC-1 proposed to interact with the amino group of glutamate	(65)
	D394, TM8	D444 (EAAC-1), TM8	R447 in EAAC-1 proposed to interact with the γ -carboxyl group of glutamate	(64)
	R397, TM8	R447 (EAAC-1), TM8		
	N401, TM8			
Na⁺ binding site #1	S278, HP1 G306, TM7 N310, TM7 N401, TM8 D405, TM8	Y403 (GLT-1), TM7 S440 (GLT-1), HP2 S443 (GLT-1), HP2	Y403 in GLT-1 is implicated in sodium binding	(66)
		D439 (EAAC-1), TM8	S440 and S443 in GLT-1 influence sodium ion discrimination	(69)
Na⁺ binding site #2	T308, TM7	D439 (EAAC-1), TM8	Residue D439 in EAAC-1 controls high-affinity sodium binding to glutamate bound transporters	(72)
	S349, HP2			
	I450, HP2			
	T352, HP2			
Transient Na⁺ binding site #3a	T92*, TM3	T101 (EAAC-1), TM3	T101 and D367 in EAAC-1 appear critical for sodium binding to the substrate-free transporters	(70, 78)
	N310*, TM7	N365 (EAAC-1), TM7		
	D312*, TM7	D367 (EAAC-1), TM7	N365 in EAAC-1 forms a β -bridge with D367 and is also important for Na ⁺ binding.	(77)
	G404*, TM8			
Na⁺ binding site #3b	T314*, TM7	T370 (EAAC-1), TM7	T370S disrupts the ability of lithium ions to support substrate transport.	(68)
	A353*, HP2		Both T370 and N451 bind to Na ⁺ before glutamate has bound	(75)
	N401*, TM8	N451 (EAAC-1), TM8		
K⁺ binding site		Y403 (GLT-1), TM7 E404 (GLT-1), TM7 R447 (EAAC-1), TM8	These three residues when mutated lock the carriers in an obligatory exchange mode and are proposed to be involved in the potassium-induced translocation of substrate-free transporters	(64, 66, 79)
		D454C (EAAC-1), TM8	D454 contributes to potassium binding.	(81-82)
H⁺ binding site		E373 (EAAC-1), TM7	E373 in EAAC-1 proposed to be a H ⁺ acceptor	(85)

1.5 MECHANISMS OF SUBSTRATE TRANSPORT

Secondary active transporters including glutamate transporters are thought to function through an alternating access mechanism (86). In this model, the substrate binding site is alternatively accessible from the extracellular and intracellular sides through a process that depends on one or more conformational changes. Several studies have been carried out to probe the conformational transitions that occur during substrate transport. Early work by Grunewald and Kanner compared how trypsin cleaves EAATs into different sets of proteolytic fragments in the absence or presence of substrates, and demonstrated that conformational changes triggered by substrate transport expose additional trypsin sites (67). Larsson *et al.* used voltage-clamp fluorometry to directly measure fluorescence changes in a neuronal EAAT covalently labeled with a fluorescent reporter. Their results showed that alterations in concentrations of glutamate and co-transported ion and in the membrane voltage induce conformational rearrangements in EAATs (87). More recently, Mim *et al.* determined the activation parameters of rapid, glutamate-induced processes by analyzing the temperature dependence of glutamate transport at steady state and pre-steady state. They proposed that two conformational changes accompany glutamate translocation and at least one conformational change accompanies relocation of the empty transporter based on the large calculated enthalpies associated with these processes (88). Although these studies do not have sufficient resolution to reveal the nature of these conformational changes, they do suggest the potential for multiple discrete conformational transitions during the transport cycle.

The substrate binding site of Glt_{ph} is cradled by the two helical hairpins (HP1 and HP2). These hairpins have thus been proposed to act as inner and outer gates for glutamate transporters, and the Glt_{ph} structure with substrate bound (PDB ID: 1XFH) represents an occluded state with two gates closed. The structural evidence supporting HP2 as the outer gate comes from the

TBOA-bound Glt_{ph} structure (PDB ID: 2NWW). The structure provided a clear view showing that when TBOA is bound, HP2 is locked in an open conformation, thus precluding the binding of a sodium ion and further conformational changes (**Figure 5A**). The opening of HP2 was also suggested by molecular dynamics simulations based on the apo-state (unliganded state) of the Glt_{ph} structure and is considered to be an intrinsic feature of glutamate transporter dynamics that occurs within tens of nanoseconds in simulations (74, 89). Indeed, substituted cysteine modification studies performed on human EAAT1 and GLT-1 showed that substrates and coupled ions can modify solvent accessibilities of the residues in HP2, consistent with the idea that this region undergoes conformational changes during substrate translocation in the mammalian EAATs (90-91).

On the other hand, more limited data exist to support HP1 as the inner gate. Biochemical studies showed that a conserved motif of three consecutive serine residues at the HP1 tip can be accessed by hydrophilic agents from both sides of the membrane in the bacterial transporter GltT_{Bs} (47). In addition, Shlaifer and Kanner (92) probed the reactivity of cysteines introduced into the C-terminal part of GLT-1 to membrane permeable agent N-ethylmaleimide (NEM). They reported an increase in the modification of cysteine substituted mutants in TM7, TM8 and HP1 when external Na⁺ is replaced by K⁺, a condition expected to increase the proportion of inward-facing transporters. By contrast, the modification of these cysteines was decreased by non-transportable analogs, which presumably lock transporters in the outward-facing state. Based on these observations, the authors suggested that the inward movement of HP1 leads to the opening of a pathway between the binding pocket and the cytoplasm, lined by parts of TM7 and TM8. Interestingly, our lab demonstrated that a disulfide crosslink that limits the movement of HP1 appears to abolish transport, whereas constraint of HP2 movement alters the apparent

affinity for substrates with no effect on the maximal transport rate. These results link the movement of HP2 to initial substrate binding events and the movement of HP1 to later steps in translocation, consistent with the view that these two domains may function as outer and inner gates of the translocation pore, respectively (52).

While HP2 can move freely toward the large aqueous basin formed by the three subunits, HP1 is tightly packed with TM7, TM8 and the surrounding scaffold structure in the substrate-bound Glt_{ph} structure (**Figure 5B**). It was therefore proposed that HP1 first moves vertically towards the cytoplasm and then laterally away to create a pathway along the polar face of TM7 and TM8, exposing the serine-rich HP1 tip (48). Evidence for such vertical movement of HP1 is revealed in a recent inward-facing structure of Glt_{ph} (PDB ID: 3KBC) in which two substituted cysteines (K55C/A364C) in TM2 and HP2 regions are crosslinked by divalent mercury (Hg²⁺) (50). The most striking feature of this structure compared to the original substrate-bound Glt_{ph} structure is that not only HP1, but the whole C-terminal transport domain moves approximately 18 Å towards the cytoplasm (**Figure 5C**). Such movements significantly increase the exposure of the transport domain to the cytoplasm allowing the potential gating movement of HP1, which contradicts the earlier proposal that only small-scale molecular motions are required to accomplish glutamate uptake in EAATs (93). The inward-facing conformation of Glt_{ph} is recapitulated by a modeling study based on the symmetric considerations of the transporter (inverted-topology structural repeats) (94). The equivalent residue pairs of K55C/A364C can also be crosslinked in human EAAT1 and EAAC-1 (94-95), reinforcing the idea that Glt_{ph} and the mammalian EAATs share similar dynamic movements during substrate transport.

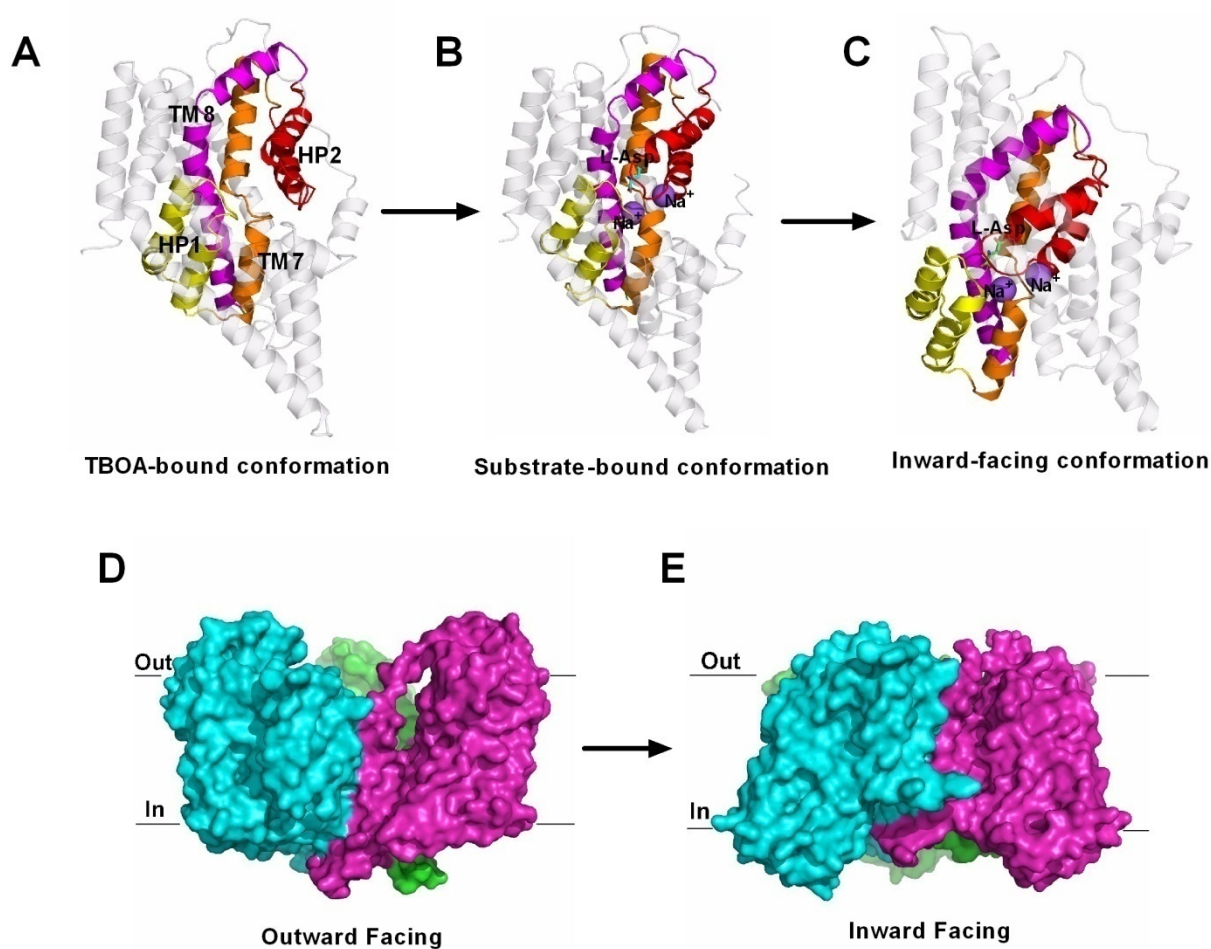


Figure 5. Mechanisms of substrate transport

(A) The TBOA-bound Glt_{ph} structure (PDB ID: 2NWW) showing HP2 displaced from the substrate binding site (TBOA is removed from the structure for clarity). (B) The substrate-bound Glt_{ph} structure (PDB ID: 2NWX) showing the closed HP2, two sodium ions and the bound substrate, L-aspartate. (C) The inward-facing Glt_{ph} structure (PDB ID: 3KBC) in which the whole C-terminal transport domain moves towards the cytoplasm. (D) Surface representation of the outward-facing Glt_{ph} (as the substrate-bound conformation) before the transport domain moves into the cytoplasm. (E) Surface representation of the inward-facing Glt_{ph}. The three protomers are colored in either green, magenta or cyan. The illustrations are made using the software Pymol (Schrödinger, LLC).

Thus, a general picture of how glutamate transporters uptake substrate emerges (Figure 5). HP2 opens up spontaneously to expose the substrate binding site. After glutamate and co-transported ions bind, HP2 closes and seals the substrate binding site, and the transporter is in an occluded, outward-facing conformation (**Figure 5D**). The whole transport domain then moves in a piston-like motion toward the cytosol which permits the opening of the internal gate, presumably HP1, and the transporter is in an occluded, inward-facing conformation (**Figure 5E**). After the release of substrate, K^+ binds to and facilitates reorientation of the carrier back to the outward-facing state.

1.6 THE STRUCTURAL BASIS FOR THE TRANSPORTER-ASSOCIATED ANION CONDUCTANCE

In addition to transporting substrates, glutamate transporters have also been shown to possess an anion channel activity (11, 28). The anion current is activated by coupled Na^+ (the Na^+ -activated anion leak current) and is significantly increased with the addition of substrates (the substrate-activated anion current). At present it is not known if the two anion currents share the same pathway or go through different ones. The relative anion permeability sequence for the Na^+ -activated anion leak current determined in human EAAT1 is $I^- > NO_3^- > Br^- > Cl^-$ and is different from that for the substrate-activated anion current ($NO_3^- > I^- > Br^- > Cl^-$). If the two anion currents share a similar pathway, the selective filter that controls anion interaction must experience subtle changes when substrate binds to the transporter. Nevertheless, the anion channel activity of glutamate transporters is thermodynamically uncoupled from the substrate transport process. Modification of substituted cysteines in the HP2 region completely abolishes

uptake activity in the mutated carriers, but preserves the glutamate-activated anion current (96-98). Studies have also shown that the substrate-activated anion current can still occur at 4 °C or at membrane potential >70 mV when glutamate uptake is abolished (29). In addition, the temperature coefficient (Q_{10}) of EAAC-1 for the Na^+ -activated anion leak current and the substrate-activated anion current are 1.9 and 1.7 at 0 mV membrane potential, respectively (88). These values are similar to the Q_{10} value for diffusion-limited processes in an aqueous solution (1.3 to 1.6) and are smaller than that of substrate transport (3.7 at 0 mV and 3.2 at -30 mV) (29, 88). Thus, while substrate transport requires substantial conformational changes and is temperature dependent, small structural rearrangements might be sufficient to maintain the anion channel activity of glutamate transporters.

The molecular determinants of the transporter-associated anion conductance have been explored by Vandenberg and colleagues (95, 99). They initially focused on polar or charged residues in the TM2 region of human EAAT1 because such residues form ion permeation pathways of many ion channels (100-101). Mutations of several polar or charged residues in TM2 affected various properties of the anion channel activity, but not the transport of glutamate (95). Consistent with the idea that they form a chloride permeating pore, most of the characterized residues are solvent accessible, as judged by their reactivity to either thiol-modifying methanethiosulfonate reagents or HgCl_2 . Two mutant carriers show particularly interesting phenotypes. The glutamate-activated anion currents in the mutant carrier S103V display an altered sequence of anion permeation, $\text{Cl}^- < \text{NO}_3^- < \text{Br}^- < \text{I}^-$ (for the wild type EAAT1, $\text{Cl}^- < \text{Br}^- < \text{I}^- < \text{NO}_3^-$), suggesting that S103 contributes to the selectivity filter of the channel. In addition, the mutant carrier D112A has a greatly increased Na^+ -activated anion leak current, but a decreased substrate-activated anion current. It was proposed that D112 may serve as a gating

residue for the anion channel. When mutated, the channel is locked in an open state, which leads to a large increase in anion leak current. Thus, little additional current can be activated by glutamate (95). This interpretation assumes that the Na⁺- and substrate- activated anion channel pathways are closely related. Alternatively, the D112A mutation may facilitate opening of the leak conductance pathway, but prevent opening of a separate substrate-activated anion pathway (102).

An additional study investigated charged residues that are within 5 Å of S103 and D112 based on a 3-dimensional homology model of human EAAT1. Residues D272 in TM5 and K384/R385 in TM7 show an altered anion leak conductance and substrate-activated anion conductance when mutated to neutral or oppositely charged amino acids (99). Unlike the D112A transporter, the mutant carriers D272A and D272K display increased amplitudes of both the leak and substrate-activated anion conductance. On the other hand, mutants K384A and R385A have increased leak conductance with little change in the substrate-activated anion current. Mutants K384D and R385D have both increased leak and substrate-activated anion conductance even though the increased amplitude of the leak conductance is smaller than that of the respective alanine mutants. These results suggest that both the position and charge of residues in the intracellular region of EAAT1 influence the two components of the anion conductance.

Because Glt_{ph} also have anion channel activity (32), it is intriguing to look at the anion channel function of EAATs in light of the Glt_{ph} structures. The mutant carrier S65V in Glt_{ph} (equivalent to S103V in human EAAT1) displays reduced substrate-activated Cl⁻ influx compared to the wild type transporter, suggesting that the chloride permeation pathway is conserved in Glt_{ph} and human EAAT1 (32). The residue equivalent to D112 is located at the TM2-TM3 loop, which undergoes significant conformational changes to accommodate the large

movement of the C-terminal transport domain as revealed by the inward-facing Glt_{ph} structure. Whether this large inward movement of the transport domain is linked to the transporter associated anion conductance warrants further exploration.

1.7 THESIS GOALS

Although several high resolution structures of Glt_{ph} in different conformations provides clarity in regards to the structural domains involved in substrate transport, our knowledge on the conformational dynamics of the carrier is far from complete. The regions that participate in permeation and gating of the anion channel activity are also not yet established, nor is the structural linkage between substrate transport and the anion channel function. The goal of this thesis is to use biochemical, electrophysiological and functional assays in combination with computational simulations to identify key domains and conformational changes involved in the glutamate transporter's dual functions.

2.0 LARGE COLLECTIVE MOTIONS REGULATE THE FUNCTIONAL PROPERTIES OF GLUTAMATE TRANSPORTER TRIMERS

2.1 INTRODUCTION

Glutamate transporters, like many other proteins, carry out their biological activities by sampling an ensemble of conformations (67, 87-88). The equilibrium motions accessible to the transporter can vary over a wide range of length- and time- scales, *e.g.*, from fluctuations in bond lengths, bond angles and dihedral angles (local motions) to cooperative movements of entire domains or subunits (global motions). The crystallization of Glt_{ph} in several different conformational states greatly expanded our understanding of substrate transport achieved via an alternating access mechanism. Local conformational changes in HP1 and HP2 allow for the opening or occlusion of the substrate-binding site, whereas the piston-like movement of the transport domain provides a means for transition between the outward- and inward-facing states (**Figure 5**). However, transport is inherently a dynamic process and cannot be completely understood solely on the basis of static pictures, even if they are of high resolution.

Ideally, researchers would like to observe individual atoms moving within a protein to study the conformational changes associated with protein functions. This goal is not possible to achieve experimentally at present and the dynamics of proteins are largely inferred from sophisticated biophysical methods that measure physical properties (103). In one such study of

glutamate transporters, Larsson and colleagues employed fluorescence/Förster resonance energy transfer (FRET) analysis to determine the relative positions of different TM domains of human EAAT3. FRET is a phenomenon by which a donor fluorophore transfers its excitation energy to a nearby acceptor fluorophore. The efficiency of FRET depends on and can be used to estimate the relative distance of the donor and acceptor fluorophores. This study suggested very little structural changes in glutamate transporters during substrate transport (93). Mutagenesis studies can also provide valuable information on the in-depth mechanism of proteins if mutations or sulfhydryl modifications of cysteine substitutions lock biomolecules in specific conformational states (104). One good example of this strategy is to constrain the movement of certain areas of proteins by crosslinking two exogenously introduced cysteines that are spatially close with each other. Using this method, our lab has successfully restricted the movements of the HP2 or HP1 domains and provided insights into the mechanism of the substrate translocation (52). Finally, computational simulations have the unbeatable power to putatively describe protein dynamics in detail, because they can simulate the precise position of each atom at any instant time, provided that a high resolution structure of the protein is known (103). In this chapter, we utilized cysteine crosslinking study in combination with computational modeling to identify a series of large-scale collective motions that are intrinsic to glutamate transporter trimers.

Using a cysteineless version of the human excitatory amino acid transporter EAAT1, we show that single cysteine residues introduced into the extracellular gate (helical hairpin HP2) on each of the three subunits form reversible intersubunit crosslinks spontaneously and/or catalyzed by the oxidizing reagent copper phenanthroline (CuPh). After crosslinking, substrate uptake, but not the substrate-activated anion conductance, is completely inhibited in these mutants. The formation of disulfide bridges between pairs of cysteines that are more than 40 Å apart in the

static structure can be explained by the concerted subunit movements predicted by anisotropic network model (ANM) analysis. The existence of these global motions is further supported by the observation that single cysteine substitutions at the N-terminal part of TM8 helix can also be crosslinked by CuPh, as predicted by the ANM analysis. Interestingly, the transport domain in the third (uncrosslinked) subunit of the trimer assumes an inward-facing orientation, suggesting that individual subunits potentially undergo separate transitions between outward-facing and inward-facing forms, rather than an all-or-none transition of the three subunits, a mechanism also supported by ANM-predicted intrinsic dynamics. These results shed light on how large collective motions contribute to the functional dynamics of glutamate transporters.

2.2 RESULTS

2.2.1 Inhibition of substrate transport by CuPh and cadmium ions in mutants V449C and I453C

Previously, our lab used CuPh-catalyzed crosslinking of cysteine pairs introduced into a highly functional cysteineless version of human EAAT1 (CSLS) to examine the interaction of key domains associated with substrate translocation (52). To serve as a control, single cysteine mutants were also treated with CuPh to confirm that crosslinking occurs between cysteine pairs within a single subunit. We unexpectedly found that for one single cysteine mutant, V449C, incubation with 300 μM CuPh for 5 min completely abolishes transport activity. V449C-transfected COS7 cells show $36.68 \pm 2.84\%$ of the transport activity of the CSLS control when 5 μM L-glutamate is used as substrate (**Figure 6B**). After 5 min exposure to 300 μM CuPh,

V449C-expressing COS7 cells display minimal transport, even at high substrate concentrations (up to 1 mM, **Figure 6E**). In contrast, no change in transport is observed for CSLS-transfected cells after CuPh treatment (**Figure 6A and 6D**). To confirm that the effect of CuPh is associated with the formation of disulfide bonds, we incubated cells expressing V449C first with 300 μ M CuPh and then with 20 mM dithiothreitol (DTT) for 5 min to reduce crosslinks. To our surprise, incubation with DTT not only recovers, but also increases substrate accumulation by this mutant. Consistent with this observation, treatment with DTT alone also enhances the uptake activity of V449C, suggesting disulfide bonds form spontaneously (**Figure 6B**).

We also explored the effect of CuPh on another mutant, I453C, a residue one helical turn away from V449. Before crosslinking, the I453C mutant exhibits $60.67 \pm 2.64\%$ of the transport activity of CSLS. After 5 min treatment with 300 μ M CuPh, this mutant displays modest transport activity ($\sim 50\%$ compared to the untreated control, **Figure 6C**). Analysis of the kinetic properties of the mutant carrier I453C shows that CuPh treatment results in a decrease of V_{max} (35% - 62.5% of the untreated control), but the K_m remains essentially the same ($34.82 \pm 9.82 \mu$ M for the untreated control vs. $33.25 \pm 5.48 \mu$ M for the CuPh treated group). The residual uptake activity after CuPh treatment arises from uncrosslinked I453C, because prolonged incubation with CuPh or additional treatment with a thiol-modifying reagent, MTSET, further reduces its uptake activity (**Figure 7**). The inhibition of I453C by CuPh can be completely reversed by 20 mM DTT, though no enhancement of transport activity is seen as for V449C (**Figure 6C**).

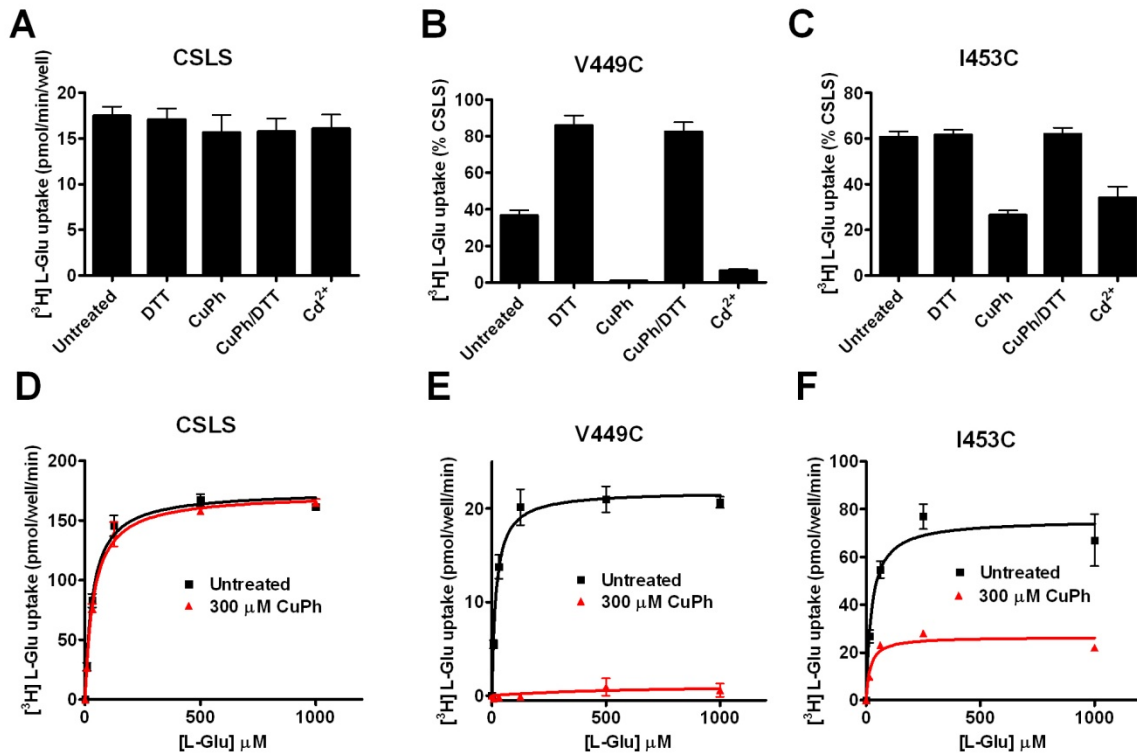


Figure 6. Inhibition of substrate transport by CuPh and cadmium ions in mutants V449C and I453C

COS7 cells expressing CSLS, V449C and I453C were treated with 20 mM DTT, 300 μM CuPh, or 300 μM CuPh followed by DTT, for 5 min. Uptake assays were performed for 10 min at room temperature using 5 μM L-[³H] glutamate as substrate in **panel A-C** or using various concentrations of L-[³H] glutamate as substrate in **panel D-F**. The effect of Cd²⁺ on transport activity was determined by including 100 μM cadmium chloride in the uptake solution. Data for V449C and I453C are expressed as the percent of uptake activity relative to the CSLS control in Panel A-C.

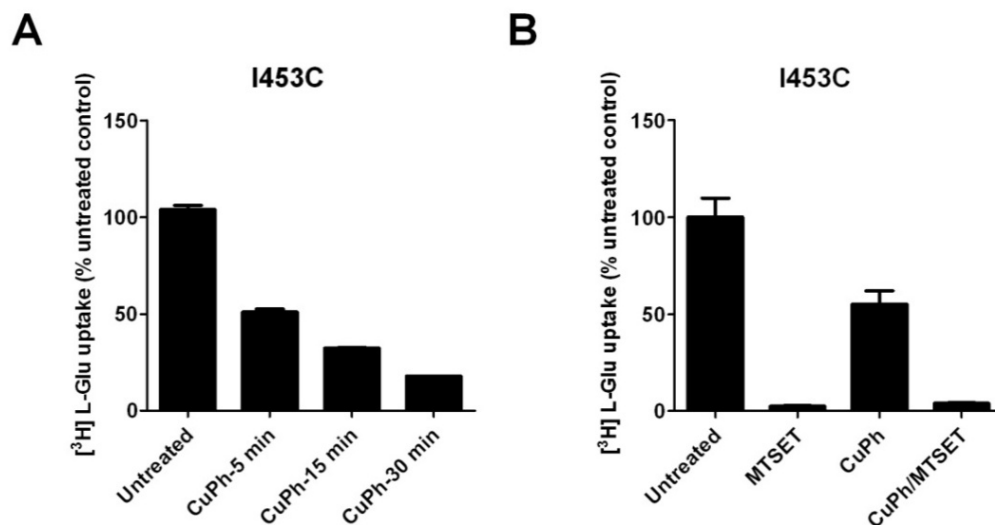


Figure 7. The effect of prolonged incubation of CuPh or additional incubation with MTSET on uptake activity of the I453C mutant carrier

(A) COS7 cells expressing I453C were treated with 300 μ M CuPh for indicated time. (B) Cells expressing I453C were treated with 300 μ M CuPh, 1 mM MTSET or 300 μ M CuPh followed by MTSET, for 5 min. Uptake assays were performed for 10 min at room temperature using 5 μ M L-[³H] glutamate as substrate. Data are expressed as the percent of uptake activity relative to the untreated control.

As a complementary method to determine the proximity of cysteine residues, we performed transport assays with V449C or I453C in the presence of 100 μ M cadmium ions. This divalent cation interacts with cysteinyl side chains and the affinity of the interaction is dramatically increased if Cd²⁺ can be coordinated by two cysteines (95). The presence of Cd²⁺ in the uptake solution abolishes the transport activity of V449C (**Figure 6B**) and significantly inhibits that of I453C (**Figure 6C**).

2.2.2 Single cysteine substitutions at the N-terminal end of helix HP2b are more reactive to CuPh and form spontaneous crosslinks

Residues V449 and I453 are located at the N-terminal end of helix HP2b, which along with HP2a forms the helical hairpin HP2 (**Figure 8A**). To determine whether other residues in HP2b can also crosslink, we measured the effect of CuPh on single cysteine mutants within the HP2b helix from A446 to V458. All but three cysteine mutants in this region are able to accumulate L-glutamate above background levels when expressed in COS7 cells (90). Upon treatment with CuPh, the most reactive cysteine substitutions are L448C and V449C, and their uptake activities are completely inhibited after 5 min incubation with 300 μM CuPh (**Figure 8C**). The mutant carrier V449C readily forms disulfide bonds because CuPh concentrations as low as 5 μM CuPh are sufficient to completely inhibit transport activity (**Figure 8B**). The second order rate constant of CuPh is $1790 \pm 263 \text{ M}^{-1}\text{s}^{-1}$ for V449C. By contrast, residues near the C-terminal end of HP2b (L455C, T456C and V458C) still accumulate substrate comparably to untreated controls, indicating they do not achieve sufficient proximity to form disulfide bonds. Mutants V452C, I453C, and V454C in HP2b show intermediate inhibition by CuPh. The inhibition of all these mutants by CuPh can be reversed by additional incubation with 20 mM DTT, as demonstrated in **Figure 8D**. Furthermore, DTT significantly increases transport activity of L448C, to an even greater degree than that observed for V449C, suggesting that L448C also forms spontaneous crosslinks.

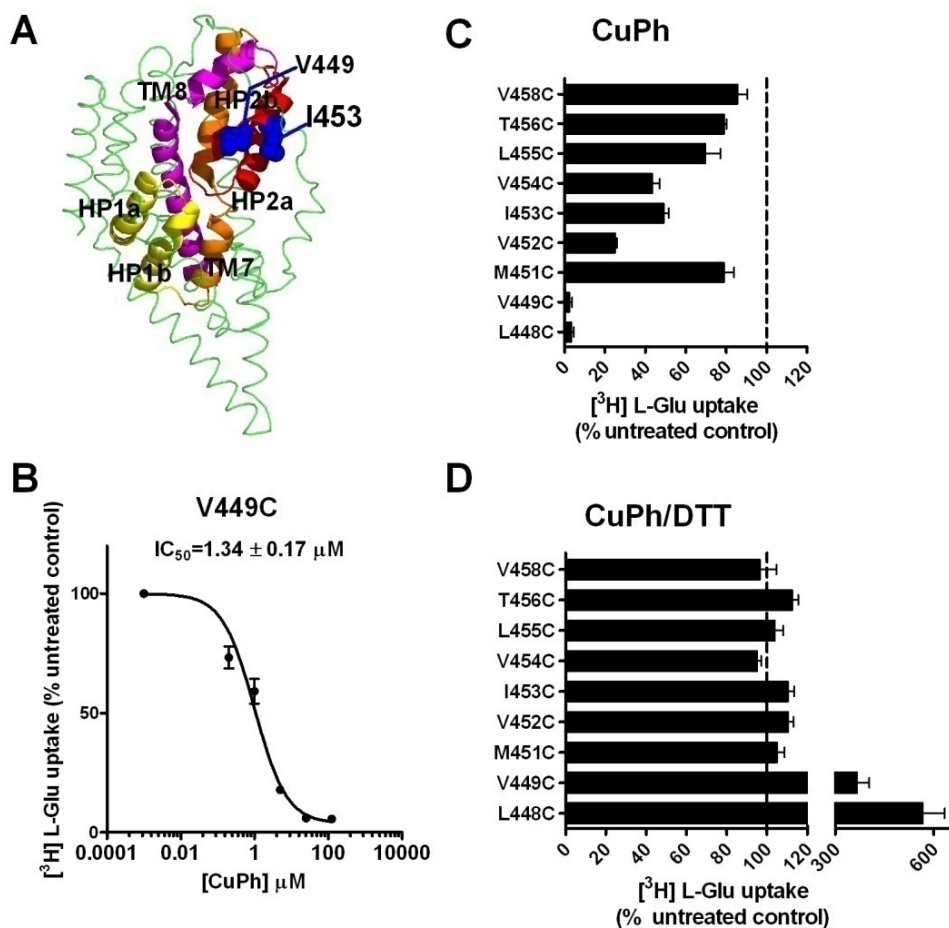


Figure 8. Single cysteine substitutions at the N-terminal end of the helix HP2b are more reactive to CuPh and form spontaneous crosslinks.

(A) Locations of V449 and I453 on the helix H2b of the HP2 hairpin, shown for one subunit (viewed in the plane of the membrane). (B) COS7 cells expressing V449C were treated with different concentrations of CuPh for 5 min and uptake activity was measured. (C) The effects of 300 μM CuPh for 5 min on the L-glutamate transport activity of transporters with a series of single cysteine substitutions in HP2b. (D) Substrate transport by mutant transporters after additional treatment with 20 mM DTT for 5 min. Uptake assays were performed for 10 min at room temperature using 5 μM L- ^3H glutamate as substrate. Data are represented as the percentage of untreated controls in two to four experiments done in triplicate.

2.2.3 The formation of disulfide bonds in V449C and I453C as confirmed by biochemical assays

We next sought to obtain biochemical evidence of disulfide bond formation after CuPh treatment. Because of their propensity to form both spontaneous and CuPh-catalyzed crosslinks, we focused on the V449C and I453C mutant carriers. V449C and I453C each contain only one cysteine residue per subunit within the trimer, the covalent disulfide bridges must span two subunits, and should be readily detectable as dimers by non-reducing SDS-PAGE. However, glutamate transporters tend to form oligomers in polyacrylamide gels when overexpressed in COS7 cells. We thus turned to *Xenopus* oocytes which predominantly show transporter species corresponding to monomers when analyzed by SDS-PAGE (57), and used a method for isolating plasma and microsomal membranes from oocytes originally described by Kobilka *et al.* (105). In oocytes, CuPh and DTT have similar effects on the uptake activity of V449C and I453C as in COS7 cells (**Figure 9**). When oocyte membrane proteins are separated by non-reducing SDS-PAGE and immunoblotted, the CSLS control exhibits two species at molecular mass of ~70 kDa and ~50 kDa, corresponding to fully glycosylated and unglycosylated/partially glycosylated monomers, respectively (**Figure 9**). With V449C and I453C, bands migrating at ~70 kDa and ~50 kDa are seen in untreated oocytes, whereas an additional ~140 kDa species appears after the oocytes are treated with 300 μ M CuPh for 5 min, consistent with the predicted size of a crosslinked transporter dimer. A weak dimer band signal is also observed in untreated V449C-expressing oocytes, confirming the existence of spontaneous crosslinks. The high molecular weight band disappears in V449C-expressing oocytes and is significantly less in I453C-expressing oocytes after additional incubation with 20 mM DTT. These results strongly suggest that V449C and I453C form CuPh-catalyzed, DTT-reversible disulfide bonds.

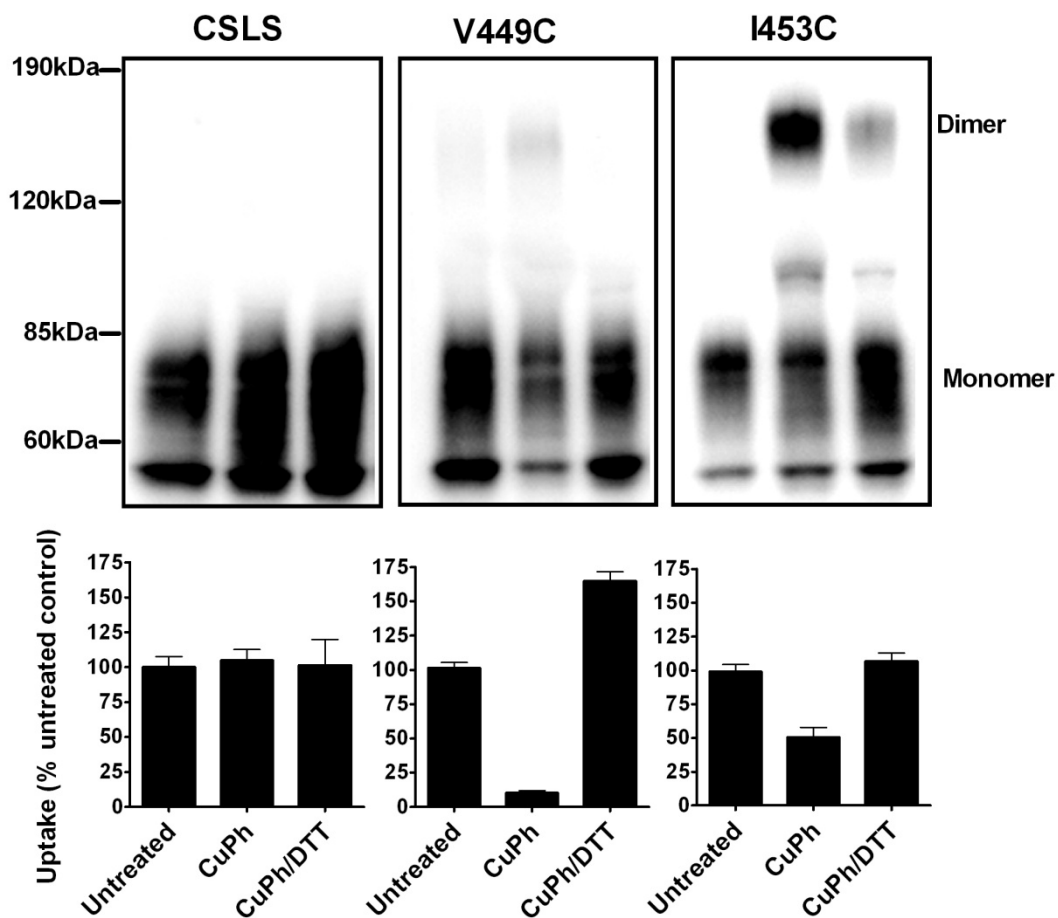


Figure 9. CuPh catalyzes the formation of disulfide bonds in V449C and I453C as confirmed by biochemical assays

Transporters were expressed in *Xenopus* oocytes and treated with 300 μ M CuPh, or 300 μ M CuPh followed by DTT, for 5 min. Oocyte membranes were lysed and separated by non-reducing gradient SDS-PAGE, and subjected to western blotting analyses. Glutamate transporter proteins were identified using an anti-EAAT1 polyclonal antibody directed against the C-terminus. Uptake assays in oocytes were carried out at room temperature using 5 μ M L-[3 H] glutamate as substrate for 15 min and data are normalized to untreated controls.

The mutant I453C shows a stronger dimer band signal compared to V449C after crosslinking, although transport by I453C is less dramatically inhibited. In addition, a weak dimer band signal of I453C is observed after additional DTT treatment even though DTT completely reverses the inhibition of uptake by CuPh. During CuPh incubation, a portion of crosslinked I453C may be internalized and are no longer accessible to DTT. The weak dimer band signal in V449C could also result from the instability of disulfide bonds in this mutant carrier during the process of biochemical assays. We therefore treated V449C-expressing oocytes with a bifunctional crosslinking reagent, 1,8-Octadiyl Bismethanethiosulfonate (M8M). 5 min incubation with 1 mM M8M significantly inhibits the uptake activity of the mutant carrier V449C (**Figure 10A**) and induces a prominent dimer species when analyzed by non-reducing SDS-PAGE (**Figure 10B**).

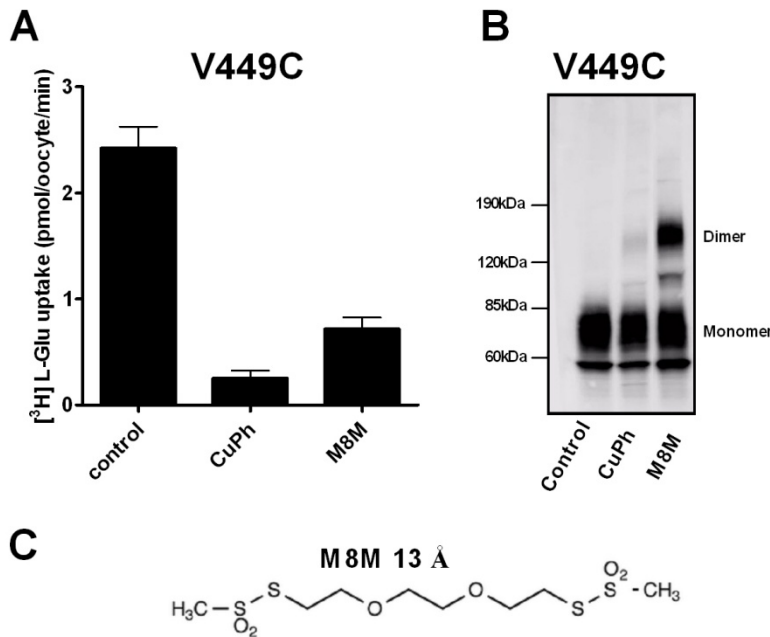


Figure 10. The effect of a bifunctional crosslinking reagent, M8M, on the mutant V449C.

(A) Oocytes expressing V449C were treated with 300 μ M CuPh or 1 mM M8M for 5 min. Uptake assays were performed at room temperature using 5 μ M L-[3 H] glutamate as substrate for 15 min. (B) After indicated treatment, oocyte membrane samples were collected and subjected to

western blotting analyses using an EAAT1-specific antibody. (C) The chemical structure of M8M.

2.2.4 Crosslinks in the mutant carrier V449C take place between two transporter subunits in the same trimer

Although the additional high molecular weight species appeared after CuPh treatment in the mutant carrier V449C migrates at the predicted size of the transporter dimers, it is possible that the crosslinks might take place between a transporter subunit and an unknown protein with a similar apparent molecular mass. To exclude this possibility, we constructed an N-terminus GFP tagged V449C. When expressed in *Xenopus* oocytes, 5 min incubation with 300 μ M CuPh significantly inhibits the uptake activity of GFP-V449C, similar to that is observed for non-tagged V449C (**Figure 11A**). We then expressed V449C, GFP-V449C or a 1:1 ratio of V449C/GFP-V449C mixture in oocytes and treated the cells with 1 mM M8M for 5 min, which induces stronger crosslinked dimer band signals (**Figure 10**). When membrane protein samples are separated by non-reducing SDS PAGE, three different species of crosslinked dimers are detected, corresponding to V449C/V449C, V449C/GFP-V449C, and GFP-V449C/GFP-V449C (**Figure 11B**). If the subunits were crosslinked to an unknown protein, we would expect to see two crosslinked species, one between V449C and the unknown protein, and the other between GFP-V449C and the unknown protein. Thus, CuPh catalyzes V449C crosslinks between two transporter subunits.

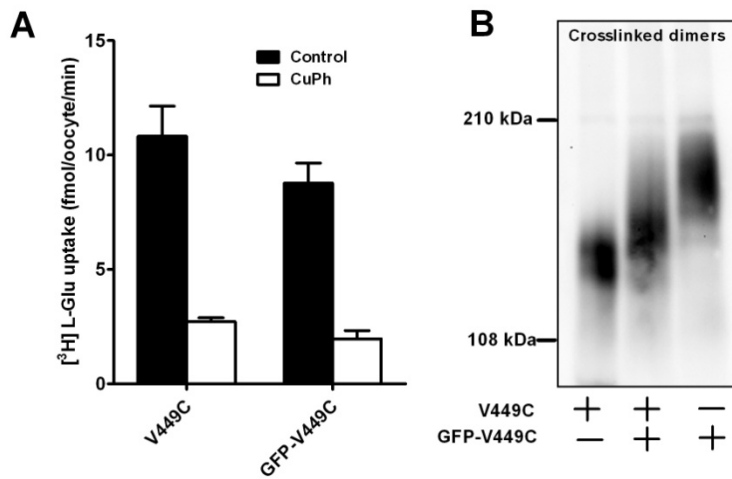


Figure 11. CuPh-catalyzed V449C crosslinks take place between two transporter subunits

(A) Oocytes expressing V449C or GFP-V449C were treated with 300 μM CuPh for 5 min. Uptake assays were performed for 15 min at room temperature using 5 μM L-[³H] glutamate as substrate. (B) V449C, GFP-

V449C or a 1:1 ratio of V449C/GFP-V449C mixture were expressed in oocytes. After treatment with 1 mM M8M for 5 min, oocyte membrane samples were collected and subjected to western blotting analyses using an EAAT1-specific antibody.

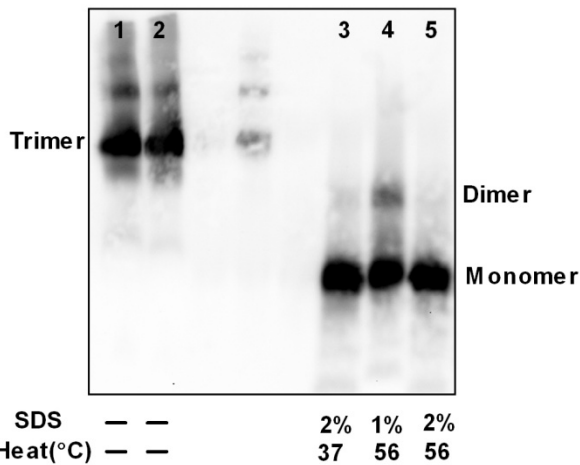


Figure 12. human EAAT1 forms trimers

CSLS glutamate transporters were expressed in *Xenopus* oocytes. Oocyte membranes were collected for blue native polyacrylamide gel electrophoresis (BN-PAGE) analyses (left two lanes). The native samples were further treated with SDS and heat as indicated to dissociate the oligomer structure (right

three lanes). The western blotting was probed with a C-terminally-directed EAAT1-specific antibody.

The Glt_{Ph} structure is comprised of three identical subunits and the trimeric stoichiometry has also been suggested for both bacterial (Glt_{T_{Bc}}, Glt_{T_{Bs}} and Glt_{P_{Ec}}) and mammalian (GLT-1 and EAAC1) glutamate transporters (55-57). The subunit stoichiometry of human EAAT1 has not been explored, although its homologous subtype in rat (GLAST) forms either dimers or trimers (54). Thus it is possible that the CuPh-catalyzed disulfide bonds observed in our study might form between two protomers of adjacent transporter multimers. Previous studies using freeze-fracture, immuno-gold labeling and electron microscopy have shown that glutamate transporters concentrate in ~200 nm protein-rich islands in the plasma membrane (106), suggesting that transporters can be very close spatially. To determine if crosslinks take place within a single transporter multimer or between adjacent multimers, we used blue native polyacrylamide gel electrophoresis (BN-PAGE) analysis, which permits gel electrophoresis under non-denaturing conditions and thus the determination of the oligomeric structure of proteins.

Similar to what has been reported for human EAAT2 (57), the CSLS transporter expressed in *Xenopus* oocytes migrates predominantly as a single band in blue native polyacrylamide gels. When the protein samples were incubated at 56 °C for 1 hour in the presence of 1% SDS, two bands at lower molecular weight appear, corresponding to the dimer and monomer forms of the transporter. Increasing SDS concentration to 2% completely dissociates transporters to monomer form (**Figure 12**). These data suggest that human EAAT1 exists in the plasma membrane as trimers. Thus, if crosslinks occur between adjacent transporter multimers, single cysteine-substitution mutants would form at minimum, a hexameric structure after CuPh treatment.

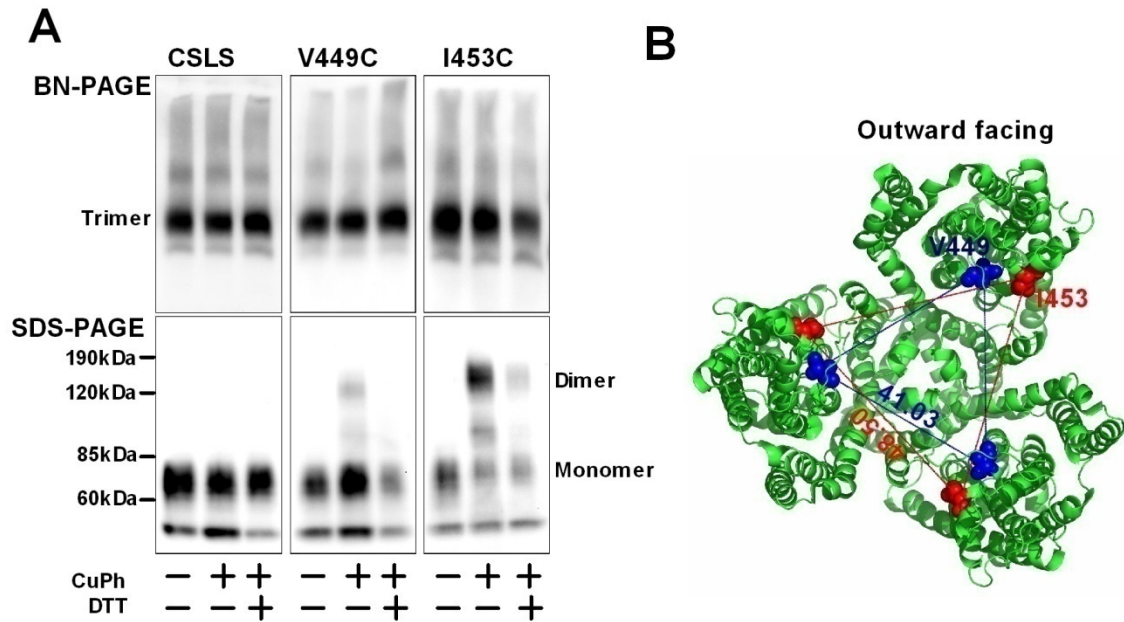


Figure 13. CuPh induced crosslinks occur within the trimeric structure

CSLS and mutant transporters were expressed in *Xenopus* oocytes. Oocytes were treated with 300 μ M CuPh, or 300 μ M CuPh followed by DTT, for 5 min. Oocyte membranes were collected for BN-PAGE analysis (**A**) and The native samples were further incubated at 56 $^{\circ}$ C for 1 hour in the presence of 2% SDS, which completely disrupted trimeric CSLS transporters to monomers. Glutamate transporter proteins were identified using an anti-hEAAT1 polyclonal antibody directed against the C-terminus. (**B**) Estimated distances (in \AA) between the three V449 residues, and the three I453 residues in an EAAT1 trimer, a model based on the crystal structure of Glt_{ph} in the outward-facing state (PDB ID: 1XFH). The transporter is viewed from the extracellular region. Glt_{ph} counterparts of V449 and I453 are I361 and M365, respectively.

The mutants V449C and I453C display trimer species of similar intensity before and after treatment with 300 μ M CuPh and no higher molecular weight crosslinked species observed when analyzed by BN-PAGE (**Figure 13A**). We further dissociated the native samples by incubating them at 56 °C for 1 hour in the presence of 2% SDS, which completely disrupted trimeric CSLS transporters to monomers when separated in SDS gels. We found that V449C and I453C with CuPh treatment display dimer bands in addition to their monomer forms (**Figure 13A**), suggesting that the trimeric species obtained by blue native gel analysis after CuPh treatment in the mutants V449C and I453C is comprised of two covalently linked subunits and one uncrosslinked subunit. V449C and I453C thus form disulfide bridges within their trimeric structures after CuPh treatment.

In the absence of substrate, glutamate transporters spend the majority of time in the outward-facing orientation, waiting to clear extracellular glutamate. Interestingly, the C α atoms of the intersubunit disulfide bridge forming residues, V449C and I453C, are separated in the equilibrium structure by more than 40 Å based on the outward-facing crystal structure of Glt_{Ph} (PDB ID: 1XFH, **Figure 13B**). In order to form a CuPh-catalyzed disulfide bond, the α -carbons of the two cysteines would need to be within 7 Å of each other (107) and this distance would need to be even shorter (within 5 Å) to form spontaneous crosslinks (108). The observed formation of intersubunit disulfide bridges suggests that large conformational transitions must take place to bring the HP2b helices of two subunits together and enable covalent bonding between cysteines of different subunits. To gain insight into the mechanism that allows these residues to interact, we examined the dynamics of the transporter at multiple scales using computational simulations based on the available crystal structures of Glt_{Ph}. Although Glt_{Ph}

shares only ~25% sequence identity with human EAAT1 (**Figure 14**), its structural features and trimeric organization agree with many aspects of the models originally proposed based on biochemical assays (109). Thus, Glt_{ph} provides a framework for investigating the structural changes associated with carrier functions.

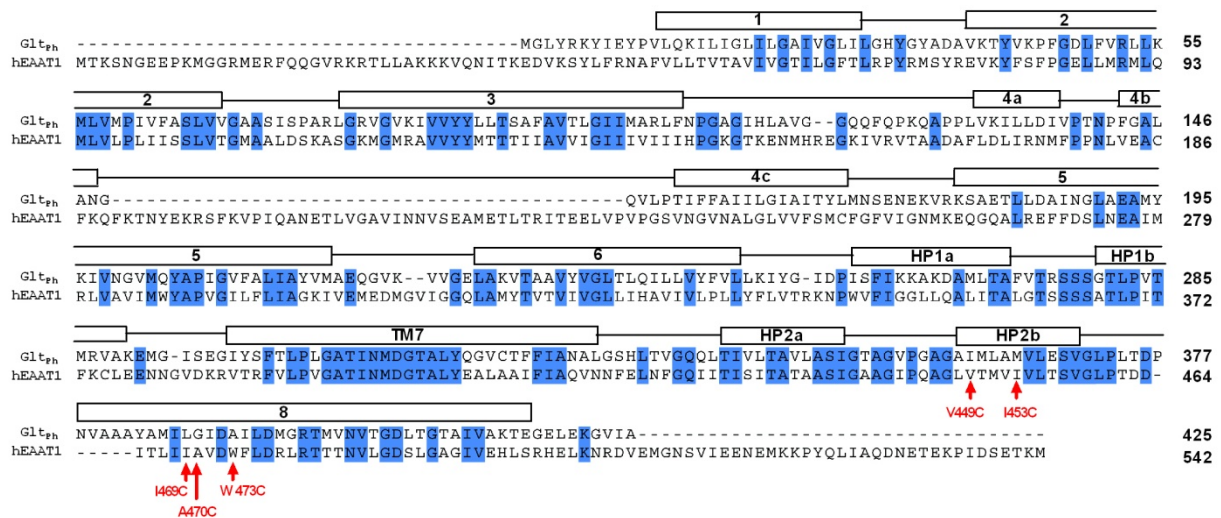


Figure 14. Sequence alignment of Glt_{ph} and human EAAT1

Boxes above the alignment correspond to transmembrane domains and sequences highlighted in blue are regions of exact identity between the two carriers. The mutants used for experiments in part 2 of this dissertation are indicated with red arrows (V449C and I453C in HP2 region, and the mutants I469C, A470C and W473C in TM8). The alignment was made using ClustalW and adjusted manually. Sequences used in the alignment are *P. horikoshii* Glt_{ph} (pubmed access number: NP_143181) and human EAAT1 (P43003).

2.2.5 Molecular dynamics (MD) simulations show spontaneous opening of the HP2 loop

We first explored the dynamic motions of glutamate transporters using molecular dynamics simulations. This computational method calculates the time dependent behavior of a molecular system and can provide detailed information on the fluctuations and conformational changes of proteins (110). The simulations were performed for 40 ns using the outward-facing structure of Glt_{ph} (PDB ID: 1XFH) embedded in a lipid bilayer as the initial conformation. The most striking motion observed in the simulation is the large amplitude fluctuations of the HP2 loop moving away from the substrate binding site toward the aqueous basin (**Figure 15A**). This type of motion is evidenced by the change in the distance between residues S278 and G354 at the tips of the respective helical hairpins HP1 and HP2 (**Figure 15B**). When HP2 is closed and shields the substrate binding site, the distance between the hydrogen bond-forming backbone nitrogen and oxygen on the respective residues G354 and S278 is ~ 1.9 Å in all three subunits. The distance is increased by more than 9 Å in subunit A (black curve in **Figure 15C**) succeeding the reconfiguration of the HP2 loop. The HP2 loop in subunit B (red curve) exhibits a displacement of about 7 Å at 17 ns, whereas that in subunit C (green curve) remains closed throughout the entire duration of the MD simulations (**Figure 15C**). Once the original tight packing of the two hairpins is disrupted, the HP2 loop tends to remain open and disordered as indicated by the large fluctuations in the HP1-HP2 distance for both subunits A and B. The opening of HP2 loop exposes the substrate binding site to the aqueous basin, suggesting that HP2 serves as the external gate.

In light of our crosslinking results, we examined the MD trajectories to determine the time evolution of the C α distance between the same residues of adjacent subunits that have shown to form intersubunit crosslinks. We found that the C α atoms of residue I361 (equivalent to

V449 in human EAAT1, **Figure 14**) between two subunits reach a minimum of $\sim 30\text{\AA}$, a distance too far to allow for disulfide bond formation. Larger movements, which are outside the range of MD simulations, are required to explain the data. Thus, we turned to anisotropic network model (ANM) analysis (111-112) to investigate the collective dynamics of Glt_{Ph}.

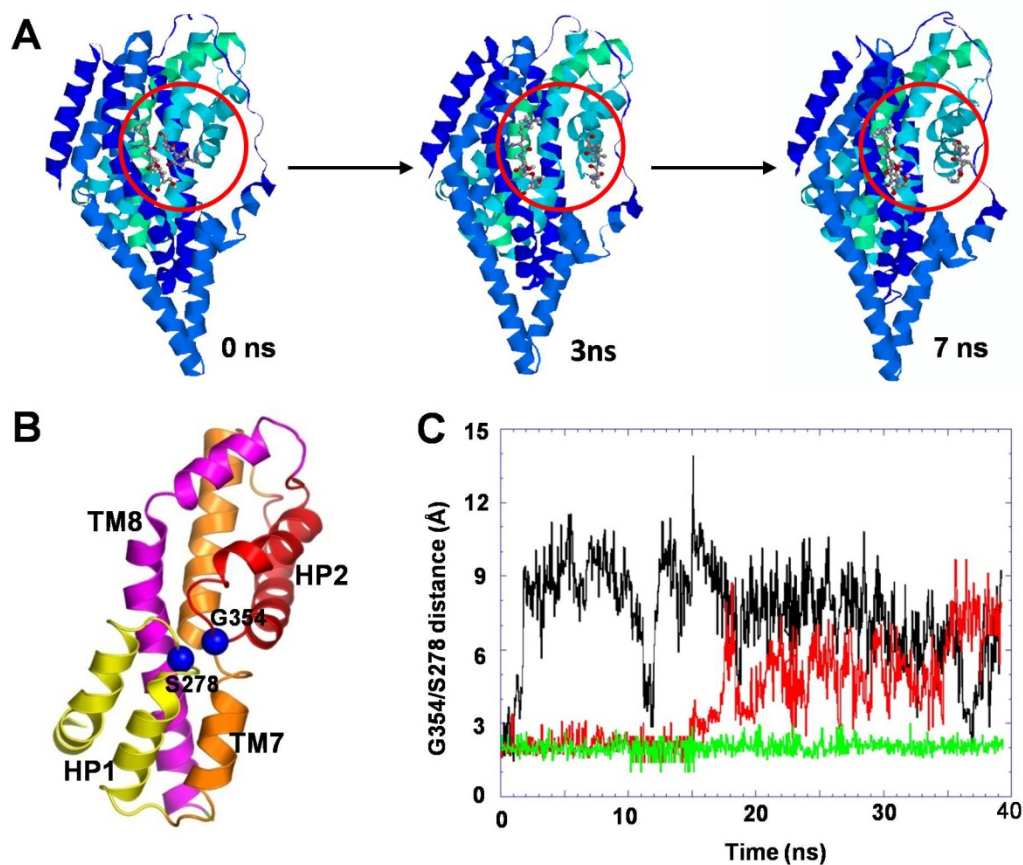


Figure 15. Molecular dynamics (MD) simulations show spontaneous opening of the HP2 loop

Simulations were performed for 40 ns using the outward-facing structure of GltPh (PDB ID: 1XFH) embedded in a lipid bilayer as the initial conformation. **(A)** Three snapshots at $t = 0, 3,$ and 7 ns of simulations display an increase in the separation between the helical hairpins HP1 and HP2 (see circled region). **(B)** Positions of residue S278 and G354 at the tips of the respective helical hairpins HP1 and HP2. The two residues are highlighted as blue spheres. **(C)** Time evolution of the distance between hydrogen bond-forming backbone S278(N) and G354(O), observed in subunit A (black), B (red), and C (green).

2.2.6 ANM analysis suggests that large collective motions of glutamate transporter trimers significantly alter intersubunit distances

ANM analysis explores collective fluctuations or so-called global motions that are intrinsically accessible to a given protein structure under physiological conditions. In this approach, the structure is modeled as a network of harmonic oscillators. The nodes of the network are identified by the C α atoms and the springs, usually taken to be uniform (identical force constants), account for inter-residue interactions. The collective dynamics of such a network is uniquely defined by the network topology, and resolved by a normal mode analysis into $3N-6$ modes of motions (N is the total number of amino acids of the given protein). The top-ranking modes are characterized by low frequency/large amplitude movements that generally occur within a micro- to millisecond time range. These so-called the soft modes usually play a dominant role in defining the structural changes involved in the biological activity of the protein, as has been demonstrated for both water-soluble and membrane proteins (113-114) .

Three ANM global modes accessible to Glt_{ph} are distinguished by their high collectivity. The first two (modes 1 and 2) are degenerate, *i.e.*, they have the same frequency and complement each other. In these two modes, the extracellular domains of two subunits move towards each other, while those in the third move away from them, and *vice versa* (**Figure 16A**). The third (mode 3) is a non-degenerate mode that cooperatively induces a 3-fold symmetric opening/closing of the three subunits (**Figure 16C**). Residues at the bottom of the transporter, within the membrane, remain rigid in either mode. In view of their mechanistic features, we refer to these modes as asymmetric stretching/contraction (mode 1 and 2), and symmetric opening/closing (mode 3).

In principle, a multitude of modes simultaneously drive the dynamics of the carrier to bring HP2 domains together, with the softest modes, including the two shown here, providing the largest contributions. We examined the potential change in intersubunit distances at the region of interest as the molecule would gradually move along the asymmetric stretching/contraction and the symmetric opening/closing modes. As shown in **Figure 16B** and **16D**, the central (bold, red) curves display the equilibrium distance between the two approaching subunits, used as reference for the residues listed along the abscissa, and the other curves display the distances sampled upon collective fluctuations of the trimeric structure along the respective mode. Residues on HP2b, and particularly those at the N-terminal end, tend to come into close proximity, whereas those at the C-terminal end remain well-separated, consistent with experimental data in **Figure 8**.

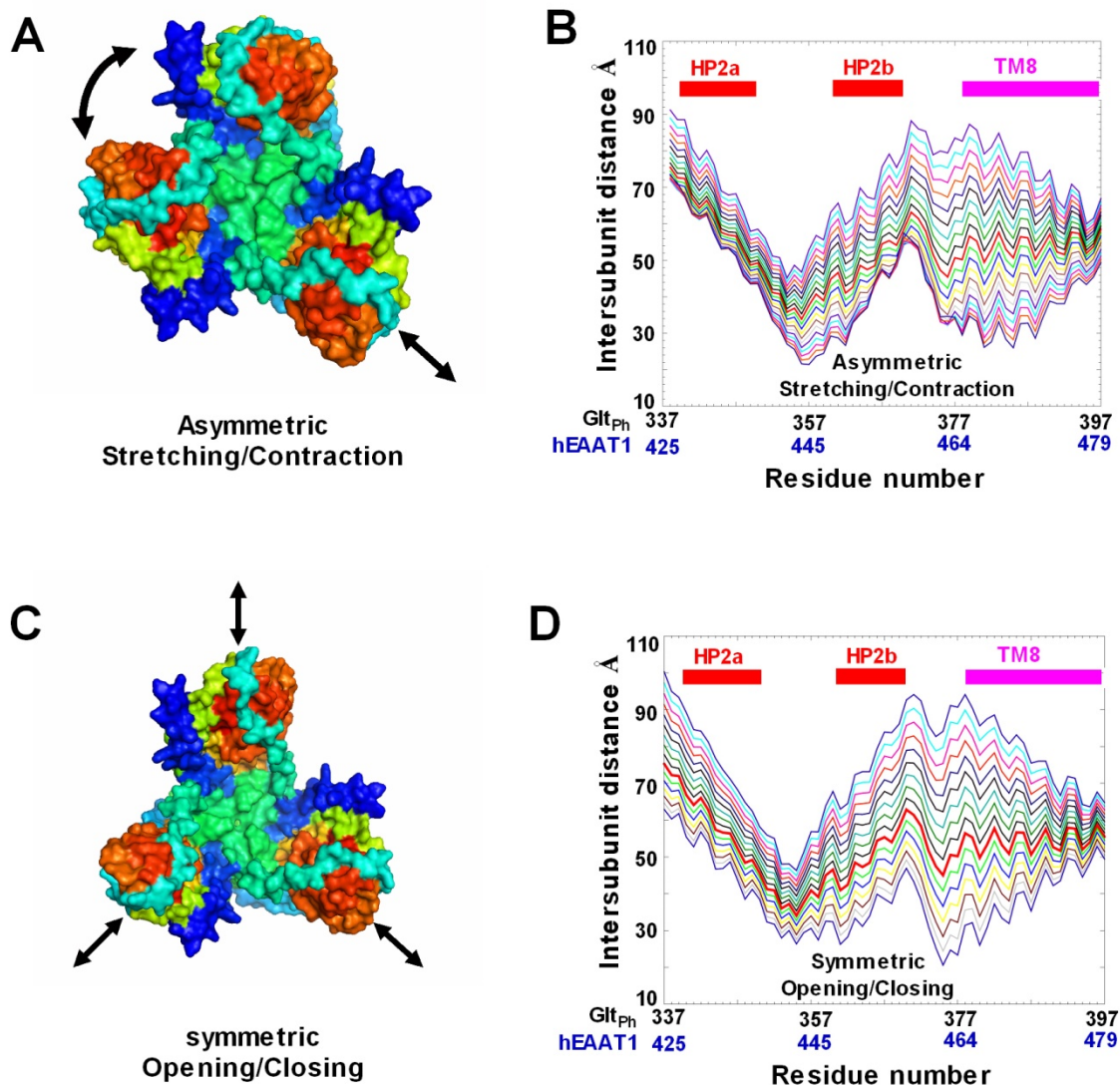


Figure 16. Large collective motions of glutamate transporter trimers predicted by ANM analysis

(A) and (C) show schematic representations of the asymmetric stretching/contraction mode and the symmetric opening/closing mode, respectively, viewed from the EC face. The arrows indicate the direction of motions of the three subunits. Intersubunit distances of residues in HP2 and TM8 (based on Glt_{Ph} C_α atoms between two approaching subunits) are significantly altered along the asymmetric stretching/contraction mode (B) and the symmetric opening/closing mode (D). The thick red curve refers to the equilibrium distances derived from the X-ray structure (PDB ID: 1XFH), and the series of curves above and below refer to different extents of deformation along the respective softest mode in positive and negative directions. Human EAAT1 residue numbers are denoted in blue, below the abscissa.

2.2.7 Crosslinking cysteine substituted mutants of several residues at the N-terminal end of TM8

Interestingly, the analysis of global motions suggests that residues at the N-terminal end of TM8 and at the loop connecting TM8 and HP2b also come into close proximity (**Figure 16B and 16D**). Inspired by this observation, we substituted cysteines for several additional residues at the N-terminal end of TM8 and examined the effects of CuPh and/or DTT on transport activity. **Figure 17A** shows the uptake activity for TM8 mutants I469C, A470C and W473C. Consistent with the residue proximities predicted by ANM analysis, the transport activity of these mutants is significantly impaired by 5 min incubation with 300 μM CuPh, and this inhibition can be reversed by DTT. The second order rate constants of crosslinking for I469C, A470C and W473C are $6,375 \pm 1,344 \text{ M}^{-1}\text{s}^{-1}$, $372 \pm 116 \text{ M}^{-1}\text{s}^{-1}$, and $5,882 \pm 2,094 \text{ M}^{-1}\text{s}^{-1}$, respectively (**Figure 17B**). Furthermore, I469C and W473C form spontaneous disulfide bonds, because DTT significantly increases their uptake activity compared to untreated controls. We also observed dimer band signals in I469C and W473C after treatment with the bifunctional crosslinker M8M (**Figure 17C**). These data confirm and reinforce the idea that large collective motions of glutamate transporters, consistent with the softest modes predicted by ANM analysis, underlie the unexpected proximities of residues within the trimer.

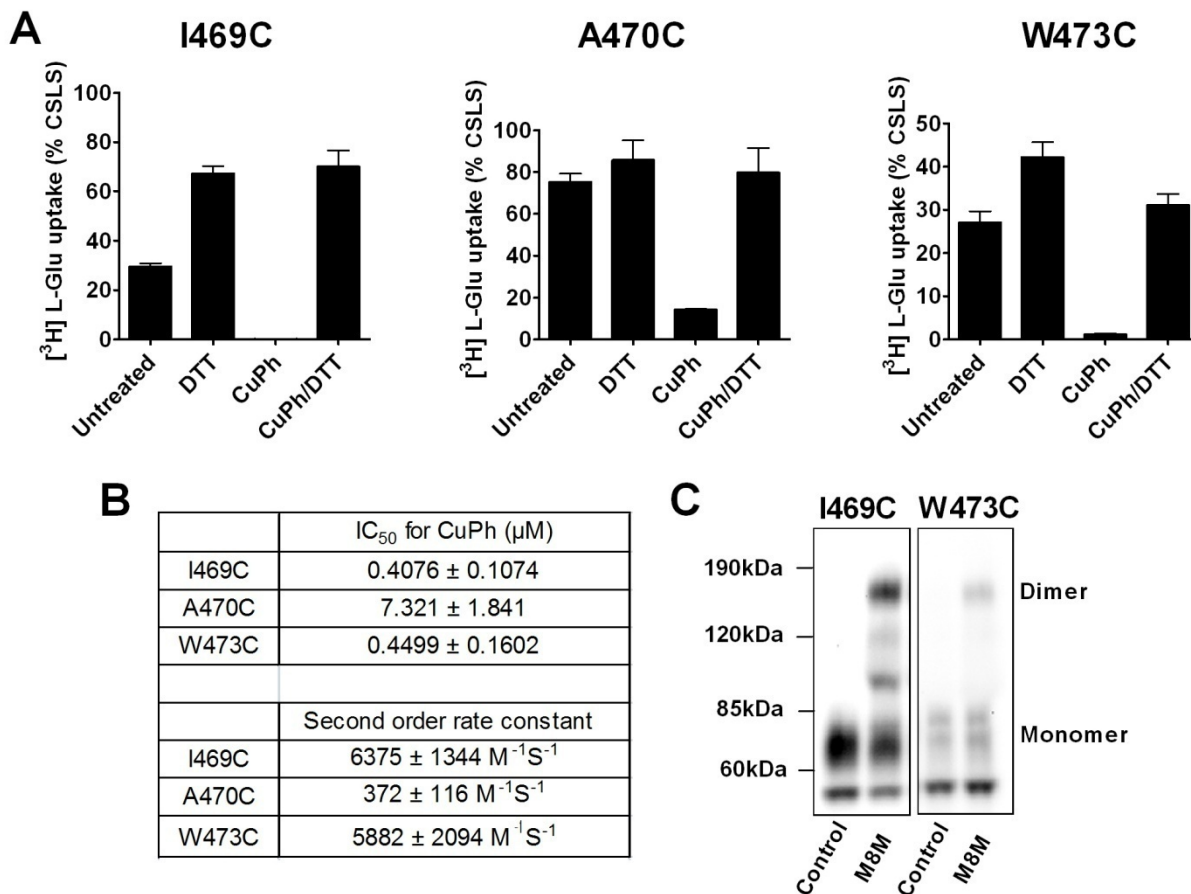


Figure 17. Crosslinking cysteine substituted mutants of several residues at the N-terminal end of TM8

(A) COS7 cells expressing wild type or mutant transporters were treated with 20 mM DTT, or 300 μM CuPh, or 300 μM CuPh followed by DTT, for 5 min. Uptake assays were performed for 10 min at room temperature using 5 μM L-[³H] glutamate as substrate. Data are expressed as the percent of uptake activity relative to the CSLS control obtained in 2-4 different experiments in triplicate. (B) COS7 cells expressing V449C were treated with different concentrations of CuPh for 5 min and uptake activity was measured. IC₅₀ was obtained by fitting data with the Michaelis-menten equation and the second order rate constants were also calculated. (C) Oocytes expressing I469C or W473C were treated with 1 mM M8M for 5 min. Oocyte membrane samples were collected and subjected to western blotting analyses using an EAAT1-specific antibody.

2.2.8 Residue V449C in the uncrosslinked subunit is inaccessible for modification after crosslinking

We further examined the functional significance of these large collective motions with regard to the transport cycle. A critical step after substrate and co-transported ions bind to the transporter is that the transport domain of each subunit moves inward into the cell cytosol, which allows for the exposure of the substrate-binding site to the cytoplasm and the release of substrate upon opening of the internal gate (50). We hypothesized that the large collective motions might be important for the transport domain movement. To test this hypothesis, we focused on the V449C mutant, which exhibits a high propensity to crosslink, and asked whether the transport domain in the uncrosslinked V449C subunit within the trimer is in an outward- or inward-facing state.

Earlier studies have shown that V449C can be modified from the extracellular environment in Na⁺-containing solution and modification of V449C completely inhibits substrate transport (96). In the inward-facing conformation of Glt_{Ph}, the equivalent residue of V449 moves toward the cytoplasm and is shielded by surrounding TM domains (**Figure 18A**). We therefore first determined whether the V449C cysteine in the uncrosslinked subunit is accessible to thiol-modifying reagents from the outside. We treated cells expressing V449C with 300 μM CuPh to completely crosslink two subunits, and then attempted to react the V449C residue in the uncrosslinked subunit with NEM, an irreversible thiol-modifying reagent. As a control, PBS or a reversible thiol-modifying reagent, MTSET, was used in place of NEM. After treatment with modifying reagents, cells were further treated with 10 mM DTT to reduce disulfide bonds and remove reversible modifying groups. If NEM could modify V449C in the uncrosslinked subunit, then the uptake activity of the mutant treated with NEM could be reduced by as much as one third compared to the PBS or MTSET treated group, assuming that the three subunits operate

independently as has been proposed (56, 115). Our results showed that V449C-expressing cells treated with CuPh/NEM/DTT exhibit uptake activity comparable to those treated with CuPh/PBS/DTT or CuPh/MTSET/DTT (**Figure 18B**).

The above data suggest that either the V449C residue in the uncrosslinked subunit is inaccessible to NEM or modification in one subunit does not affect the function of the transporter trimer. To exclude the latter possibility, we used a biotin-conjugated thiol-modifying reagent (maleimide-PEO₂-biotin) to react with V449C in the uncrosslinked subunit and then allowed the transporter proteins to bind to avidin-conjugated agarose beads. As a control, V449C-expressing cells were treated with DTT to reduce spontaneously crosslinked cysteines. Although the control group could readily react with the biotin reagent and affinity purified, no significant amount of transporter proteins could be obtained in this manner from V449C-expressing cells treated with CuPh (**Figure 18C**). Thus, V449C in the uncrosslinked subunit cannot be accessed by NEM, indicating that the uncrosslinked subunit exists in an inward-facing conformation.

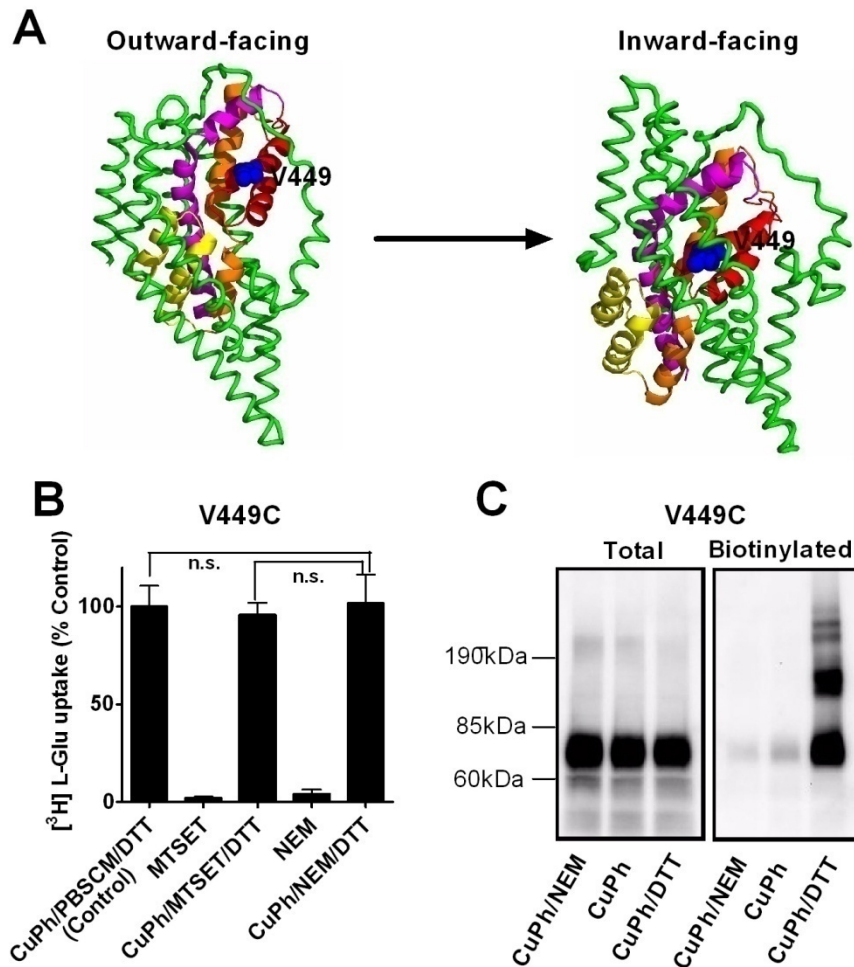


Figure 18. Residue V449C in the uncrosslinked subunit is inaccessible for modification after crosslinking

(A) Location of the equivalent V449 residue (human EAAT1 numbering) in the context of the outward-facing and inward-facing Glt_{ph} crystal structure (PDB ID: 1XFH and 3KBC). (B) COS7 cells expressing V449C were treated for 5 min sequentially with 300 μM CuPh, 1 mM MTSET, 0.5 mM NEM, or 10 mM DTT as indicated. Uptake assays were performed for 10 min at room temperature using 5 μM L-[³H] glutamate as substrate. Data are represented as the percentage of control in four experiments done in triplicate (n.s., not significant). (C) After indicated treatments, surface proteins were biotinylated with maleimide-PEO₂-biotin and subjected to western blotting analyses. Glutamate transporter proteins were identified using an anti-EAAT1 polyclonal antibody directed against the C-terminus.

2.2.9 Residue L376C in the uncrosslinked subunit is exposed intracellularly after crosslinking of V449C

The alternating access model predicts that distinct sets of residues are exposed to the intracellular environment depending upon whether the carrier faces inward or outward. An earlier study (92) reported that several cysteine substitutions in HP1, TM7, and TM8 of a rat glutamate transporter (GLT-1) display increased accessibility to NEM when external Na^+ was replaced by K^+ , a condition expected to increase the proportion of inward-facing transporters. We generated single cysteine mutations in CSLS background corresponding to the ones identified in GLT-1. As expected, the uptake activity of several mutants (A355C, T368C, L376C and V390C) was more significantly inhibited after treatment with NEM in a K^+ -containing solution compared to a Na^+ -containing solution (**Figure 19A**). Thus, these residues are exposed intracellularly as the transport domain moves toward the cytoplasm, which agrees with their positions in the outward-facing and inward-facing Glt_{Ph} structures (**Figure 19B**).

To determine whether the uncrosslinked subunit in the V449C mutant is inwardly oriented, we introduced these cysteine substitutions into the V449C mutant and asked whether these conformationally-sensitive residues in the uncrosslinked subunit were accessible intracellularly after V449C crosslinking. Cells were treated with 10 mM DTT to reduce spontaneous V449C crosslinks, followed by incubation with 300 μM CuPh. As a control, the membrane impermeant thiol-modifying reagent, MTSET, was used to protect V449C from further modification, and lock transporters in an outward-facing conformation (96). Cells were then incubated with the membrane permeant thiol-modifying reagent, NEM. Finally, CuPh-induced disulfide bonds and MTSET modifications were reversed with 10 mM DTT. We found that substrate transport by V449C_L376C is significantly inhibited after sequentially treated with

DTT/CuPh/NEM/DTT compared to that treated with DTT/MTSET/NEM/DTT. By contrast, other double mutants (V449_A355C, V449C_T368C, and V449C_V390C) show no differences in substrate transport between these two treatments (**Figure 19C**). We also used a membrane permeable biotin-conjugated thiol-modifying reagent (maleimide-biotin) to react with the cysteines in uncrosslinked subunits and then allowed the transporters to bind to avidin-conjugated agarose beads. Significant amounts of V449C_L376 are affinity-purified after crosslinking, but not the mutant carrier V449C_T368C (**Figure 19D**). Interestingly, L376C is most proximal to the cytoplasm among the residues tested, and would be the first exposed to the IC environment as the transport domain moves down (**Figure 19B**). These data confirm that the transport domain in the uncrosslinked subunit is inwardly oriented when the two remaining subunits are crosslinked extracellularly.

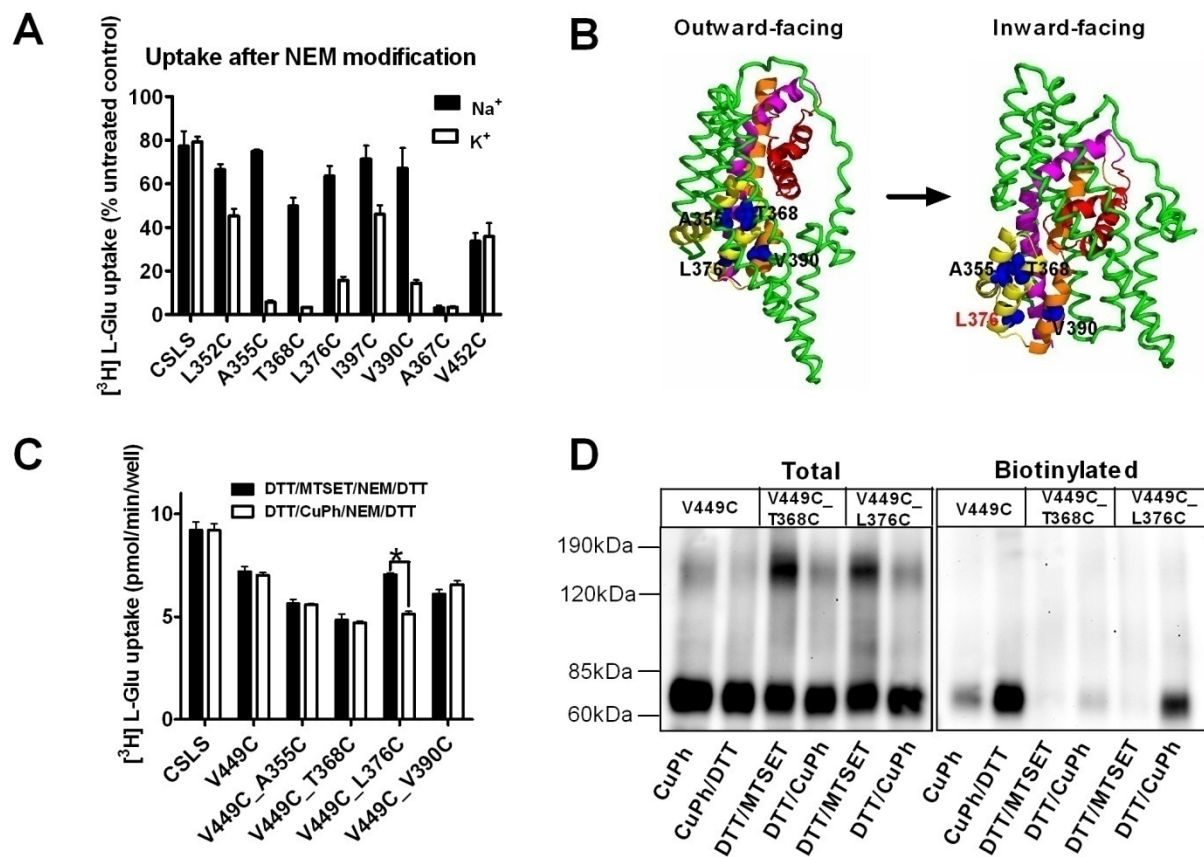


Figure 19. Residue L376C in the uncrosslinked subunit is exposed intracellularly after crosslinking of V449C

(A) COS7 cells expressing wild type or mutant transporters were treated with 0.25 mM NEM, except for the mutant L352C where 1 mM NEM was used, for 5 min in Na⁺- or K⁺-containing solution. Uptake assays were carried out for 10 min at room temperature using 5 μ M L-[³H] glutamate as substrate. The remaining uptake activity was presented after normalizing to untreated controls in respective cation condition. (B) Location of the equivalent residues (A355, T368, L376 and V390, human EAAT1 numbering) in the context of the outward-facing and inward-facing Glt_{ph} crystal structure (PDB ID: 1XFH and 3KBC). (C) COS7 cells expressing wild type or mutant transporters were treated with 10 mM DTT, 1 mM MTSET, 0.5 mM NEM or 300 μ M CuPh for 5 min as indicated before assaying for transport activity (*, p<0.05). (D) After indicated treatments, surface proteins were biotinylated with maleimide-biotin and subjected to western blotting analyses. Glutamate transporter proteins were identified using an anti-EAAT1 polyclonal antibody directed against the C-terminus.

2.2.10 Glutamate transporters favor stepwise transitions between outward-facing and inward-facing states

The above experimental data suggest that the glutamate transporter trimer transits through a state where two subunits are outward-facing and approach each other while the third moves inward. However, the available crystal structures of Glt_{ph} show that all three subunits assume the same conformation, facing either outward or inward (PDB ID: 1XFH and 3KBC). Whether the conformation state we observed is an on-pathway structure towards achieving the fully-inward conformation or a consequence of intersubunit crosslinks, is not known. In other words, whether glutamate transporters tend to undergo an all-or-none transition (of all three subunits) between inward-facing and outward-facing states or a stepwise transition, to enable alternating access, is yet to be understood.

To address this question, we examined the distribution of ANM modes that contribute to the structural transition between different states. Many studies have compared the structural change between two structurally resolved forms (*e.g.*, open and closed states) of a given protein, with the soft modes predicted by ANM analysis for one of the conformers (116). The difference between any pair of structures is quantitatively described by a $3N$ -dimensional deformation vector \mathbf{d} , evaluated by overlaying the two structures to remove rigid-body translations and rotations. The deformation vector \mathbf{d} is then compared with the eigenvectors of individual predicted ANM modes and the correlation cosines squared represents the contribution of each ANM modes to the overall structural change between two endpoints. In principle, because the eigenvectors form a complete orthonormal basis set, the correlation cosines squared sum up to unity 1. The summation (cumulative overlap) is performed over the subset of modes of interest, usually starting from the lowest-lying modes. These studies show that a very small subset of soft

modes (if not the top 1–3) yields a cumulative overlap of 0.80 ± 0.15 with experimentally observed structural changes (117). Cumulative overlap also provides a means to compare the ease of different transitions because soft modes are by definition the most energetically favorable modes, and undertaking a structural change along softer modes is more likely than another which involves higher-frequency (or stiffer) modes.

We consider four possible states of Glt_{ph} , with the numbers of outward/inward-facing subunits being 3/0, 2/1, 1/2 and 0/3, as illustrated in **Figure 20A**. The states 3/0 and 0/3 are the experimentally resolved 3-fold symmetric structures, and 2/1 and 1/2 are models reconstructed by assembling the outward-facing and inward-facing subunits upon superimposition of their trimerization domains. **Figure 20B** provides a schematic view of possible transitions between these states. The left vertical path (designated as **4** and **4'** for the clockwise and counterclockwise steps, respectively) refers to an all-or-none transition, and the other three steps (**1-3** and **1'-3'**) refer to the stepwise transitions, between the two experimentally known structures. We examined cumulative overlaps between ANM-predicted low frequency modes and the structural change at each step (**Figure 20C and 20D**). Panel C compares the all-or-none transition from the outward-facing state to the inward-facing state (blue curve) to the stepwise transitions in the same direction (red, green and black curves). Each of the three transitions that involve intermediate states is achieved by fewer number of low frequency modes (*i.e.* energetically more favorable) and is thus 'easier' than the all-or-none transition. A similar pattern is observed for the reverse transition as well (**Figure 20D**). These results support the notion that the conformation state we observed is a physically viable step towards achieving the fully-inward conformation.

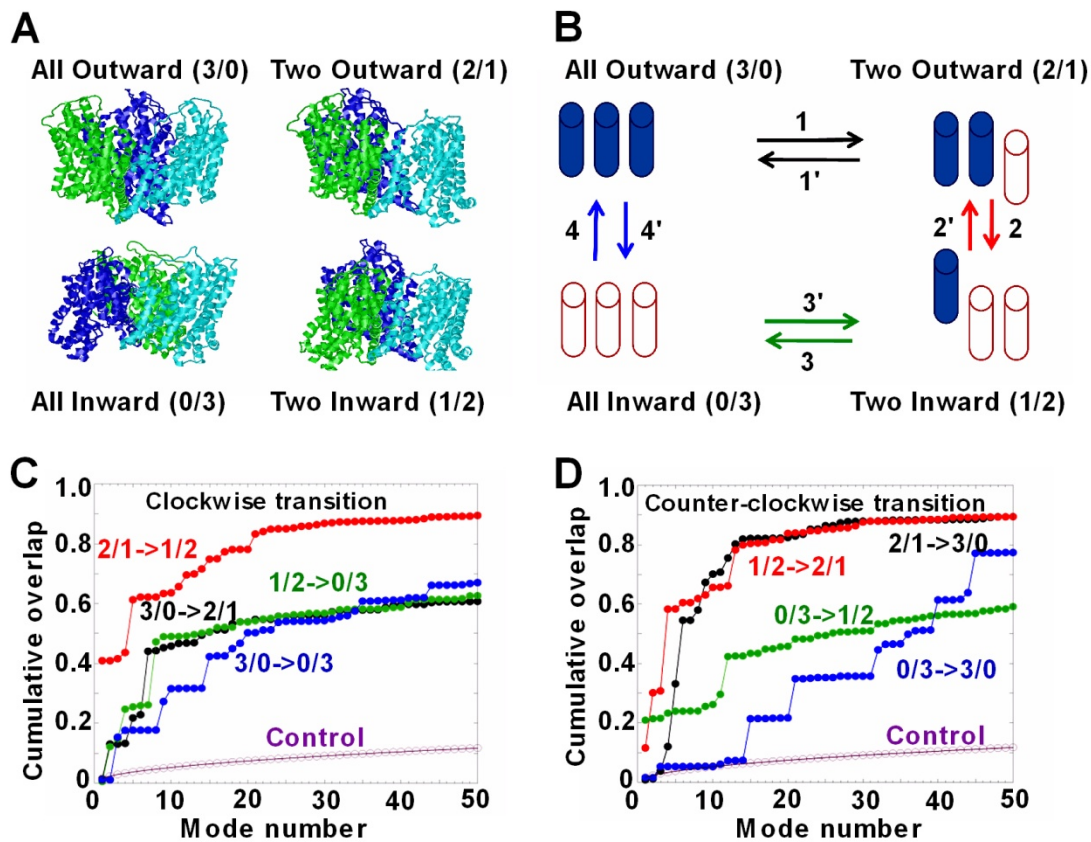


Figure 20. Cumulative overlap of ANM modes and transitions between pairs of conformations

(A) Cartoon representation of the four structures used for transport domain transitions. The All Outward (3/0) and the All Inward (0/3) conformations represent the 1XFH and 3KBC structures, respectively. In the Two Outward structure (2/1), one subunit faces inward (cyan), while in the Two Inward structure (1/2), two subunits face inward (green and cyan). (B) A schematic representation of the passages between different conformations. (C) and (D) Cumulative overlap of the ANM modes with the deformation vector between pairs of conformations indicated by the labels on the paths. The control curves refer to the case of randomly oriented modes that contribute equally to conformational transitions.

2.2.11 Impact of crosslinking on the substrate-gated anion flux

In addition to transporting substrates, which generate two positive charges into the cell per transport cycle, glutamate transporters also function as a substrate-activated anion channel. Thus, glutamate elicited currents are comprised of a substrate-coupled component that dominates at membrane potential of -100 mV, and a substrate-activated uncoupled anion component that dominates at +60 mV. To examine the impact of crosslinking on the anion channel activity, we focused on V449C, which displays minimal transport activity after crosslinking in oocytes, thus no substrate-coupled currents. In Cl⁻ containing solution, the control CSLS transporter exhibits similar glutamate-elicited currents before and after CuPh treatment. When the mutant carrier V449C was treated with 300 μM CuPh, substrate-elicited currents at -100 mV are significantly decreased and the currents reverse near the oocyte chloride reversal potential. Further incubation with 20 mM DTT increases the amplitude of currents at -100 mV induced by glutamate and the reversal potential becomes more positive compared to the untreated control, as the spontaneous crosslinks are reduced (**Figure 21A**). We also substituted the more permeable anion NO₃⁻ for Cl⁻, and observed comparable glutamate-elicited NO₃⁻ currents in V449C-expressing oocytes after DTT or CuPh treatment (**Figure 21B**). These results suggest that, remarkably, glutamate can still activate the anion conductance even when two subunits are constrained by crosslinking, and substrate transport no longer occurs.

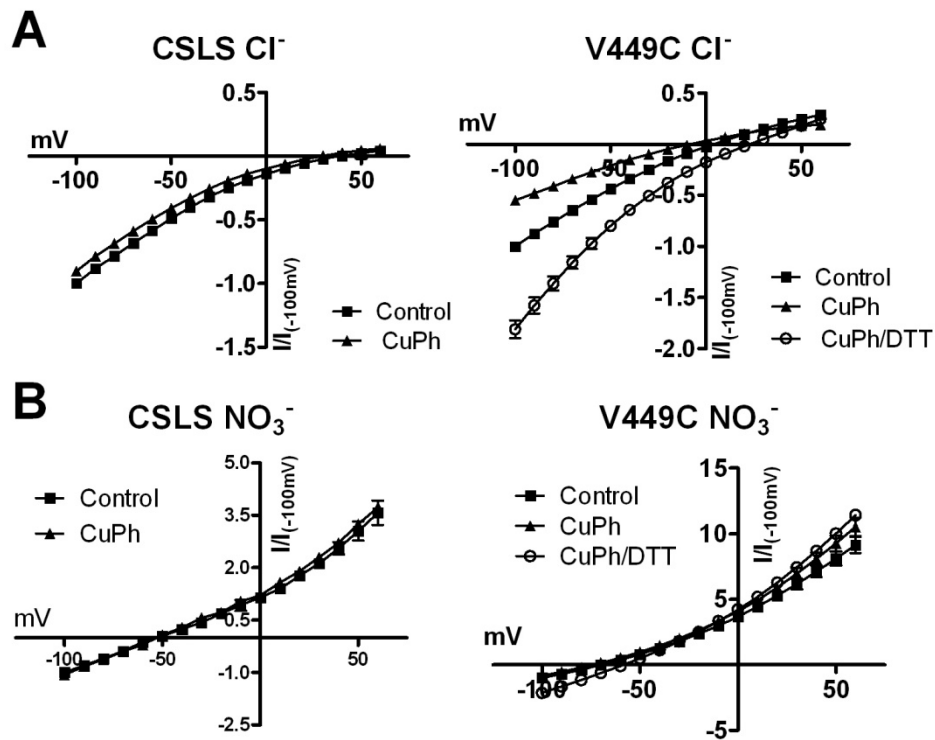


Figure 21. V449C retains substrate-activated anion conductance after crosslinking

Using a two electrode voltage clamp, currents from oocytes expressing CSLS or V449C were recorded in Cl^- -containing solution (**A**), and in a solution in which Cl^- was replaced by NO_3^- (**B**). Recordings were made before (filled square) and after (filled triangle) application of 300 μM CuPh (5 min), as well as after additional treatment with 20 mM DTT (5 min, open circle). Currents obtained in the absence of glutamate were subtracted from those elicited by 1 mM L-glutamate. Currents were normalized to the control currents at -100 mV.

2.3 DISCUSSION

The present study was driven by the observation that single cysteine substitutions for residues of HP2b in the human glutamate transporter EAAT1, form spontaneous and/or CuPh-catalyzed intersubunit crosslinks. Substrate translocation activity is abolished in the mutant transporters as a consequence of crosslinking, but the substrate-activated anion conductance associated with the carrier is retained. Evidence for the close proximity of two inter-subunit cysteines and their capacity to form disulfide bonds comes from the following observations: first, although the mutants V449C and I453C fractionate as monomers by non-reducing SDS-PAGE before CuPh treatment, they migrate as both monomers and dimers after CuPh treatment (**Figure 9**); second, the addition of the reducing reagent, DTT, reverses both the transport inhibition and the formation of crosslinked dimers (**Figure 6 and 9**); and third, the presence of cadmium ions in the uptake solution also inhibits the transport activity of V449C and I453C (**Figure 6**). This latter observation is consistent with the idea that the two cysteines are near each other to coordinate Cd^{2+} , although it should be noted that Cd^{2+} can bind to the thiol-group of a single cysteine residue. Previous studies have shown that modification of cysteine substituted residues in HP2b region by other thiol-modifying reagents such as MTSET significantly inhibits substrate transport (90). Thus, the inhibition of substrate transport by Cd^{2+} in the mutant carriers V449C and I453C could be a consequence of interaction between Cd^{2+} and single cysteines instead of the coordination of Cd^{2+} by two adjacent cysteines. At present, we are unable to rule out this possibility and the Cd^{2+} experiment can only be viewed as complementary evidence to support the proximity of substituted cysteines between two adjacent subunits.

We noticed that the mutant I453C shows a stronger dimer band signal compared to V449C, although transport by I453C is less dramatically inhibited after crosslinking (**Figure 9**).

This inconsistency would be explained by either the complete inhibition of substrate transport by CuPh in V449C is partially due to the oxidization of single cysteines, or alternatively, by the instability of disulfide bonds during the biochemical assays. It is suggested that CuPh treatment, under some cases, oxidizes cysteine residues to sulfinic and sulfonic acids (118). However, these high oxidation states of cysteine cannot be reduced by DTT and in our study, the functional inhibition of the cysteine substituted mutants is completely reversed by DTT (**Figure 8**). These results suggest that the complete inhibition of substrate transport in V449C is a result of CuPh-catalyzed disulfide bond formation. Additional experiments revealed that the V449C disulfide bonds are less stable during oocyte membrane preparation, because we observed a similar inhibition of uptake, but a substantially more prominent V449C dimer species using a bifunctional crosslinking reagent instead of CuPh (**Figure 10**).

We further excluded several other scenarios in which CuPh-catalyzed crosslinks might occur in single cysteine substituted glutamate transporters. First, we considered the possibility that disulfide bonds form between a transporter subunit and an unknown protein of similar molecular mass. Because mutant glutamate transporters are overexpressed in both the COS7 cell and *Xenopus* oocyte expression systems, the unknown protein would need to be a membrane protein expressed abundantly in both systems in order to crosslink one-to-one with transporter subunits, making this scenario less attractive. One way to experimentally exclude this possibility is to coexpress two different tagged mutant transporters (*e.g.* HA-V449C and myc-V449C) and see if antibody against one tag could pull down the other after crosslinking. This strategy is problematic because we and others have shown that glutamate transporters tend to aggregate during biochemical assays even without crosslinking (43, 77). Instead, we took advantage of size difference between the untagged V449C and an N-terminus GFP-tagged V449C. When

coexpressed, we observed crosslinked bands corresponding to three dimer species (V449C/V449C, V449C/GFP-V449C, and GFP-V449C/GFP-V449C). If crosslinking the subunits to an unknown protein, we would expect to see two crosslinked species, one between V449C and the unknown protein, and the other between GFP-V449C and the unknown protein (**Figure 11**). These results suggest that crosslinks in V449C take place between two transporter subunits. Second, we considered the possibility that disulfide bonds form between two transporter subunits of adjacent trimers. If this occurred, we would expect to see at least hexamer species (crosslinking of two transporter trimers) when separated by BN-PAGE, which preserves oligomeric structures of proteins. Our results showed that both V449C and I453C migrate as trimer species in blue native gels and no higher molecular weight bands are observed after CuPh treatment, suggesting that disulfide bonds form between two transporter subunit in a single trimer (**Figure 12**). These results further support that crosslinking does not occur between a transporter subunit and an unknown protein. In addition, we have successfully constructed a functional concatenated glutamate transporter trimer that physically links the three transporter subunits with flexible peptide linkers. This construct allows the introduction of either one or two V449C subunits in the trimer. We found that CuPh inhibits the uptake activity of the concatenated carrier when it contains two V449C subunits, but not when it contains only one V449C subunit (Data not shown, and see chapter 4 in this dissertation for concatemer information). Taken together, we concluded that several single cysteine substitutions for residues of HP2b form spontaneous or CuPh-induced disulfide bonds between two transporter subunits of a single trimer.

Based on the outward-facing crystal structure of the Glt_{ph} trimer, the distances between the crosslinkable residues of HP2b in adjacent subunits are significantly greater than that

required to form disulfide bonds, suggesting that domains within the glutamate transporter trimer are capable of large-scale movements in the absence of substrate. In collaboration with Dr. Ivet Bahar's group in the Department of Computational and Systems Biology at the University of Pittsburgh, we explored the dynamics of glutamate transporters using computational simulations. Our molecular dynamics (MD) simulations revealed that the HP2 loop possesses an intrinsic, structure-induced ability to 'open up' and expose the substrate binding site to the aqueous basin, thus acting as an extracellular gate (**Figure 15**). These results agree with the TBOA-bound crystal structure of Glt_{Ph}, which revealed the displacement of HP2 from the substrate binding site (49). However, detailed analysis of the MD trajectory suggest that such local motions fall short of bringing two HP2b helices sufficiently close to form crosslinks. ANM analysis, on the other hand, predicts two major types of large collective motions to be energetically more favorable: an asymmetric stretching/contraction and a symmetric opening/closing mode. Residues in the EC domains of adjacent subunits approach each other in either modes, and thus enable the formation of intersubunit disulfide bridges (**Figure 16**). By contrast, residues at the bottom of the transporter, within the membrane, remain rigid, in agreement with earlier findings (119). ANM calculations also suggest that residues at the N-terminal end of TM8 between two subunits tend to come into close proximity. This prediction was confirmed experimentally by crosslinking of single cysteine substituted mutants in this region (**Figure 17**). Our current study thus underscores the existence of large-scale, intrinsic movements of subunits in glutamate transporters shown experimentally and predicted computationally.

Because global motions of proteins are usually intrinsic and driven by their tertiary and quaternary structures, the presence of substrate is unlikely to disrupt such collective movements (120). Experiments to confirm this argument are complicated by the fact that substrate or

inhibitors may influence conformational changes other than large collective motions that also contribute to observed crosslinks. We noted that the ability of cysteine substituted mutants in HP2b to form disulfide bonds, parallels their modification rates by sulfhydryl-reactive reagents reported previously (90). In particular, mutants L448C, V449C, V452C and I453C exhibit fast rates of modification whereas M451C, V454C, L455C, T456C and V458C have much slower rates. Similarly, transporters with mutations near the HP2 loop, L448C, V449C, V452C, I453C, V454C, readily form crosslinks after CuPh treatment. Furthermore, the mutant carriers L448C and V449C form spontaneous crosslinks (**Figure 8**). These results suggest that local rearrangements of the HP2 region may also contribute to bringing residues in HP2b between two subunits into close proximity. Nevertheless, there is growing evidence for the functional relevance of the global movements predicted by coarse-grained network models in substrate-free forms (120-121). Although the crosslinking captured in the current study occurs in non-transporting carriers, the large collective motions that enable crosslinking will also take place and have functional impact in actively-transporting carriers. Supporting this idea, the inward movement of the transport domain, which was proposed based on crosslinking two introduced cysteines in TM2 and HP2, readily occurs in the absence of Na⁺ and substrate, and has been suggested to be a critical step of the transport cycle (50, 94).

In contrast to our report, Koch *et al.* proposed that small-scale molecular motions around the substrate binding site are sufficient to accomplish glutamate uptake in human glutamate transporters (93). Their findings can be easily reconciled with our observations. Koch *et al.* used FRET assays as a means to compare the relative positions of extracellularly exposed EAAT residue pairs in a choline-substituted solution in the absence of substrate (non-transporting state) to those in a Na⁺-containing solution with 1 mM glutamate (transporting state). No significant

changes in FRET efficiencies were observed between the two conditions. FRET assays determine the distance of residue pairs averaged from a population of proteins and over the experimental timeframe of signal acquisition when proteins undergo a broad range of conformational fluctuations. Because the large collective motions proposed in our study are likely to occur in both substrate-free and actively-translocating transporters, the average distances measured by FRET assays under the two conditions would be comparable.

In fact, such collective motions are essential to the transition of the transporter from outward-facing to inward-facing state and *vice versa*, during the completion of the transport cycle. After crosslinking of V449C, the uncrosslinked subunit assumes an inwardly-facing orientation, as evidenced by the inaccessibility of the V449C cysteine from the extracellular environment in the uncrosslinked subunit (**Figure 18**) and the exposure of the L376C cysteine to the cytoplasm (**Figure 19**). Thus, crosslinking captures a conformational state during the transport cycle in which two subunits of the trimer approach each other in the outward-facing state while the transport domain of the third subunit moves inward. These results suggest that the large changes in structure observed in our study can be functionally linked to the inward movement of the transport domain, a critical step for substrate transport.

ANM calculations confirm that a stepwise transition of individual transport domain is a more viable mechanism to enable alternating access of the transporter to the EC and IC regions, compared to an all-or-none transition of all three subunits. Several studies introduced mutations to alter the function of one or more subunits, determined their impact on overall function, and concluded that each subunit functions independently during substrate transport (56, 115, 122). Yet it is still debatable whether allosteric interactions modulate the anion channel function (115, 123). Although our results generally agree with the idea that each subunit can function

independently (the transport domain moves individually), the experiments presented here, which disrupt the collective motions of the trimer, reveal a higher order cooperative nature of subunit-subunit interactions. Such cooperativity would not be captured in earlier studies because the mutations used would have no effect on global motions. In chapter 4, we will further explore the subunit interactions of transport functions using a concatenated glutamate transporter trimer.

Finally, although the V449C mutant is unable to transport substrates after crosslinking, it retains substrate-elicited anion currents. Since the uncrosslinked subunit in V449C is restricted in an inward-oriented conformation and is likely not accessed by substrate, anions have to flow through the two crosslinked subunits. The apparent K_m for glutamate activation of the anion conductance is reduced after V449C crosslinking ($K_m = 8.35 \pm 1.02 \mu\text{M}$ for V449/CuPh vs. $K_m = 30.98 \pm 3.05 \mu\text{M}$ for V449C/DTT), consistent with the idea that HP2 remains open in the two crosslinked subunits. Similarly, Seal *et al.* showed that modification of V449C also abolishes substrate transport, but increases the substrate-gated anion conductance (96). It is currently debatable which step in the substrate transport cycle conducts anion currents, but our results support the idea of a conducting state at an early step of the transport cycle after substrate binding. Further studies will shed light on how the substrate transport is linked to the anion conduction (See chapter 3) and whether the alternating access mechanism is facilitated by visiting intermediate states with different conformations of the subunits (*i.e.* inward- and outward-facing).

3.0 A CONSERVED POSITIVE CHARGE IN TM7: A KEY PLAYER IN GLUTAMATE TRANSPORTER DUAL FUNCTIONS

3.1 INTRODUCTION

In Chapter 2, we showed that after crosslinking of V449C, substrate cannot be transported into the cell, but is still able to elicit anion currents. We suggested that the substrate-activated anion currents are generated by the two crosslinked subunits which have a more restricted capacity to undergo conformational changes. Thus, a conducting state occurs at an early step after substrate binds to the transporter and does not require substantial structural rearrangement. Supporting this idea, studies have shown that the substrate-activated anion currents can still occur at 4°C when substrate transport is abolished (29).

In addition to this anion conducting state activated by substrate at the early step(s) of the transport cycle, glutamate transporters allow anions to traverse the cell membrane in the absence of the substrate (33). This current requires extracellular Na^+ and is referred to as the Na^+ -activated anion leak current. Other anion conducting states during the transport cycle have also been suggested (124-125). Because of technical challenges to isolate individual steps of the transport cycle following glutamate binding, the assignment of the anion conducting states was achieved by chemical-kinetic simulations that model recorded transport and anion currents. In addition, by using fast application of glutamate to measure the pre-steady state of the transport

current and the anion current, these studies show that both pre-steady state currents rise quickly after glutamate application and decay to a steady state, suggesting that the substrate transport process is closely linked to the substrate-gated anion conductance (124, 126). However, despite gains in knowledge of transporter domains and conformational changes required for substrate transport, limited evidence exists to show how the anion channel is activated by Na^+ and substrate, and how anion channel activation and substrate transport are coordinated.

Establishing the anion permeation pathway will also facilitate our understanding of the anion channel function. It is suggested that anions permeate glutamate transporters through a pathway different from the substrate. As we have observed for the crosslinked V449C, three separate studies showed that modification of cysteine substituted residues in HP2 disrupts glutamate transport, but allows glutamate binding and activation of the anion channel (96-98). Mutants that abolish substrate-activated anion current without interfering with substrate transport have yet to be identified. Ryan *et al.* reported that mutations of several polar or charged residues in TM2 influence various properties of the anion channel, but not the transport of substrate (95). In particular, residue S103 in human EAAT1 is implicated in forming part of the selectivity filter of the anion channel, because glutamate-activated anion current in the mutant carrier S103V displays an altered rank order of relative permeability to different anions (95). In addition, one mutant, D112A in human EAAT1 has a greatly increased Na^+ -activated anion leak currents, but decreased substrate-activated anion currents. Residue D112 was proposed to serve as a gating residue for the channel (95).

Based on the crystal structure of Glt_{Ph} (PDB ID: 1XFH), we hypothesized that residues in TM7 might be involved in the anion channel function because TM7 is spatially very close to TM2, and is also a critical domain for binding Na^+ and substrate. While we were testing this

hypothesis, Huang *et al.* identified additional residues in TM7 and TM5 that are involved in mediating the leak and substrate-activated anion current (99). In this study, they investigated charged residues within 5Å from residues S103 and D112 in EAAT1 based on the Glt_{Ph} structure, which could influence the conformations of these two residues. Their results showed that residues D272 in TM5 and K384/R385 in TM7 display changed amplitudes of leak conductance and substrate-activated anion conductance when mutated to neutral or oppositely charged amino acids (99). Thus, TM2, 5 and 7 appear to contribute to the formation of the anion permeation pathway. It should be noted that both this study and one by Ryan *et al.* directly compare uptake activities and current amplitudes between wild type and mutant transporters, without considering the surface expression of individual carriers. Most of their data can also be attributed to the altered surface expression by the mutations. Thus, more rigorous characterization of these mutant carriers or identification of new mutants around this region may further elucidate the molecular determinants of the anion channel function.

In the present study, we identified a conserved residue, R388 in TM7 of human EAAT1 that is involved in both substrate transport and anion conduction. Neutralizing R388 with the amino acid alanine significantly impairs uptake activity compared to wild type transporters, and increases the Na⁺-activated anion leak current. Reversing the positive charge of R388 with either amino acid aspartate or glutamate results in accumulation of substrate through an electroneutral process. More interestingly, the mutant carriers R388D and R388E display no substrate-activated anion current. A similar phenotype is also observed in an equivalent mutant of rat EAAT4, rEAAT4 R410E. Detailed characterization of the mutant transporter R388D show that this carrier predominantly exists in the anion leak state, indicating the gating mechanism of substrate-activated anion current is disrupted. Finally, we demonstrate that the transport domain of the

mutant carrier R388D spends a longer time in the inward-facing orientation in the absence of substrate. These results not only suggest that R388 is an important element in the functional coupling between substrate transport and the anion channel activity, but also illuminate the role of the inward transport domain movement in anion permeation.

3.2 RESULTS

3.2.1 Residue R388 plays an important role in substrate transport

Residue R388 is highly conserved in mammalian glutamate transporters (**Figure 22A**) and is one helix turn away from residues K384 and R385 in TM7. To determine the importance of this residue in transporter functions, we first neutralized R388 by replacing arginine with a small non-polar amino acid, alanine, and assessed its transport activity relative to the wild type transporter. It should be noted that the initial EAAT1 mutations in this chapter were generated within a cysteineless version of the transporter because it enables the use of cysteine accessibility assays to probe the conformation of the transport domain (see section 3.2.6). Previous studies have shown that the activity of the CSLS carrier is very similar to the wild type EAAT1 (41), however, we have also reconfirmed critical observations using mutant carriers generated within the wild type EAAT1 background.

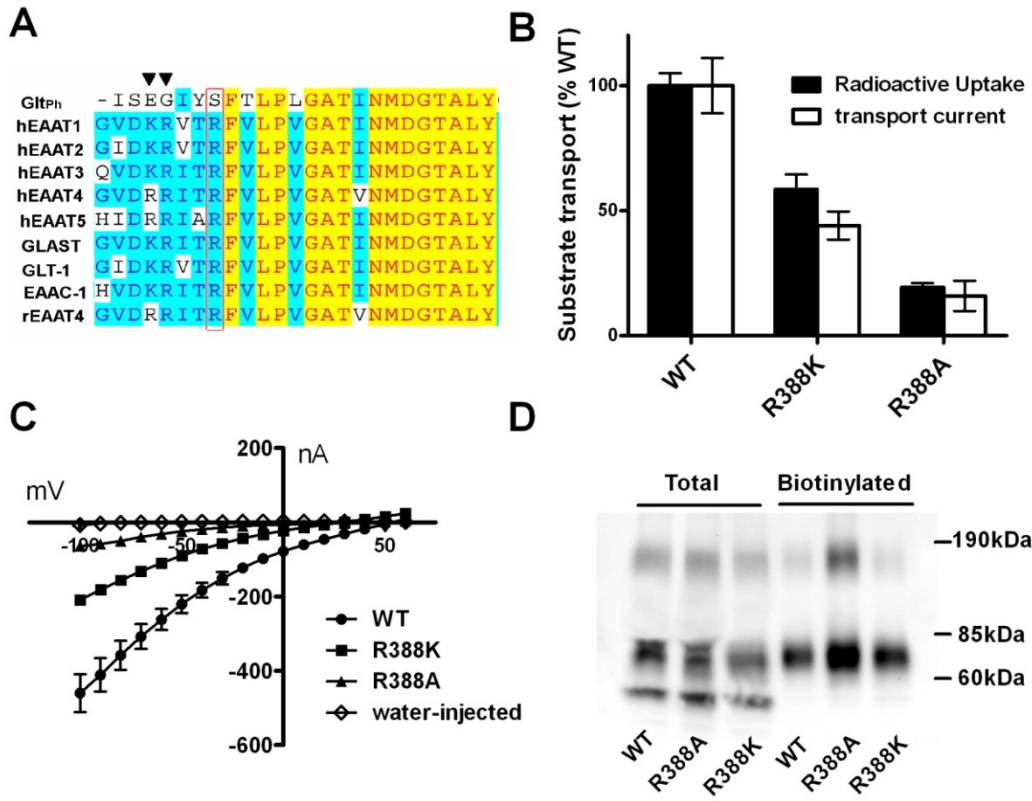


Figure 22. Neutralizing the charge of residue R388 with amino acid alanine impairs substrate transport

(A) Sequence alignment of the highly conserved TM7 region. R388 is highlighted with red box, and residues K384 and R385 are indicated with inverted triangles. (B) Wild type human EAAT1 transporters and mutant carriers (R388K or R388A) were expressed in *Xenopus* oocytes. Uptake assays were carried out at room temperature using 100 μ M L-[³H] glutamate as substrate for 15 min and data are normalized to wild type transporters. (C) I-V relation of 100 μ M L-glutamate elicited current recorded in Cl⁻ solution using two-electrode voltage clamp for oocytes expressing wild type transporters (filled circle), R388K (filled square), R388A (filled triangle) or water-injected oocytes (open diamond). (D) Representative surface biotinylation assays of oocytes expressing wild type and mutant transporters. Glutamate transporter proteins were identified using an anti-EAAT1 polyclonal antibody directed against the C-terminus.

Using radioactive glutamate uptake assays, we found that the transport activity of R388A is reduced to ~20% of the wild type transporters (**Figure 22B**). We also recorded substrate-elicited currents in Cl⁻ solution using two-electrode voltage clamp recordings (the current in the absence of substrate was subtracted from that in the presence of substrate). Because the influx of one glutamate molecule is associated with the inward movement of two positive charges and glutamate transporters also possess an anion channel function, the recorded current is comprised of substrate-coupled current and substrate-activated uncoupled anion current. At a membrane potential of -100 mV, the majority of current arises from the substrate-coupled transport current with its amplitude being proportional to the substrate transport activity. Consistent with the results obtained with uptake assays, application of 100 μM glutamate to the R388A mutant carrier generates a significantly decreased inward current at -100mV compared to wild type transporters (**Figure 22B and 22C**), although the voltage dependence of glutamate-elicited currents remains unchanged (**Figure 22C**). The decreased substrate transport activity of R388A cannot be explained by reduced surface expressions because cell surface biotinylation assays show that R388A has a comparable surface level as wild type transporters (**Figure 22D**).

The mutant carrier R388K, which conserves the positive charge, also shows a reduced substrate transport activity compared to the wild type EAAT1, but is less impaired than R388A (**Figure 22 B-D**). In contrast, when we replace arginine with the negatively charged amino acid aspartate or glutamate, the mutant carriers R388D and R388E accumulate 10%-15% radioactive substrates compared to the wild type EAAT1 (**Figure 23A**). R388D and R388E also express less at the cell surface, which may contribute to their reduced transport activity. To our surprise, even though these two mutant carriers accumulate substantial amounts of radioactive substrate, no substrate-coupled transport currents at -100 mV are observed (**Figure 23B**). These data suggest

that R388D and R388E uptake substrate through an electroneutral process. Thus, arginine at position 388 in human EAAT1 plays an important role in substrate transport. Mutating arginine to alanine significantly decreases substrate transport activity and reversing the positive charge with either aspartate or glutamate results in accumulation of substrate through an electroneutral process.

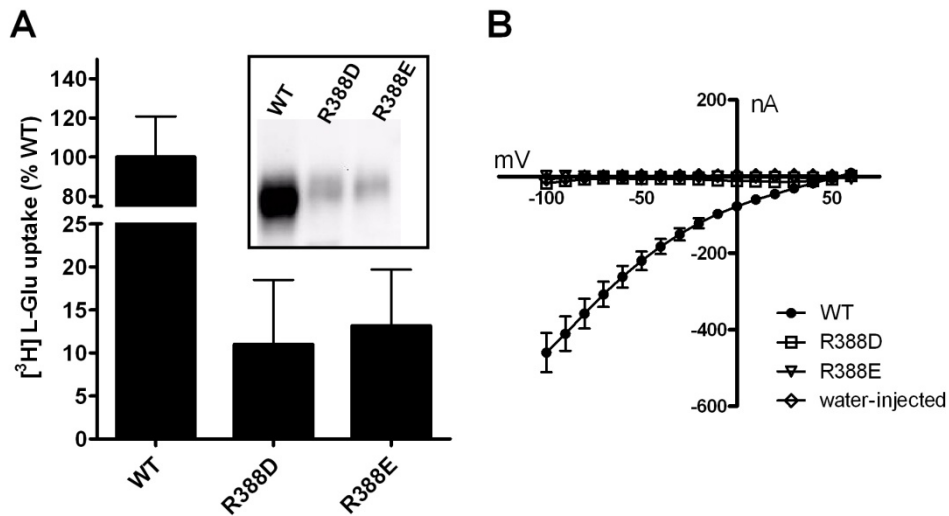


Figure 23. The mutant carriers R388D and R388E accumulate substrate through an electroneutral process

(A) Wild type human EAAT1 transporters and mutant carriers (R388D or R388E) were expressed in *Xenopus* oocytes. Uptake assays were carried out at room temperature using 100 μ M L-[3 H] glutamate as substrate for 15 min and data are normalized to wild type transporters (Note the segmented y-axis). Representative surface expression of wild type and mutant transporters is shown in the boxed inset. **(B)** I-V relation of 100 μ M L-glutamate elicited current recorded in Cl⁻ solution using two-electrode voltage clamp for oocytes expressing wild type EAAT1 transporters (filled circle), R388D (open square), R388E (inverted open triangle) or water-injected oocytes (open diamond).

3.2.2 Residue R388 is critical for the anion channel function

To determine the role of residue R388 on the anion channel function, we substituted NO_3^- , a more permeant anion for extracellular Cl^- to increase the amplitude of anion currents. Under this condition, the recorded current is largely contributed by anions flowing through the transporter and the substrate-coupled current is negligible. Because anion conductance associated with glutamate transporters can be activated by Na^+ alone (in the absence of substrate, termed as $I_{\text{Leak}}^{\text{Glutamate}}$ in the following sections) and is significantly increased with the addition of substrate (in the presence of substrate, as $I_{\text{Total}}^{\text{Glutamate}}$), we directly plotted I-V curves of recorded currents without subtracting $I_{\text{Leak}}^{\text{Glutamate}}$ from $I_{\text{Total}}^{\text{Glutamate}}$ as we did in previous sections. Such analysis allows assessment of the magnitude of the Na^+ -activated anion leak current and also enables a quick determination of whether the transporter is expressed on the cell surface. In addition, the ratio of $I_{\text{Total}}^{\text{Glutamate}}$ to $I_{\text{Leak}}^{\text{Glutamate}}$ (usually at positive membrane potentials) is not dramatically influenced by the surface expression level of transporter proteins and can be used to assess any selective changes in either the anion leak current or the substrate-activated anion current.

Oocytes expressing wild type or mutant transporters R388A and R388K display significantly larger $I_{\text{Leak}}^{\text{Glutamate}}$ compared to water-injected oocytes, indicating that transporter proteins are expressed on the cell surface and that leak anions flow through (**Figure 24A-C**, black circle vs. open diamond). The mutant carrier R388A in general has larger current in the absence of glutamate ($I_{\text{Leak}}^{\text{Glutamate}}$) than the wild type EAAT1 transporter or the mutant carrier R388K, but less additional current elicited by glutamate. The ratio of $I_{\text{Total}}^{\text{Glutamate}}$ to $I_{\text{Leak}}^{\text{Glutamate}}$ at +60 mV for R388A is 1.395 ± 0.032 , and is significantly smaller than that of the wild type EAAT1 transporter (2.571 ± 0.1) and the mutant carrier R388K (2.511 ± 0.09) (**Figure 24D**). These

results suggest that either the Na^+ -activated anion leak current or the substrate-activated anion current is altered in the mutant carrier R388A.

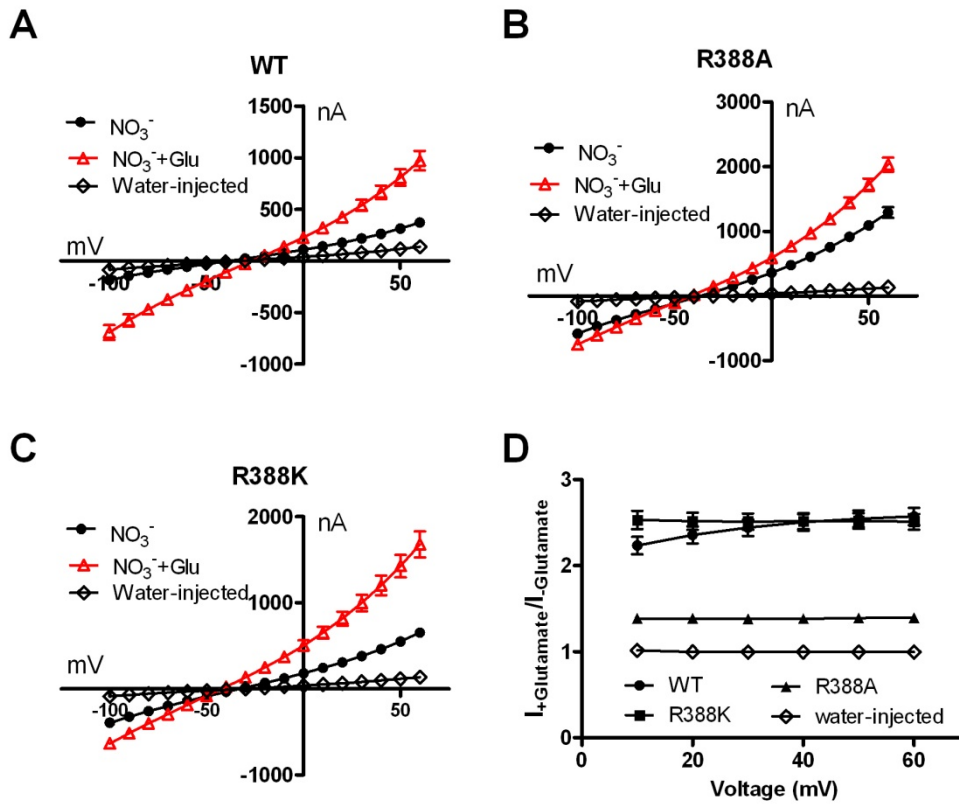


Figure 24. Neutralizing the charge of Residue R388 alters the anion channel function of EAAT1

Oocytes expressing wild type transporters (A), R388A (B) or R388K (C) were recorded in the absence and presence of 1 mM L-glutamate using NO_3^- as external anions in replacement of Cl^- . Endogenous currents were also included by recording water-injected oocytes (open diamond). The ratio of current in the presence of substrates ($I_{+\text{Glutamate}}$, red triangle) relative to that in the absence of substrate ($I_{-\text{Glutamate}}$, black circle) at positive potentials in (A-C) was calculated and shown in (D).

Oocytes expressing the mutant carriers R388D and R388E also display larger $I_{\text{-Glutamate}}$ compared to water-injected oocytes (**Figure 25**, black circle vs. open diamond). This current can be inhibited by 400 μM TBOA, confirming that the current arises from the anion leak conductance through the mutant carriers (**Figure 25**, inverted triangle). Interestingly, current recorded in the presence of 1 mM glutamate ($I_{\text{+Glutamate}}$) superimposes on the top of that in the absence of glutamate ($I_{\text{-Glutamate}}$) (**Figure 25**, red triangle vs. black circle), suggesting that substrate no longer elicits additional anion currents in either mutant carrier. Thus, R388 is also critical for the anion channel function. Mutating arginine to alanine significantly decreases the ratio of current in the presence of substrate ($I_{\text{+Glutamate}}$) to that in the absence of substrate ($I_{\text{-Glutamate}}$), and reversing the positive charge with either aspartate or glutamate abolishes the substrate-activated anion current.

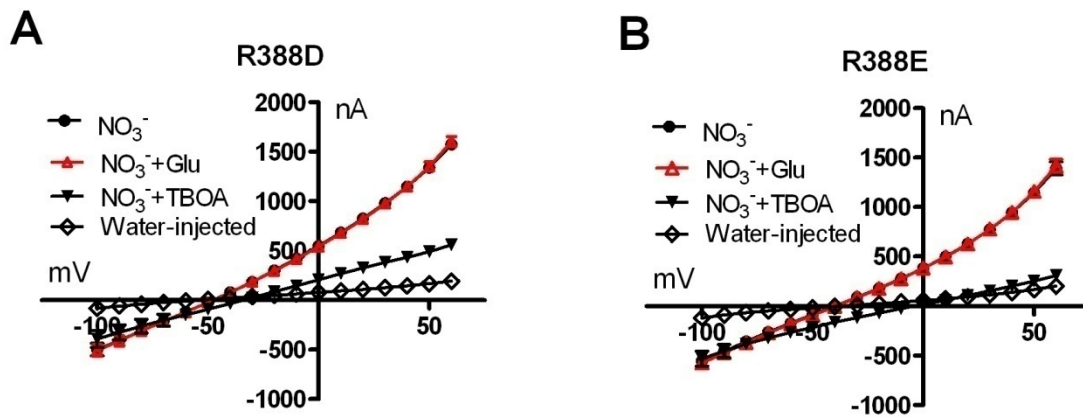


Figure 25. Substrate no longer elicits additional currents in the negatively-charged R388 mutants

The mutant carriers R388D (A) and R388E (B) were expressed in *Xenopus* oocytes. Currents in the absence (black circle) and presence of 1 mM L-glutamate (red triangle) were recorded using NO_3^- as external anions. Currents in the presence of 400 μM TBOA was shown as inverted triangle and endogenous currents were also included by recording water-injected oocytes (open diamond).

3.2.3 The mutant carrier R388D predominantly exists in the anion leak state

The inability of L-glutamate or D-aspartate (data not shown) to elicit additional currents in the mutant carriers R388D and R388E suggests that the link between glutamate binding and the gating mechanism may be disrupted, and thus the mutant carriers spend more time in the anion leak state (I_{Leak}). Alternatively, the mutated carrier may exist in a conformation in which the channel reaches the I_{Leak} state even in the absence of substrate. To resolve these possibilities, we focused on unique properties that distinguish the substrate-gated and anion leak conductance. It has been shown that substrate alters the relative permeability to different anions in EAAT2 and EAAT4. In other words, the relative conductance of various anions differs between the I_{Leak} and I_{Leak} states (127). We therefore determined the relative permeability of anions for the I_{Leak} and I_{Leak} states by measuring the ratio of macroscopic currents at +60 mV in one anion relative to another.

In oocytes expressing wild type EAAT1, the relative conductance of $\text{NO}_3^-/\text{Cl}^-$ and SCN^-/Cl^- is 1.91 ± 0.11 and 6.90 ± 0.51 in the I_{Leak} state, respectively. Application of 1 mM glutamate (the I_{Leak} state) increases the respective relative conductance of $\text{NO}_3^-/\text{Cl}^-$ and SCN^-/Cl^- to 4.62 ± 0.42 and 23.96 ± 1.78 (**Figure 26A and 26B**). Because glutamate cannot elicit additional currents in the mutant carrier R388D, the relative conductance in the I_{Leak} state would be the same as that in the I_{Leak} state. Indeed, our results showed that the relative conductance of $\text{NO}_3^-/\text{Cl}^-$ and SCN^-/Cl^- measured for R388D is 1.89 ± 0.26 and 6.81 ± 1.0 in the I_{Leak} state, and is 1.91 ± 0.26 and 6.90 ± 1.13 in the I_{Leak} state, respectively. These ratios are remarkably similar to those of the I_{Leak} state of the wild type EAAT1 transporter (**Figure**

26B), suggesting that the mutant carrier R388D predominantly exists in the anion leak state and the gating mechanism by glutamate might be impaired with the introduced negative charge.

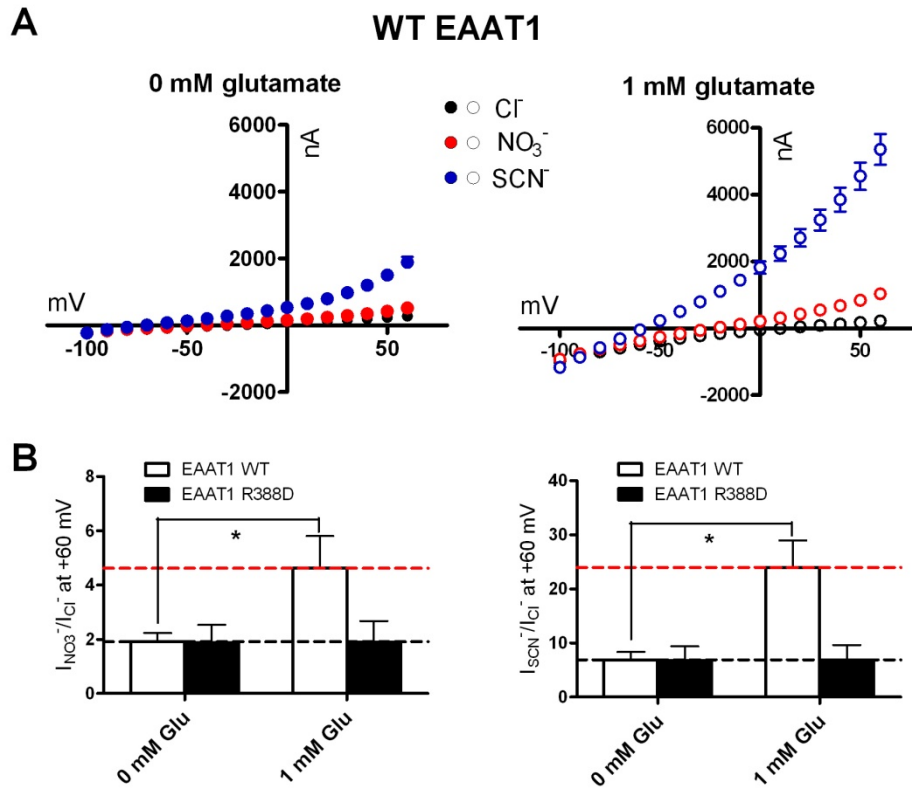


Figure 26. The mutant carrier R388D predominantly exists in the anion leak state

(A) Wild type EAAT1 and the mutant carrier R388D were expressed in *Xenopus* oocytes. Currents in the absence (filled circle) and presence of substrate (open circle) were recorded in Cl⁻, NO₃⁻ or SCN⁻ containing solutions. (B) Ratio of the current measured at +60 mV with different permeating anions (NO₃⁻ to Cl⁻ and SCN⁻ to Cl⁻) for both wild type and mutant carriers. Black dashed lines represent the ratio of currents recorded in the absence of substrate and red dashed lines represent the ratio of currents recorded in the presence of substrate for the wild type EAAT1 transporter. *, p<0.05.

3.2.4 The corresponding mutant carrier R410E of rat EAAT4 predominantly exists in the anion leak state

Because the arginine residue is highly conserved in all of the mammalian glutamate transporters, we replaced the equivalent arginine residue in rat EAAT4 (rEAAT4) by the amino acid glutamate and asked if the mutation also abolishes the glutamate-gated anion channel activity. Just as we observed with R388D and R388E in EAAT1, no additional macroscopic anion current is observed upon glutamate application in oocytes expressing the rEAAT4 R410E mutant carrier, while glutamate elicits a large NO_3^- current in those expressing the wild type rEAAT4 transporter (**Figure 27A**). rEAAT4 R410E transporter proteins are expressed on the cell surface because the current recorded in the absence of substrate ($I_{\text{Glutamate}}$) is significantly larger than that obtained in water-injected oocytes, as a result of the anion leak conductance through the expressed transporters (**Figure 27A**). Glutamate increases the relative conductance of $\text{NO}_3^-/\text{Cl}^-$ from 1.77 ± 0.11 in the $I_{\text{Glutamate}}$ state to 6.31 ± 0.65 in the $I_{+\text{Glutamate}}$ state for the wild type rEAAT4 transporter, and increases the relative conductance of SCN^-/Cl^- from 11.59 ± 1.42 in the $I_{\text{Glutamate}}$ state to 24.26 ± 2.13 in the $I_{+\text{Glutamate}}$ state. The mutant carrier rEAAT4 R410E has similar relative conductance as the wild type rEAAT4 in the $I_{\text{Glutamate}}$ state (**Figure 27B**). The relative conductance of $\text{NO}_3^-/\text{Cl}^-$ is 2.94 ± 0.14 in the $I_{\text{Glutamate}}$ state and 2.93 ± 0.15 in the $I_{+\text{Glutamate}}$ state, and that of SCN^-/Cl^- is 10.62 ± 0.84 in the $I_{\text{Glutamate}}$ state to 10.87 ± 0.78 in the $I_{+\text{Glutamate}}$ state. These results indicate that with both isoforms (human EAAT1 and rEAAT4), mutating the arginine to a negatively charged amino acid prevents glutamate from gating the anion channel and therefore glutamate is no longer able to increase anion permeation.

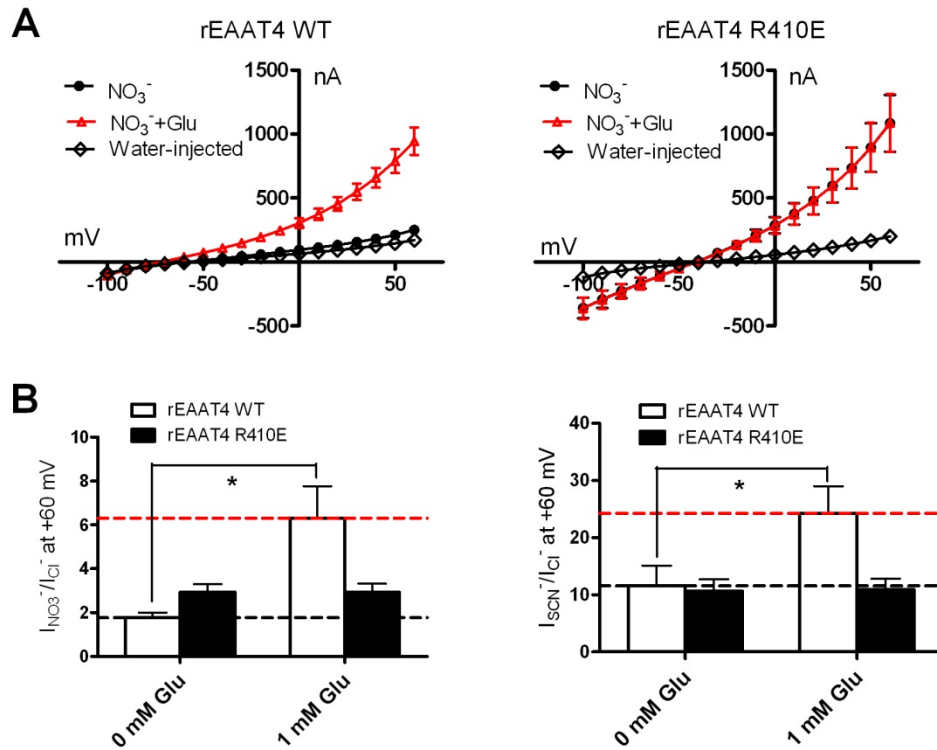


Figure 27. The mutant carrier rEAAT4 R410E predominantly exists in the anion leak state

(A) Currents in the absence (black circle) and presence of 1 mM L-glutamate (red triangle) were recorded using NO_3^- as external anions. Endogenous currents were also included by recording water-injected oocytes (open diamond). (B) Currents were recorded in Cl^- , NO_3^- or SCN^- containing solutions. Ratio of the current measured at +60 mV with different permeating anions (NO_3^- to Cl^- and SCN^- to Cl^-) for both wild type and mutant carriers. Black dash lines represent the ratio of currents recorded in the absence of substrate and red dash lines represent the ratio of currents recorded in the presence of substrate for the wild type rEAAT4 transporter. *, $p < 0.05$.

3.2.5 The mutant carriers R388A and R388D have dramatically increased anion leak currents

The smaller ratio of $I_{+Glutamate}$ to $I_{-Glutamate}$ at +60 mV in the mutant carrier R388A compared to the wild type EAAT1 transporter and the mutant R388K indicates either changed anion leak conductance or substrate-activated anion current when neutralizing the arginine charge (**Figure 24**). Because the mutant carrier R388D displays no glutamate-activated anion current and the transporter exists predominantly in the anion leak state (**Figure 25 and 26**), we hypothesized that the anion leak conductance might also be increased in the mutant carrier R388A, which would result in a decreased ratio of $I_{+Glutamate}$ to $I_{-Glutamate}$ at +60 mV. Consistent with this idea, the $I_{-Glutamate}$ of R388A is generally larger than that of the wild type EAAT1 or the mutant R388K (**Figure 24**). Alternatively, R388A could express more on the cell surface, leading to large $I_{-Glutamate}$, but have decreased $I_{+Glutamate}$, which will also result in a decreased ratio of $I_{+Glutamate}$ to $I_{-Glutamate}$ at +60 mV. Thus we assessed the relative surface expression levels of transporter proteins, and normalized the anion leak current to transporter surface density. We recorded $I_{-Glutamate}$ using NO_3^- as the permeating anion and also determined the cell surface expression of transporter proteins from the same batch of injected oocytes. When normalizing the NO_3^- current at +60 mV to their respective surface expression levels, we found that the Na^+ -activated anion leak current of the mutant R388A is significantly increased relative to the wild type EAAT1 transporter, and the anion leak current of the mutant carrier R388D is even larger (**Figure 28A**).

R388 is located close to TM2 residue D112 in the outward-facing Glt_{Ph} structure (**Figure 28B**). Previous studies have shown that neutralizing D112 with alanine also leads to a large increase in the anion leak current, raising the possibility that R388 may interact with D112 to control gating of the anion channel in human EAAT1. To test this hypothesis, we attempted to

restore substrate-elicited anion currents in the mutant R388D by introducing a positive charge at position D112. Unfortunately, this attempt was not successful. Even though the double mutant carrier R388D_D112R expresses well on the cell surface as indicated by a larger $I_{\text{Glutamate}}$ compared to water-injected oocytes, it does not display substrate-elicited anion currents (**Figure 28C**).

3.2.6 The mutant carrier R388D spends more time in the inward-facing conformation in the absence of substrate

During substrate transport, the transport domain moves toward the cell cytosol to allow cytoplasmic access of the substrate binding site. Such movement is intrinsic to the transporter protein and occurs in the absence of the substrate (50). Crisman *et al.* (94) have also shown that substrate accelerates the inward movement of the transport domain, while the non-transportable inhibitor TBOA blocks it (94). The characteristics of the inward movement of the transport domain are reminiscent of those of the anion channel function. Like the transport domain movement, the anion conductance occurs in the absence of substrate (activated by Na^+), is blocked by TBOA and is increased by substrate. Thus, it is interesting to hypothesize that the transport domain movement may be linked to the anion channel function, and that the negative charge we introduced at position R388 might alter the conformation or limit the movement of the transport domain.

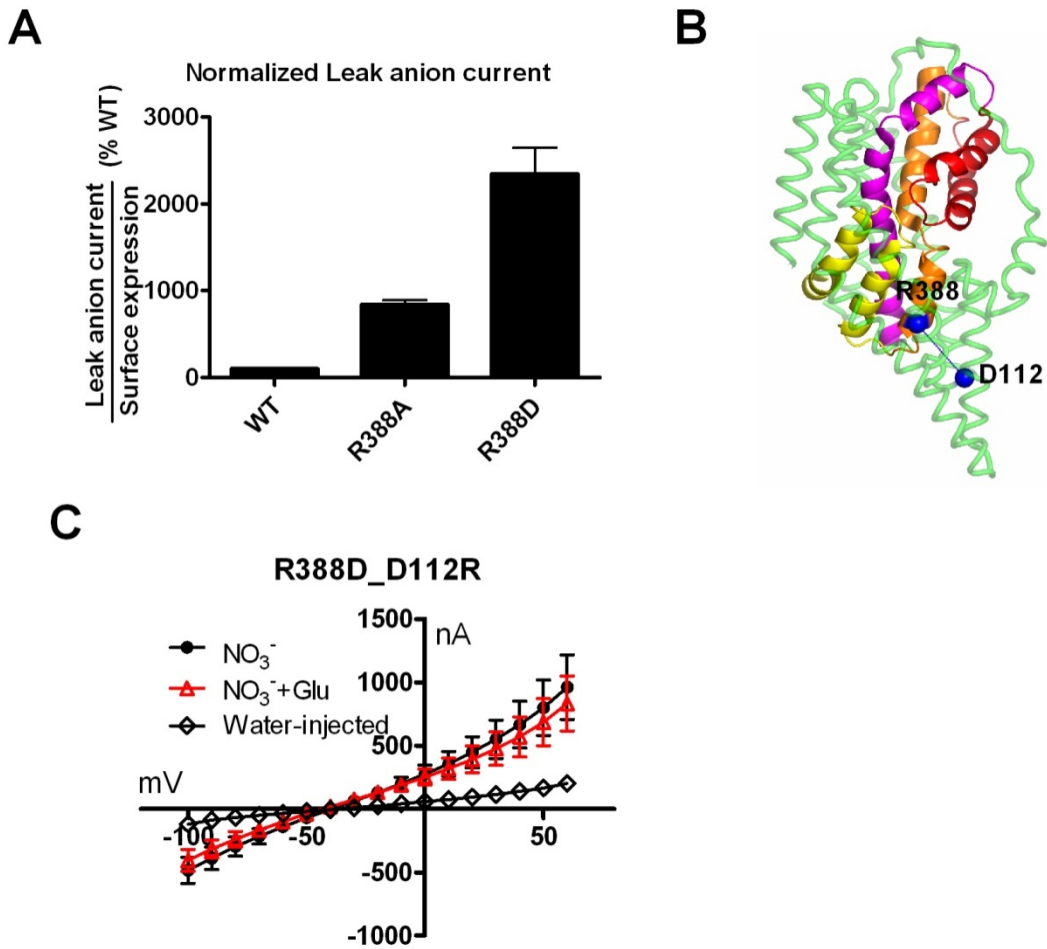


Figure 28. The mutant carriers R388A and R388D have dramatically increased anion leak currents

Wild type EAAT1 and the mutant carriers (R388A, R388D, and R388D_D112R) were expressed in *Xenopus* oocytes. **(A)** Currents in the absence of substrate were recorded in NO_3^- containing solutions. Surface expression levels were determined using cell surface biotinylation assays from the same batch of injected oocytes. Relative anion leak currents were obtained after normalizing to respective surface expression levels and data were normalized to wild type EAAT1 transporters. **(B)** Residues equivalent to R388 and D112 of human EAAT1 were highlighted in blue spheres based on the crystal structure of Glt_{Ph} (PDB ID: 1XFH). **(C)** Currents in the absence (black circle) and presence of 1 mM L-glutamate (red triangle) were recorded using NO_3^- as external anions. Endogenous currents were also included by recording water-injected oocytes (open diamond).

We first assessed the affinity of substrate for the mutant carrier R388D, reasoning that any change in the conformation of the transport domain could affect the extracellular accessibility of the substrate binding site. Because R388D accumulates substrate very poorly, but has a large Na^+ -activated anion leak current (**Figure 23 and 26**), we determined the affinity of TBOA by measuring TBOA-blocked anion leak current. Our results showed that the K_m for TBOA is increased in the mutant carrier R388D compared to the wild type transporter ($2.22 \pm 1.08 \mu\text{M}$ for the wild type EAAT1 and $12.83 \pm 1.08 \mu\text{M}$ for the mutant R388D), consistent with the idea that the substrate binding site in the mutant carrier is less accessible (**Figure 29A**).

To probe the conformation of the transport domain in the mutant carrier R388D, we took advantage of several previously characterized cysteine substitutions that demonstrate conformational sensitivity to thiol modification, particularly with respect to the transport domain movement (**Figure 18A**). We have observed that L376C displays the greatest sensitivity to conformational changes in the transport domain among the residues we have examined so far. We thus introduced L376C into the R388D background, and determined the accessibility of L376C to the membrane permeable thiol-modifying agent, NEM, under Na^+ (the transport spends most of the time in the outward-facing orientation) or K^+ conditions (in the inward-facing orientation). As expected, glutamate elicits a large NO_3^- current in the single mutant carrier L376C, but no additional glutamate-elicited currents are seen in the double mutant carrier R388D_L376C (**Figure 29B**). R388D_L376C is expressed on the oocyte cell surface because oocytes expressing the mutant carrier have a larger $I_{\text{Glutamate}}$ compared to water-injected oocytes (**Figure 29B**). We treated oocytes expressing transporter carriers with 0.25 mM NEM, a condition that has very different modification rates of L376C in Na^+ and K^+ containing solutions. 5 min incubation with 0.25 mM NEM in Na^+ solution does not inhibit the uptake activity of

L376C. In contrast, L376C shows $63.21 \pm 9.82\%$ of transport activity after NEM treatment in K^+ solution (**Figure 29C**), due to the increased frequency of the inward movement of the transport domain by high extracellular K^+ and the intracellular exposure of L376C enabling NEM modification. It should be noted that when expressed in COS7 cells, treatment with 0.25 mM NEM in a solution with high extracellular K^+ almost completely inhibits the uptake activity of L376C. The large cell volume of *Xenopus* oocytes might affect the effective intracellular NEM concentration. Supporting this idea, we have observed that NEM non-specifically inhibits transport activity of the CSLS control carrier by approximately 20% in COS7 cells, but not of the R388D single mutant carrier expressed in *Xenopus* oocytes. After 5 min treatment with 0.25 mM NEM in the Na^+ condition, oocytes expressing the mutant carrier R388D_L376C displays $42.51 \pm 4.38\%$ of transport activity compared to the untreated control, suggesting that residue L376C is already exposed intracellularly in the Na^+ condition. Modification with NEM in the K^+ condition does not further inhibit the transport activity of the mutant carrier R388D_L376C (**Figure 29C**). Thus, the mutation of R388 to aspartate appears to cause the transport domain spend more time in the inward-facing orientation in the absence of substrate, which is in line with the decreased accessibility of the substrate binding site from the extracellular environment.

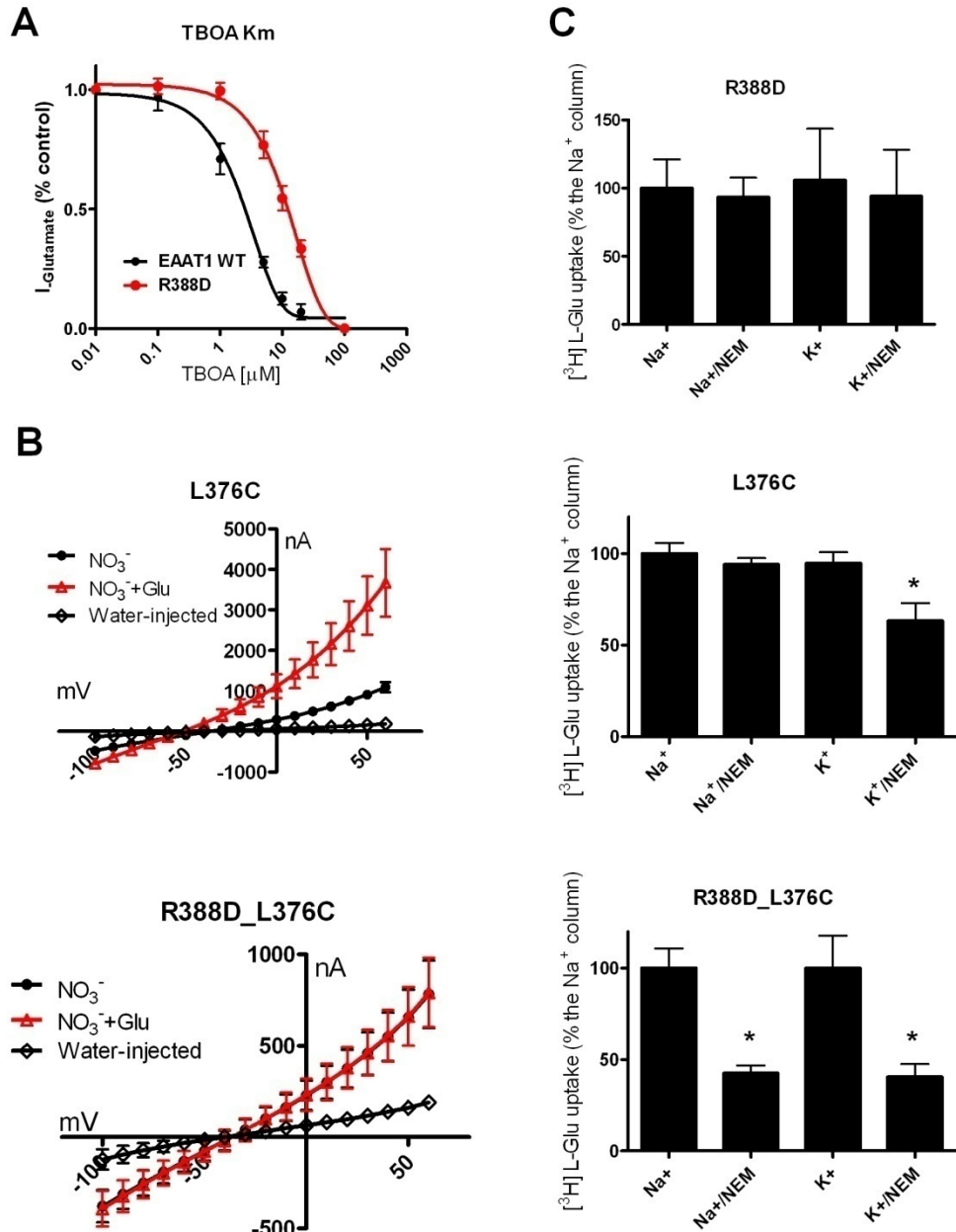


Figure 29. The mutant carrier R388D spends more time in the inward-facing conformation in the absence of substrate compared to the wild type transporter

Wild type EAAT1 and mutant carriers (R388D, L376C, and R388D_L376C) were expressed in *Xenopus* oocytes.

(A) Currents in the presence of various concentrations of TBOA were recorded in NO₃⁻ containing solutions.

Currents at +60 mV in the presence TBOA were normalized to that in the absence of TBOA. Note that the basal

current ($I_{\text{Glutamate}}$ recorded in the presence of maximal concentration of TBOA) was subtracted for the normalization. **(B)** Currents in the absence (black circle) and presence of 1 mM L-glutamate (red triangle) were recorded using NO_3^- as external anions. Endogenous currents were also included by recording water-injected oocytes (open diamond). **(C)** Oocytes expressing mutant carriers were treated with 0.25 mM NEM for 5 min under Na^+ or K^+ conditions as indicated. Uptake assays were performed for 15 min at room temperature using 5 μM L-[^3H] glutamate as substrate. Data are normalized to the Na^+ column.

3.3 DISCUSSION

Glutamate transporters possess dual functions to clear extracellular glutamate and to conduct anions. Mutagenesis studies obtained so far suggest that these two functions seem to be mediated by independent processes. Modification of cysteine substituted residues in HP2 abolishes substrate transport, but the substrate-activate anion channel activity remains (96-98). On the other hand, mutating several charged or polar residues in TM2, 5 and 7 affects the anion channel function with modest changes in the substrate transport (95, 99). However, because both substrate transport and the substrate-activated anion current require the presence of Na^+ and glutamate, these two functions must utilize similar structural components at various steps in the two processes. The present study shows that a conserved residue R388 in TM7 of human EAAT1 serves a critical role in both substrate transport and anion conduction. Neutralizing R388 with amino acid alanine significantly impairs uptake activity compared to wild type transporters, and increases the Na^+ -activated anion leak current. The mutant carriers R388D and R388E accumulate substrate through an electroneutral process and also abolish the substrate-activated anion current (**Figure 22-25**).

R388 is located one helix turn away from two other conserved basic residues, K384 and R385 in TM7. Mutant carriers with K384 or R385 replaced by either amino acid alanine or aspartate generally have similar rates of substrate transport and the voltage dependence of transport currents compared to wild type transporters. In addition, they display both changed Na^+ -activated anion leak current and the substrate-activated anion current (99). In our study, the mutant carrier R388A accumulates only ~20% of radioactive L-glutamate relative to the wild type transporter. The transport current at -100 mV is also decreased to a similar degree, although the voltage dependence of the transport current is unchanged (**Figure 22**). We also examined the cell

surface expression of R388A and concluded that the impaired substrate transport is not due to the decreased surface protein level. Thus, residue R388 is important for substrate transport. This is not so surprising in that TM7, as part of the transport domain, contributes to form the binding pocket for substrate and coupled ions, and moves inward to enable the alternating access of the binding pocket to the EC or IC environment.

The involvement of the residue R388 in substrate transport is also supported by the phenotype of the mutant carriers R388D and R388E. Although these two mutants still accumulate radioactive substrate, no substrate-coupled transport current is observed. For a complete transport cycle, the inward movement of each glutamate molecule is coupled to the influx of 3 Na⁺, 1 H⁺ and the efflux of 1 K⁺, which generates two positive charges (**Figure 1**). If the mutant carriers R388D and R388E accumulate radioactive substrate by making a full cycle, the absence of coupled currents would suggest that the stoichiometry of coupled ions and glutamate is altered in these two mutants. Alternatively, radioactive substrate can be accumulated through a process called exchange, in which the K⁺-induced reorientation step is impaired and the transport returns to the outward-facing state by moving intracellular substrate and coupled ions outside the cell (**Figure 1A**). The K⁺-induced reorientation step is very vulnerable and several mutations have been reported to impair this step (64, 66, 79). The general properties of forward and reverse glutamate transport are symmetric (128). Experimentally, high extracellular K⁺ applied to cells expressing the wild type transporter leads to reverse transport, with release of intracellular substrate and co-transported ions and gating of the anion conductance. However, mutants with the impaired K⁺-induced reorientation step lose their ability to elicit anion currents when high concentrations of K⁺ are applied outside. Our preliminary results show that raising extracellular concentrations of K⁺ does not elicit any NO₃⁻ current in the mutant carriers R388D

and R388E (data not shown), similar to what has been observed for the mutants that impair the K^+ -induced reorientation step. However, we found later that glutamate no longer elicit additional anion current during forward transport for these two mutants (**Figure 25**) and thus the inability of high extracellular K^+ to elicit anion currents could be due to the fact that no substrate-activated anion currents are associated with reverse transport in the mutant carriers R388D and R388E. Nevertheless, our results show that reversing the positive charge of R388 with either aspartate or glutamate results in accumulation of radio-labeled substrate through an electroneutral process, supporting the role of R388 in substrate transport.

Traditionally, the substrate-activated anion current is obtained by subtracting current in the absence of substrate from that in the presence of substrate. Because the Na^+ -activated anion leak current is blocked by non-transportable inhibitors such as TBOA, this current is obtained by subtracting current in the presence of inhibitors from that in the absence of inhibitors. In addition, more permeable anions such as NO_3^- and SCN^- are used to study anion channel function. When comparing the subtracted currents between wild type and mutant transporters, variations arise within oocytes of different batches and sometimes even of the same batch because of inconsistent expression. In our study, we plot currents recorded in the absence of substrate ($I_{-Glutamate}$) and in the presence of substrate ($I_{+Glutamate}$) without subtraction. Currents recorded at +60 mV, the most positive potential in our recording, are used to compare the anion channel activity because at this voltage the majority of current is due to the anion flow. The ratio of $I_{+Glutamate}$ to $I_{-Glutamate}$ at +60 mV is not significantly influenced by the expression of transporter proteins, even though both $I_{-Glutamate}$ and $I_{+Glutamate}$ contain endogenous oocyte currents (**Figure 24**). This is because endogenous oocyte currents are generally small compared to $I_{-Glutamate}$ or $I_{+Glutamate}$. Furthermore, comparison of $I_{-Glutamate}$ with endogenous oocyte currents from the same

batch provides a means to quickly determine if transporter proteins are expressed on the cell surface. The ratio of $I_{\text{Glutamate}}$ to $I_{+\text{Glutamate}}$ at +60 mV for the mutant carrier R388A is significantly smaller than that for the wild type EAAT1 transporter and the mutant carrier R388K, suggesting that either the Na^+ -activated anion leak current or the substrate-activated anion current is altered in the mutant carrier R388A. Further determination of the Na^+ -activated leak current after normalizing to the cell surface expression suggests that the mutant R388A has a larger Na^+ -activated leak current compared to the wild type EAAT1 transporter (**Figure 28A**).

Surprisingly, even though the mutant carriers R388D and R388E still accumulate radioactive substrate, no glutamate-elicited anion current is observed (**Figure 25**). This phenotype is also seen in the equivalent charge reversing mutant of rat EAAT4, rEAAT4 R410E (**Figure 27**). Detailed analysis of the mutant carriers R388D and rEAAT4 R410E show that these mutants predominantly exist in the anion leak state. Consistent with this observation, the mutant R388D has a larger Na^+ -activated leak current after normalizing to the cell surface expression compared to the wild type EAAT1 transporter (**Figure 28A**). Thus, mutating the arginine to negatively charged amino acids prevents glutamate from gating the anion channel and therefore glutamate is no longer able to increase anion permeation. Taken together, these results suggest that R388 in TM7 plays a critical role in the anion channel function.

We initially speculated that residue R388 might interact with residue D112 in TM2 through charge attractions based on following observations. First, the mutant carrier D112A display increased Na^+ -activated anion leak current, but decreased substrate-activated anion current (95). This phenotype is very similar to that for the mutant R388A, but is not observed in the mutant R388K when the positive charge is preserved. Second, although the residues corresponding to R388 and D112 are conserved within mammalian EAATs, in Glt_{ph} the

corresponding residues are both serine, suggesting a potential co-evolution of residues. Third, based on the outward-facing crystal structure of Glt_{ph}, the C α atom distance between residues equivalent to D112 and R388 is ~ 13 Å. Forth, the equivalent residue of D112 in Glt_{ph} is located in the TM2-TM3 loop, which undergoes significant conformational changes to accommodate the inward movement of the transport domain, where residue R388 resides (50). We attempted to restore the substrate-activated anion current by reversing the charges of R388 and D112 to maintain their potential interactions. However, glutamate does not elicit additional anion currents in the double mutant carrier R388D_D112R. The side chains of D388 and R112 in the double mutant carrier might not face the right directions to allow interaction or in wild type transporters a network of charge interactions may exist instead of a simple R388_D112 interaction. Supporting the latter explanation, mutations of several charged residues near these two residues have resulted in altered anion channel function (95, 99). It is thus possible that the introduced negative charge might interfere with the network of charge interactions and change the conformation of the transporter protein.

We considered the conformation of the transport domain because this domain contains binding sites for substrate and coupled Na⁺ that are required to activate the anion channel. In addition, the transport domain moves inward into the cell cytosol, which may disrupt charge interactions of residues in TM7 with those in TM2 and TM5, gating the anion channel. By determining the accessibility of a conformation-sensitive cysteine residue L376C, our results show that the transport domain of the mutant carrier R388D spends more time in the inward-facing orientation in the absence of substrate (**Figure 29**). Consistent with this observation, the affinity of TBOA to block Na⁺-activated anion leak currents is also decreased in the mutant carrier R388D, suggesting decreased accessibility of the substrate binding site from the

extracellular environment when the transport domain moves in. These results indicate that the movement of the transport domain, a critical step during substrate transport, is required for the anion channel gating. In the mutant carrier R388D, the transport domain shifts to the inward-facing orientation and this renders the carrier in the anion leak state.

Our results are also consistent with previous notions that the substrate transport process is tightly linked to the anion channel function. Early evidence showed that fast application of glutamate elicits pre-steady state currents for both the transport current and the anion current, which then decay to steady state currents. These currents can be mathematically modeled by going through connected states occupied at similar early steps in the transport cycle (124). Grewer and colleagues rigorously studied the kinetics, Na^+ and voltage dependence of these pre-steady state currents (34, 126). They found that the pre-steady state of the anion current rises more slowly and the rising time constant is in the same range as the fast decay phase for the transport current (both called τ_{fast}). The decay phase of the anion current is best fit with one exponential component and is similar to the slow decay phase for transport current (τ_{slow}), suggesting that at least two phases (τ_{fast} and τ_{slow}) of the pre-steady state transport currents and anion currents share similar kinetic steps of the transport cycle. Additional experiments examining the Na^+ and voltage dependence of these phases support this conclusion (88, 126). Interestingly, the activation enthalpies of these two processes are very large, indicating they are rate-limited by substantial conformational changes of the transporter (88). In light of our results, we attribute one of the conformational changes to be the inward movement of the transport domain.

Together, our results show that a positively charged residue in TM7 is involved in both substrate transport and the anion channel function. By studying the charge-reversing mutants,

this study also suggests for the first time how the inward movement of the transport domain, a critical step of substrate transport, might be linked to the anion channel function. Our study opens new avenues toward a complete understanding of the complex dual mechanism carried by glutamate transporters.

4.0 SUBUNIT INTERACTIONS OF GLUTAMATE TRANSPORTERS

4.1 INTRODUCTION

Glutamate transporters are multimeric proteins composed of three identical subunits that line a small central hole (48, 55, 57). In studies of ours (**Figure 12**) and others (57), protein samples collected from oocytes expressing human EAAT1 or EAAT2 migrate predominantly as a single trimer species in blue native polyacrylamide gels. Virtually no dimer or monomer species is seen, suggesting that the trimerization of monomers occurs efficiently during or shortly after synthesis of the individual subunits.

One fundamental question associated with multimeric structures is whether the individual subunits function independently of each other or whether there is cross-talk between them. It has been shown that the Hill coefficient for glutamate dependence of substrate transport is close to one, suggesting that only one glutamate molecule needs to bind to the transporter to be transported (34, 123). Grewer *et al.* (56) further explored this question by coexpressing wild type EAAT3 transporters and mutant transporters that have different substrate specificity and kinetic properties. Although the wild type and mutant transporters coassemble into trimers, they behave as two independent populations of transporters, leading to the conclusion that the individual subunits in the glutamate transporter trimer function independently of each other in both

substrate transport and anion conduction (56). Several other studies generally agree with this notion (115, 122).

In contrast, Torres-Salazar *et al.* observed sigmoidal glutamate concentration dependence for the anion conduction with Hill coefficients ≥ 3 in EAAT4 (123). Because it is sometimes difficult to draw conclusions about cooperativity based only on Hill coefficients, the authors also showed that in contrast to the early findings, cells coexpressing wild type EAAT4 transporters and mutant transporters do not show characteristics of two independent populations of transporters in the anion channel function (123). Based on these results, the authors concluded that multiple glutamate binding sites must be occupied to activate the anion channel, similar to ideas proposed to explain the behavior of ligand-gated channels such as acetylcholine receptors (129). Apart from the different transporter subtypes used experimentally in this study and the Grewer's (56), the basis for the differences in the results remains unresolved. One explanation might be the untested assumptions of random translation and interaction of wild-type and mutant subunits expressed at the plasma membrane. The coexpression strategy theoretically results in four populations of glutamate transporters, comprised of either three wild type subunits, two mutant and one wild type subunits, one mutant and two wild type subunits, or three mutant subunits. The steady-state data essentially come from a mixed population of transporter trimers and in practice it is very difficult to determine the percentage contribution of each population to the total transporter function. Thus, fitting data to a model based equation may be problematic, since the information on the contribution of each population is not available. To overcome this shortcoming, we constructed a tandem-linked trimeric glutamate transporter. This concatenated glutamate transporter has 3 identical subunits connected by flexible linkers, each harboring unique restriction sites that enables us to "cut and paste" mutant subunits in any combinations

desired. The advantage of this concatenated gene is that it generates a homogeneous population of transporters with fixed stoichiometry of mutant and wild type subunits. Using this concatemer strategy, our preliminary data suggest that glutamate transporters are functional as trimers and the individual subunits transport substrate independently.

4.2 RESULTS

4.2.1 Characterization of a concatenated glutamate transporter trimer

We made a concatenated glutamate transporter trimer by linking three cysteine-less EAAT1 subunits (CSLS) at the DNA level. The linkers used are “GYPYDVPDYAGSAAISAAAAAAAAAAAA” and “AAAAAAAAAAAAAGSAAISAAAAAAAAAAAA”. We named this construct as “1WT2WT3WT”, in which the number corresponds to the position of the subunit in the concatemer and the letter “WT” represents cysteine-less EAAT1. When expressed in COS7 cells, the concatenated carrier displays ~30 percent of uptake activity compared to the wild-type transporter (**Figure 30A**) and it also has comparable substrate affinity of transport activity ($53.31 \pm 15.18 \mu\text{M}$ for the wild type EAAT1 transporter vs. $28.09 \pm 8.56 \mu\text{M}$ for the 1WT2WT3WT concatemer). It should be noted that the concatenated carriers takes 3 days after cell transfection to achieve this substrate transport level. Similar to the wild type EAAT1 transporter, substrate transport of the concatenated carrier depends on sodium ions and can be inhibited by the presence of TBOA, a common non-transporting inhibitor of glutamate transporters (**Figure 30B**), suggesting that the concatenated glutamate transporter has functional characteristics similar to that of the wild type EAAT1 transporter. To exclude the possibility that the

concatenated carriers form higher order oligomers between concatemers, we performed blue native gel analysis to determine the quaternary structure of proteins. Both the wild type EAAT1 transporter and the concatenated carrier migrate predominantly as a single trimer species and no other apparent species at higher molecular weight is observed (**Figure 30C**). The concatenated carrier runs a little bit slower, which may be due to the two linkers inserted into the protein. When the concatenated carrier is denatured and separated by SDS-PAGE, the majority of species migrate at a molecular weight of >190 kDa, corresponding to the size of a trimeric glutamate transporter. In contrast, the wild type EAAT1 transporter displays a monomer species of ~70 kDa and an additional species at ~140 kDa, which arises from the aggregation of glutamate transporters (**Figure 30D**). Thus, the concatenated glutamate transporter carriers self-assemble into trimer and are highly functional.

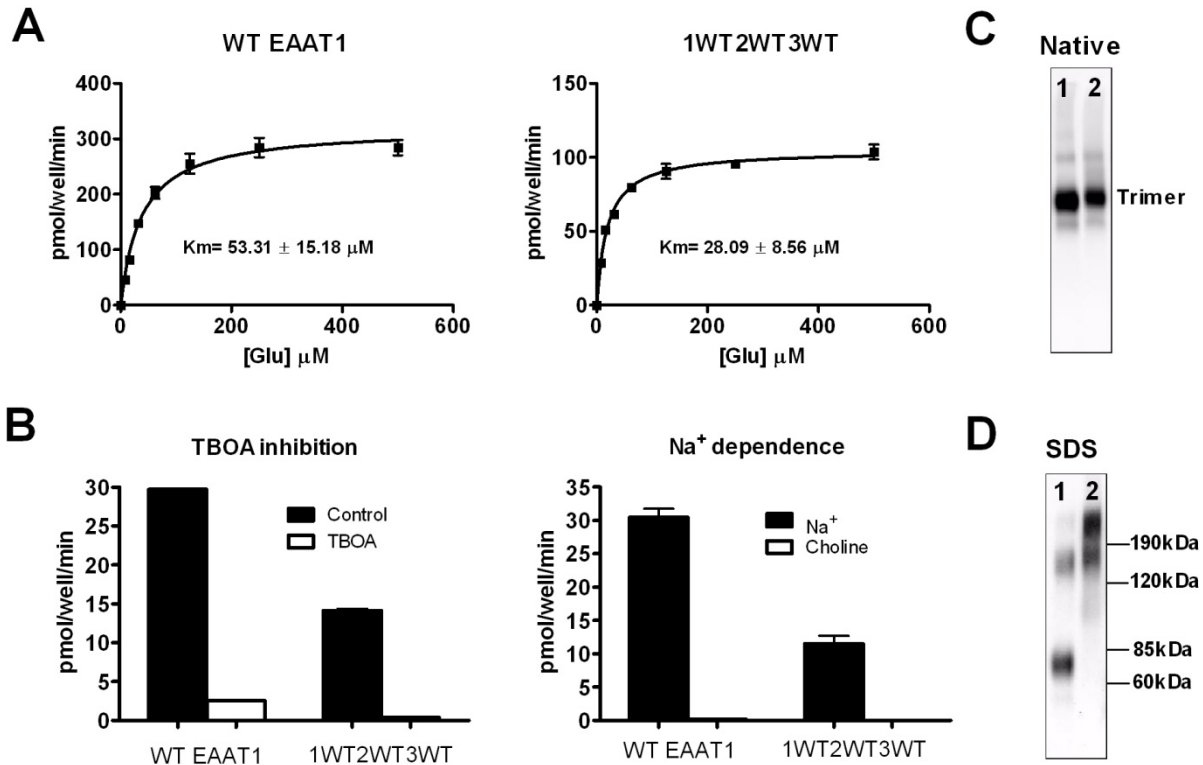


Figure 30. Characterization of a concatenated glutamate transporter trimer

The wild type EAAT1 transporter and the concatenated carrier 1WT2WT3WT were expressed in COS7 cells. **(A)** 3 days post transfection, uptake assays were performed for 10 min at room temperature using concentrations of L-[^3H] glutamate as indicated. **(B)** Uptake assays were carried out using 5 μ M L-[^3H] glutamate as substrate in the absence and presence of 384 μ M TBOA. For Na^+ dependence, sodium ions were replaced by equal molar of choline. **(C)** Proteins samples were separated by blue native PAGE. **(D)** Proteins samples were separated by SDS PAGE. Lane 1: the wild type EAAT1 transporter, Lane 2: the concatenated carrier 1WT2WT3WT. Glutamate transporter proteins were identified using an anti-human EAAT1 polyclonal antibody directed against the C-terminus.

4.2.2 The mutant carrier R479C in human EAAT1 changes its substrate specificity

It has been shown previously that the neutralization of a conserved arginine residue R447 results in the conversion to neutral amino acid substrate specificity in a neuronal glutamate transporter EAAC1. Whereas wild type EAAC1 is capable of accommodating both L-glutamate and L-cysteine as substrates, several EAAC1 R447 mutants do not bind acidic amino acids, but are able to transport L-cysteine and other neutral amino acids, such as L-serine, which is not a substrate for the wild type transporter (64). When coexpressed with the wild type EAAC1 transporter, a population of the assembled trimers are composed of individual subunits that transport either L-glutamate or L-serine. Using this strategy, Grewer *et al.* showed that the amplitudes of anion currents elicited at 0 mV by the mixture of two substrates is identical to the sum of the anion current amplitudes activated by the application of either L-glutamate or L-serine alone. Data obtained by coexpressing human EAAT4 and the equivalent arginine mutant show different results, thus reaching distinct conclusions on the subunit interactions of the anion channel function. We intend to revisit this question by generating concatenated heterotrimers that allow the expression of a single population of the heterotrimers containing subunits that transport either L-glutamate or L-serine. With these constructs, we can address the following questions: a) Is a single subunit capable of transporting substrate and conducting anions, and b) Is there cross-talk between subunits?

We first mutated the equivalent arginine residue in human EAAT1 (R479) to cysteine and tested the substrate specificity of the mutant carrier in oocytes. As shown in **Figure 31**, application of 1 mM L-glutamate to oocytes expressing the WT EAAT1 transporter elicits an outward NO_3^- current +60 mV, whereas 1 mM L-ser or L-alanine does not elicit any detectable currents. With the mutant R479C, 1 mM L-serine or L-alanine elicits an outward NO_3^- current,

but 1 mM L-glutamate does not (**Figure 31**). These results demonstrate that the function of the arginine residue is conserved in different subtypes of mammalian transporters. The mutant carrier R479C changes its substrate specificity from preferring acidic amino acids to neutral amino acids.

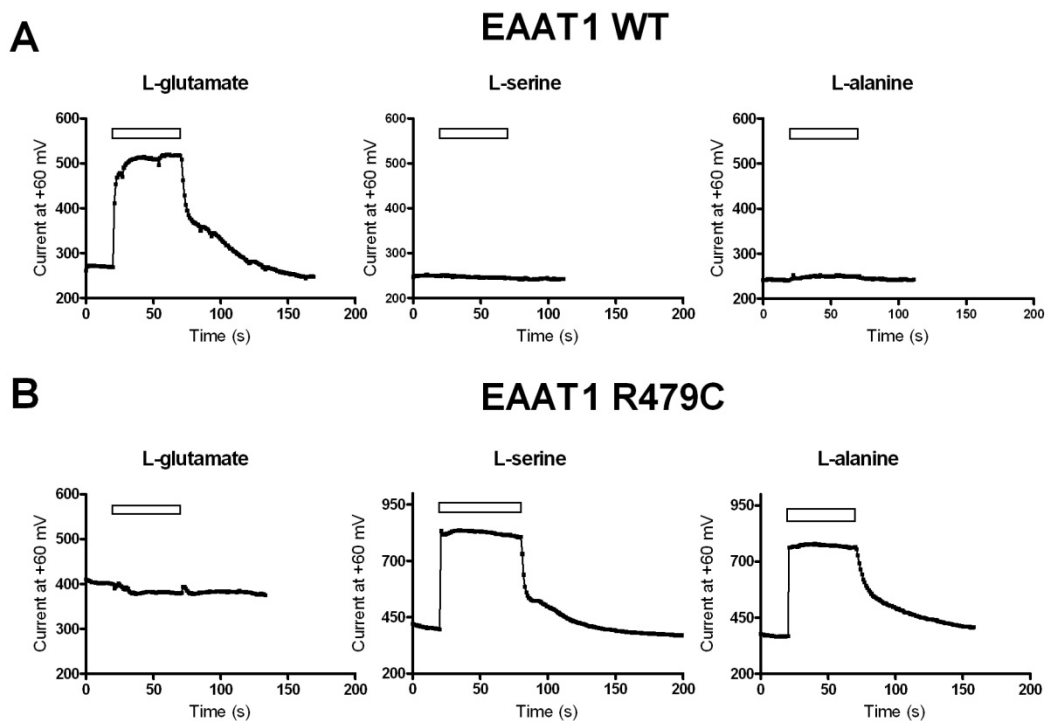


Figure 31. The mutant carrier R479C in human EAAT1 changes its substrate specificity

The wild type EAAT1 transporter and the mutant carrier R479C were expressed in *Xenopus* oocytes. Currents elicited by 1 mM L-glutamate, 1 mM L-serine or 1 mM L-alanine were recorded using NO_3^- as external anions. The oocytes were clamped at a membrane potential of +60 mV. Open bars on the top of current traces represent the application of the substrates.

4.2.3 A single subunit of glutamate transporter trimer is capable of transporting substrate

We next replaced one or two subunits in the concatenated 1WT2WT3WT with the R479C mutant subunit(s) and asked whether a single subunit is capable of transporting substrate. The concatenated carrier 1WT2WT3R479C, which contains a single R479C subunit in the third position, is able to accumulate radioactive L-serine (**Figure 32A**). Similarly, the concatenated carrier 1WT2R479C3R479C, which contains only one wild type EAAT1 subunit, transports L-glutamate (**Figure 32B**). These results indicate that a single transporter subunit within a trimer is capable of transporting substrate.

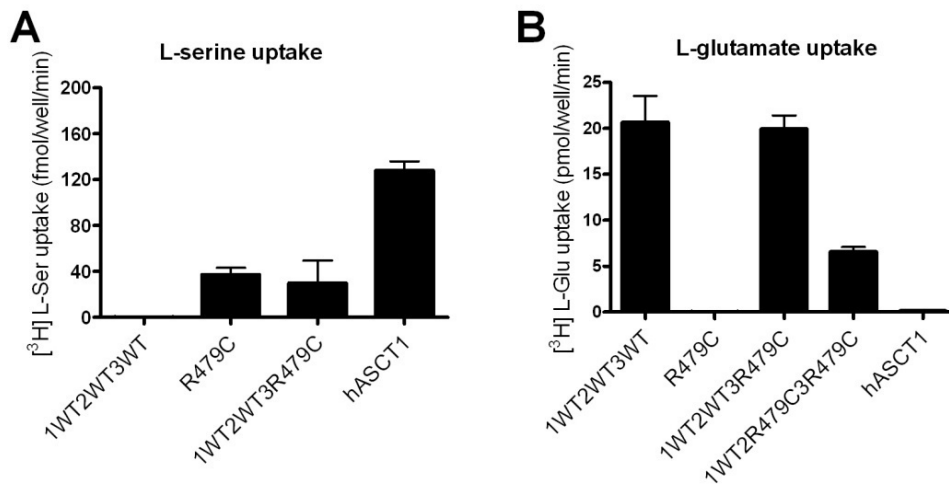


Figure 32. A single subunit of the glutamate transporter trimer is capable of transporting substrate

The concatenated carriers (1WT2WT3WT, 1WT2WT3R479C, and 1WT2R479C3R479C), the EAAT1 mutant carrier R479C and the wild type human ASCT1 were expressed in COS7 cells. 3 days post transfection, uptake assays were performed for 10 min at room temperature using 100 nM L- ^3H serine (**A**) or 5 μM L- ^3H glutamate (**B**) as substrates.

4.2.4 Each subunit of the glutamate transporter trimer uptakes substrate independently from each other

To examine the potential subunit interactions on transporting substrates, we tested whether the substrate transport capability of one subunit is influenced by the function of a neighboring subunit in the trimer. We compared the accumulation of radioactive L-glutamate by the concatenated carriers 1WT2WT3R479C and 1WT2R479C3R479C in the absence or presence of 500 μM unlabeled L-serine. No significant difference in L-glutamate accumulation is observed for both concatenated carriers 1WT2WT3R479C and 1WT2R479C3R479C using either 5 μM (**Figure 33A**) or 500 μM L-[^3H] glutamate (**Figure 33B**) as substrate, suggesting that each subunit transports substrate independently.

4.3 DISCUSSION

In this study, we made a concatenated gene by linking three glutamate transporter subunits at the DNA level. This concatenated carrier is highly functional and assembles as a trimer in mammalian cells. These results confirm that glutamate transporters can function through a trimeric stoichiometry. We further studied subunit interactions by introducing into the concatenated carrier mutant subunit(s) that only transport neutral amino acids. We found that a single glutamate transporter subunit is capable of transporting substrate. In addition, each subunit functions independently in substrate transport. To explore whether a single subunit of glutamate transporters is able to conduct anion currents and whether there are interactions between subunits during this process, we expressed the concatenated carriers in *Xenopus* oocytes. Unfortunately,

despite the success at expressing the concatenated trimer constructs in mammalian cells, expression of these carriers in oocytes has proved difficult thus far. Further studies using patch clamping in mammalian cells or improved expression in oocytes will help delineate the subunit interactions of glutamate transporters in the anion channel function.

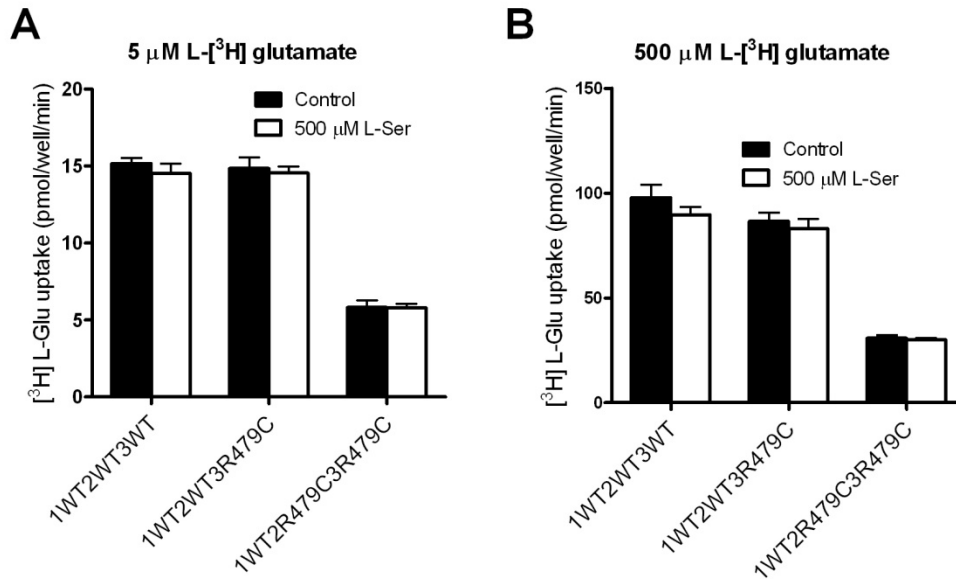


Figure 33. Each subunit of the glutamate transporter trimer uptakes substrate independently from each other

The concatenated carriers 1WT2WT3WT, 1WT2WT3R479C, and 1WT2R479C3R479C were expressed in COS7 cells. 3 days post transfection, uptake assays were performed for 10min at room temperature using 5 μM L- $[^3\text{H}]$ glutamate (**A**) or 500 μM L- $[^3\text{H}]$ glutamate (**B**) as substrate in the absence or presence of 500 μM unlabeled L-serine.

5.0 CONCLUSIONS, GENERAL DISCUSSIONS AND FUTURE DIRECTIONS

Neuronal and glial glutamate transporters function to clear synaptically released glutamate from the extracellular space. This process not only ensures the spatial and temporal fidelity of excitatory signaling, but also prevents the neuronal death triggered by excess glutamate (130). In addition, glutamate transporters possess a substrate-gated anion channel function, which may play an important role in shaping the synaptic transmission. The overarching questions that have driven this thesis project are how these two distinct functions can take place within a glutamate transporter trimer and what are the domains and domain movements required for glutamate transport and/or the anion channel function

As described in Chapter 2, we have used cysteine crosslinking in combination with computational simulations to obtain evidence for large-scale collective movements of the glutamate transporter trimer that are functionally important. Two types of these movements are suggested by the ANM analysis: asymmetric contraction/stretching and symmetric opening/closing. In both modes, the extracellular domains of adjacent subunits approach each other, whereas residues at the bottom of the transporter, within the membrane, remain rigid. Restricting these motions by the formation of disulfide bonds between two subunits of a trimer completely abolishes substrate transport. In addition, when two subunits approach each other and are crosslinked, the transport domain of the third uncrosslinked subunit assumes an inward-facing orientation, suggesting that the large collective movements of the transporter trimer are

functionally linked to the piston-like movement of the transport domain. The ANM analysis also confirms that individual subunits potentially undergo separate transitions between outward-facing and inward-facing forms, rather than an all-or-none transition of the three subunits. Finally, glutamate still elicits anion currents after crosslinking, presumably through two crosslinked subunits that have limited capability to move. Thus, substrate-activated anion conduction likely occurs at an early step of the transport cycle without significant conformational changes.

We went on to explore the anion permeation pathway and the conformational changes associated with the anion channel function in Chapter 3. A conserved arginine residue in TM7 was identified to be important for both substrate transport and the anion channel function. This positively charged residue, R388 in human EAAT1, displays impaired substrate transport activity when mutated to the neutral amino acid alanine. The mutant carrier R388A also has increased Na^+ -activated anion leak currents, but decreased substrate-activated anion currents. When R388 is replaced with a negatively charged amino acid, such as glutamate or aspartate, the mutant carriers R388D and R388E accumulate radioactive substrate through an electroneutral process, and abolish the ability of substrate to elicit additional anion currents. The transport domain in the mutant carrier R388D spends a longer time in the inward-facing orientation, pointing to the possibility that the piston-like movement of the transport domain, a critical step during substrate transport, might also be involved in the anion channel function.

Finally, we constructed a concatenated glutamate transporter trimer in Chapter 4, which has functional characteristics similar to the wild type transporter. Using this concatenated construct, we concluded that a single glutamate transporter subunit is capable of transporting substrates and its transport activity is not influenced by the activity of adjacent subunits.

In summary, data presented in this dissertation expand our understanding of domains and conformational changes associated with these domains critical for glutamate transporter dual functions. As is always true in scientific research, our results stimulate more questions than they answer. In the following sections, I will discuss the implication of our proposed mechanisms and areas of future research.

5.1 LARGE COLLECTIVE MOVEMENTS PROVIDE A DIFFERENT VIEW TO UNDERSTAND THE ALTERNATING ACCESS MECHANISM OF GLUTAMATE TRANSPORTERS

The successful crystallization of the archaeal glutamate transporter homolog Glt_{ph} marks a new chapter in studying the structure and function of this protein family, which started decades ago with the discovery of transport systems that use the gradients of ions across the cell membrane to concentrate glutamate. Each structure crystallized under a specific condition (substrate-bound, TBOA-bound and crosslinked) provides tantalizing clues of how these proteins work through the alternate accessing mechanism. This mechanism contends that the transporter isomerizes between an outward-facing and an inward-facing conformation, in which the substrate binding site is alternatively accessible from the external and internal solutions. Two conceptual models have been proposed to fulfill this mechanism by different proteins. The canonical model, called ‘gated pore’, involves the presence of two gates—one external and one internal. The two gates flank the substrate binding site and open sequentially to allow alternate accessing (86). Examples of carriers using this model include the H⁺/Cl⁻ exchanger of the CLC family (131). The ‘rocker-switch’ model, on the other hand, focuses on the rocking movements of protein domains, usually

through a global conformational change that pivots at the substrate binding site (132). Members of the major facilitator superfamily (MFS), such as lactose permease, belong to this category (133). Glutamate transporters seem to integrate both models. In the substrate-bound conformation of Glt_{ph}, the two hairpin loops HP1 and HP2 cradle the substrate binding site. Molecular dynamics simulations show that the HP2 loop opens up within tens of nanoseconds and remains open during 40 ns duration of the simulation (**Figure 15**, Chapter 2 and (89)). Consistent with these results, HP2 is displaced from the substrate binding site in the TBOA-bound conformation of Glt_{ph}, due to the hindrance of the large benzyl group of TBOA (49), supporting the idea that HP2 serves as an external gate. Based on the ‘gated pore’ model, HP1 may serve as the internal gate. Mutagenesis studies exploring the accessibility of residues in this region also support this notion (92). The conformation of Glt_{ph} with HP1 open is not yet available. Steered-MD simulations suggested the existence of two large energy barriers along the putative intracellular substrate pathway aligned by HP1, TM7 and TM8 (134). Such energy barriers will be relieved by the opening of the HP1 gate. On the other hand, initial evidence supporting the ‘rocker-switch’ model was obtained by crosslinking two introduced cysteines in TM2 and HP2. This structure, known as the inward-facing conformation, reveals the inward movement of the transport domain into the cell cytosol that is necessary to expose the substrate binding site intracellularly. The surface representations of the substrate bound and crosslinked structures clearly show the alternate access of the substrate binding site, in a similar manner as that of the ‘rocker-switch’ model in the MFS proteins (**Figure 5D and 5E**). However, the conformational changes adopted by the MFS proteins to achieve ‘rocker-switch’ model are quite different from the piston-like movement of the transport domain, but instead are similar to the large collective movements shown in our study. Thus, the large collective movements provide a

different view of how glutamate transporters achieve their functions through the alternating access mechanism.

5.2 DETERMINATION OF THE FREQUENCY OF THE LARGE COLLECTIVE MOVEMENTS AS A MEANS TO ESTABLISH THEIR PHYSIOLOGICAL RELEVANCE

Our cysteine crosslinking, accessibility and ANM analysis data are consistent with a conformational state of the glutamate transporter in which two subunits move towards each other, while the transport domain of the third subunit starts to move into the cell cytosol. Obtaining a crystal structure of a glutamate transporter trapped in this state will further confirm this prediction. Is this conformation frequently visited during substrate transport or are we just trapping some extreme condition that rarely occurs? These questions can be partially addressed by assessing the frequency of these large collective motions and how close the adjacent subunits might reach. Unfortunately, the ANM analysis is an analytical tool that only predicts the direction of global motions, and the exact amplitude and frequency of these motions cannot be inferred. In addition, current ANM technology does not include plasma membrane and it has been shown that the membrane composition influences the localization and function of glutamate transporters (135). In our study, the second order rate constants calculated for the CuPh-catalyzed functional inhibition are lower than those obtained in the previous work for Shaker K⁺ channels and the *E. coli* D-galactose receptor in which the two crosslinked cysteines are already very proximal in their respective structures (136-137). Instead, both the frequency of the large collective motions and the distance between reactive cysteines contribute to the reaction rate in

the present work and it is not possible to distinguish which has the greatest impact on the rate of bond formation. Based on the ratio of the eigenvalues computed by the ANM for the global modes to the eigenvalues computed for local (nanoseconds) events, we have estimated that the low frequency global modes take place at a time range of micro- to milliseconds. In line with the observation that intersubunit crosslinks readily occur between at least 8 cysteine pairs, we propose that the transporter does transit through the conformation(s) we capture at a relatively high and readily detectable frequency. Recently, the application of fluorescence at the single-molecular level brings to life the dream of watching a single protein molecule functioning in real time, although not at the atomic level. This kind of technique can detect transient intermediates and the sequence of events that might be hidden in population-averaged measured. Using single-molecule FRET, Diez *et al.* (138) successfully identified the step wise rotation of the γ subunit in F_0F_1 -ATP synthase driven by the proton gradient. Zhao *et al.* (139) reported a process whereby substrate binding from the extracellular side of a Neurotransmitter/ Na^+ symporter (LeuT) facilitates intracellular gate opening and substrate release at the intracellular face of the protein. Similar application of single-molecule FRET in glutamate transporters will allow the assessment of the frequency of the large collective movements, and the discovery of other conformational changes required for transporter functions.

5.3 ADDITIONAL CROSSLINKING STUDIES TO ADDRESS THE RELATIONSHIP BETWEEN LARGE COLLECTIVE MOTIONS AND THE PISTON-LIKE MOVEMENT OF THE TRANSPORT DOMAIN

Our results suggest that large collective movements of the glutamate transporter trimer can be functionally linked to the piston-like movement of the transport domain. However, it is currently unknown how they are associated. One intriguing hypothesis is that the large collective movements involving all three transporter subunits may provide the energy required for the transport domain movement, which is shown to occur in the absence of substrate and coupled ions (50). In our study, all of the intersubunit crosslinkable residues are located in the transport domain. Because the transport domain needs to move substantially during substrate transport, the inhibition of uptake could also be a consequence of inability of the transport domain to complete the required movement. Future studies could use similar strategy to crosslink residues in the scaffold domain (TM1-6) between two subunits. This kind of crosslinking would only restrict the large collective movements, but not the piston-like movement of the transport domain. Searching such crosslinkable residues based on the Glt_{ph} structures should proceed with cautions. Although the structural features of the transport domain are similar between the mammalian EAATs and Glt_{ph}, the structure of the scaffold domain in the mammalian EAATs is still an enigma. A recent study explored the proximity of residues between TM5 and TM8 in a rat transporter, GLT-1 (140). The locations of the identified residue pairs, when mapped onto the Glt_{ph} structures, do not agree with the proximity suggested by the crosslinking data. Comparing to Glt_{ph}, the mammalian EAATs have an additional segment of over 50 amino acids in TM4, which contains the N-linked glycosylation sites. The structure of this segment and its relationship to the rest of the transporter are unknown. One study suggested that this segment extends from near the center

of the protein and that the majority of the residues are positioned on the outer perimeter of the protein (62). If this is true, this segment will also influence the ability of large collective movements that bring two adjacent subunits close together. In recent years, significant progress has been made to determine the atomic structure of membrane proteins by crystallography, benefited from a raft of technical advances including the application of high throughput platforms (141). With the advances of other biophysical methods, such as NMR spectroscopy and electron crystallography of 2D crystals in the presence of lipids (142-143), it is conceivable that the atomic structure of mammalian EAATs will be available in the near future, which will help the design of additional crosslinking studies to explore the importance of the large collective movements.

5.4 LARGE COLLECTIVE MOVEMENTS AND THE GLUTAMATE BUFFERING THEORY

In addition to facilitating substrate transport, the large collective movement of the transport trimer may influence glutamatergic signaling in other ways such as changing the buffering capacity of the glutamate transporter. It is no doubt that glutamate transporters play a crucial role in glutamatergic synaptic transmission. Several studies have shown that blocking glutamate transporters increases the amplitude or the decay time of excitatory postsynaptic currents (144-145). However, the cycling time of glutamate transporters, estimated to range from 30 ms to 100 ms (125-126, 146), is significantly slower than the time course of synaptically released glutamate, leading to the hypothesis that transporters remove free glutamate from the cleft very quickly primarily by binding, with transport to following on a longer timescale (147). Supporting

this buffering theory, chemical-kinetic simulations of currents evoked by the fast application of glutamate show that binding of glutamate to the transporters is very rapid, and occurs within 10-100 μ s at typical released glutamate concentrations (34, 125). Another parameter important for the buffering hypothesis is the rate of glutamate dissociation from the substrate binding site, which has been estimate to be about 500 μ s to 2 ms (34, 125). Thus, glutamate also can come off the substrate binding site before being translocated. The three subunits of glutamate transporters form a bowl-shape structure. By measuring the binding and unbinding rates of a potent inhibitor, 4-fluorenyl-L-aspartylamide, in the presence or absence of glutamate, Kavanaugh and colleagues suggested that the three subunits surrounding the large aqueous central cavity restrict diffusion of substrates out of the basin and facilitate transport efficiency (148). We propose that the large collective motions may also help prevent the escape of glutamate from the central basin and ensure the rapid clearance of glutamate from the extracellular space. One strategy to test this hypothesis is to crosslink adjacent subunits with bifunctional crosslinking reagents of different length, which theoretically will change the size and pore of the aqueous central cavity of glutamate transporters and influence the diffusion of substrates. Such studies will also establish how flexible the extracellular domains of glutamate transporters are required to carry out their functions, as has been shown for the lactose permease LacY (149).

5.5 EXPLORING THE ANION PERMEATION PATHWAY

Our study has also identified for the first time two charge-reversing mutants of human EAAT1, R388D and R388E that abolish the substrate-activated anion current, but retain the ability to accumulate radioactive substrate. These mutants, together with others identified in the previous studies by Vandenberg and colleagues, suggest that TM2, TM5 and TM7 form the anion permeation pathway (95, 99). To obtain a complete picture of the anion permeation pathway, cysteine substituted mutants can be generated in this region and modification of the cysteines by thiol-modifying reagents should inhibit the permeation of anions if they line the pathway. This strategy has been successfully applied in $\text{Na}^+\text{-K}^+$ ATPase to identify the cation permeation pathway (150).

5.6 LINKING THE INWARD MOVEMENT OF THE TRANSPORT DOMAIN TO THE ANION CHANNEL ACTIVITY

An interesting hypothesis inferred from the characterization of the mutant carrier R388D is that the inward movement of the transport domain might be required for anion channel gating. Supporting this idea, TBOA inhibits an anion leak current when applied to the intracellular side, suggesting that the inward-facing transporter is also anion conducting (128). How deep does the transport domain have to move to gate the channel? Our results suggest that a small movement might be sufficient because glutamate is able to activate the anion current when two subunits are crosslinked and have limited ability to undergo conformational changes. Further studies can utilize cysteine crosslinking studies to restrict the transport domain at positions along its

trajectory moving towards the cytoplasm and explore the consequence on the anion channel function. In addition, computational simulations might also help to elucidate the importance of the transport domain movement for gating the channel and to identify the anion permeating pathway.

6.0 MATERIALS AND METHODS

6.1 MATERIALS

All chemical were purchased from Sigma-Aldrich unless specified. MTS derivatives were from Toronto Research Chemicals Inc.

6.2 MUTAGENESIS

Mutant transporters were generated based on the appropriate cDNA template using a PCR-based site directed mutagenesis strategy (Stratagene). PCR products were then subcloned into empty vectors to avoid unexpected mutations in vectors and the transporter insertions were sequenced using dye terminator cycle sequencing (PerkinElmer).

6.3 CELL CULTURE AND TRANSFECTION

COS7 cells were maintained in DMEM medium containing 10% fetal bovine serum, 100 U/ml penicillin and 100 U/ml streptomycin in humidified air with 5% CO₂ at 37 °C. Cells were

passaged, plated into 24-well plates or 6-well plates, and then transfected using Fugene 6 (Roche) or *TransIT*®-LT1 (Mirus Bio LLC) according to the manufacturers' guidelines.

6.4 XENOPUS OOCYTE PREPARATION

Female *Xenopus laevis* were ordered from the following commercial vendors (Nasco, Xenopus 1, and Xenopus Express). Late-stage oocytes (stage V-VI) were removed from the ovaries of the adult female. Specifically, the frog was anesthetized in a chilled 0.1% tricaine solution for 15-25 min. Once anesthetized, a one centimeter incision through the skin and abdominal muscle was made to one side of the ventral midline of abdomen. Autoclaved instruments were used for the extraction of ovarian tissue, and harvested oocytes were defolliculated for 60-90 min with 1.5 mg/ml type 2 collagenase (280 U/mg; Worthington Biochemical Corp) in sterile OR₂ solution containing: 82.5 mM NaCl, 2.5 mM KCl, 1 mM MgCl₂, and 5 mM Hepes, pH 7.4. After collagenase treatment, isolated oocytes were rinsed with OR₂ and stored in ND96++ storage solution containing: 96 mM NaCl, 2 mM KCl, 1.8 mM CaCl₂, 1 mM MgCl₂, 5 mM Hepes, 50 µg/ml of gentamicin (Invitrogen) and 100 µg/ml amikacin (Sigma-Aldrich), pH 7.4 at 17°C. Oocytes were checked daily for death and rinsed with fresh ND96++ solution.

6.5 RNA PREPARATION AND OOCYTE INJECTION

cDNA sequence transcribing wild type and mutant transporters were subcloned into an oocyte transcription vector (pOTV) that utilizes *Xenopus* 6-globin 5'- and 3'- untranslated regions

derived from pSP64T to enhance expression (18). pOTV constructs containing transporter cDNAs were usually linearized with BamH I and capped RNAs were transcribed by using T7 RNA polymerase provided in mMessage mMachine kits (Ambion). Approximately 10 ng RNAs (50 nl) were injected into defolliculated stage V to VI oocytes with a microprocessor-controlled nanoliter injector (World Precision Instruments, Inc.). The oocytes were kept at 17 °C for 2-4 days.

6.6 CUPH-CATALYZED DISULFIDE BRIDGE FORMATION AND DTT APPLICATION

COS7 cells expressing either wild type or mutant transporters were washed with phosphate-buffered saline (171 mM NaCl, 10.1 mM Na₂HPO₄, 3.35 mM KCl, and 1.84 mM KH₂PO₄, pH 7.4) and then incubated for 5 min at room temperature with various concentrations of CuPh or 20 mM DL-dithiothreitol (DTT) in phosphate-buffered saline (PBS). CuPh was generated prior to experimental use by mixing CuSO₄ and 1,10-phenanthroline in a 1:2 ratio. For DTT application after CuPh treatment, cells were washed with PBS and incubated with 20 mM DTT in PBS for an additional 5 min. Transporter-expressing oocytes were treated with CuPh or DTT in ND96 solution similarly as described.

6.7 UPTAKE ASSAYS AND TRANSPORT KINETIC MEASUREMENTS

Uptake assays in COS7 cells were usually performed two days post transfection, except for experiments involving concatenated glutamate transporters (3 days post transfection). Briefly, cells were washed with phosphate-buffered saline solution plus 0.1 mM calcium chloride and 1 mM magnesium chloride (PBSCM), and then incubated for 10 min at room temperature with 5 μM L-[^3H] glutamate (50 nM L-[^3H] glutamate and 4.95 μM unlabeled L-glutamate). After washing twice with cold PBSCM, cells were lysed in 0.1% SDS and counted in a Beckman scintillation counter. For V_{max} and K_{m} measurements, cells were washed once with PBSCM and then incubated with 7.8125, 15.625, 31.25, 62.5, 125, 250, 500, 1000 μM L-glutamate containing a fixed ratio of L-[^3H] glutamate (1:10,000) for 10 min at room temperature. V_{max} and K_{m} values were determined using the Michaelis-Menten equation with the software package Prism 4.0 (Graphpad software). Background L-glutamate uptake measured in cells transfected with the pCMV5 vector was subtracted for each condition. Uptake in *Xenopus* oocytes were performed similarly in ND96 solution using 5 μM L-[^3H] glutamate as substrate for 15 min at room temperature.

6.8 CALCULATION OF THE REACTION RATE CONSTANTS

The reaction rate constants for CuPh-catalyzed crosslinking were determined as previously described (90, 151). We plot the fraction of uptake remaining ($F = \text{uptake after}/\text{uptake before}$) as a function of the concentration of CuPh and then fit to a non-linear regression equation for one phase exponential decay, $F = F_{\text{max}} \times \exp^{(-yct)} - F_{\text{min}}$, where t is the incubation time in seconds (5

min), c is the concentration of CuPh reagent, and y is the second order reaction rate constant expressed as ($M^{-1}s^{-1}$).

6.9 CELL SURFACE BIOTINYLATION

Cell surface expression of transiently transfected transporters was assayed as previously described (152). Briefly, cells were washed with PBS and then incubated with 1.5 mg/ml NHS-SS-biotin (Pierce) in biotinylation buffer (2 mM $CaCl_2$, 150 mM NaCl, 10 mM triethanolamine, pH 8.0) for 30 min at 4 °C. For thiol-specific biotinylation assay, cells were treated with 1 mg/ml maleimide-PEO₂-biotin (Thermo Scientific) or 1 mg/ml maleimide-biotin (Vector Labs) in PBS. Following the biotinylation reaction, unreacted NHS-SS-biotin was quenched by the addition of 100 mM glycine. Cells were then lysed on ice in 1 ml lysis buffer containing 1% Triton X-100, 150 mM NaCl, 5 mM EDTA and 50 mM Tris, pH 7.5. The cell lysates were centrifuged at $10,000 \times g$ for 30 min. The supernatants were collected and divided into two portions: a 50 μ l aliquot was mixed with 50 μ l 2 \times SDS sample loading buffer to be used as total input, and the rest 950 μ l was mixed with Ultralink Immobilized NeutrAvidin beads (Pierce) overnight at 4 °C. The beads were then washed and 1.3 \times SDS loading buffer was added. Protein samples were incubated at 37 °C for 30 min before gel electrophoresis.

6.10 OOCYTE MEMBRANE PREPARATION

Oocyte membranes were prepared as described by Kobilka with some modifications (105). Briefly, 6-12 oocytes were transferred into a microcentrifuge tube and pipetted to disrupt the membrane in 200 μ l disruption buffer containing 7.5 mM NaH_2PO_4 , 1 mM EDTA, 10 mM NEM and protease inhibitors (Roche), pH 7.4. The homogenate was then centrifuged for 5 min at 3,000 \times g. The supernatant was transferred to a new tube and centrifuged at 10,000 \times g for 30 min. The yellow yolk was removed with a cotton swab and the collected membranes were dissolved with 40 μ l disruption buffer containing 2% SDS.

6.11 BLUE NATIVE POLYACRYLAMIDE GEL ANALYSIS

BN/PAGE was carried out as described (153). Protein samples were collected from oocytes as described above and then homogenized in 500 μ l of sucrose buffer (250mM sucrose, 20mM imidazole/HCl, pH 7.0). The samples were centrifuged for 10min at 10,000 \times g and the pellets were dissolved in 10% glycerol, 0.2% (wt/vol) Serva blue G, and 2% digitonin before loading onto 4-12% gradient native polyacrylamide gels (Invitrogen). For SDS PAGE, proteins were solubilized in 2% SDS and incubated at 56 °C for 1 hr before electrophoresis.

6.12 WESTERN BLOTTING

Proteins samples were generally separated on 4-12% or 8-6% Tris-glycine gradient polyacrylamide gels (Invitrogen), and transferred to a PVDF membrane (Millipore). Glutamate transporter proteins were probed with a polyclonal antibody against the C-terminus of EAAT1 (1:1,000 dilution) (43), and other proteins such as β -actin were probed with optimized concentrations of antibodies. Proteins were visualized with a horseradish peroxidase (HRP)-conjugated secondary antibody and chemiluminescent detection (PerkinElmer). For protein quantitation, multiple exposures of Western blots were collected, and densitometry of appropriate images was performed using Image J software (NIH).

6.13 ELECTROPHYSIOLOGY

Two-electrode voltage clamp recordings were performed at room temperature using glass microelectrodes filled with 3 M KCl solution (resistance $< 1 \text{ M}\Omega$) and a Ag/AgCl wire and an active bath probe. An Axon Geneclamp 500B amplifier (Axon instruments) was used with Digidata 1322A interface. The pClamp suite of programs were used to control simulation parameters and for data acquisition and analysis. Oocyte recordings were routinely done in either frog Ringers (ND96) or anion substituted Ringers. For anion substitution experiment, NaCl was replaced with equal molar NaNO_3 or NaSCN . We used a 3 M KCl/agar bridge to avoid offset voltages associated with anion buffer changes. To generate current-voltage (I-V) relationships, steady state currents were elicited by 150 ms voltage steps from a holding potential of -60 mV or 0 mV over the range of -100 to +60 mV in 10 mV increments.

6.14 MOLECULAR DYNAMICS SIMULATIONS

We simulated the dynamics of Glt_{ph} (PDB ID: 1XFH) embedded in a bilayer-solvent environment using the GROMACS program 3.2.1 with the Gromacs force field (154). The membrane consisted of 353 1-palmitoyl-2-oleoylphosphatidyl ethanolamine molecules, and the system was solvated with ~23,000 water molecules. Missing atoms on the side chains of some residues in the crystal structure of GltPh were constructed using Xplor (154). Constant number of particles (N), pressure (P), and temperature (T) conditions, with a pressure of 1 bar and a coupling constant of $\tau_p = 1.0$ ps, were adopted. Water, protein, and lipid molecules were coupled separately to a temperature bath at 310 K using a coupling constant of $\tau_t = 0.1$ ps. The van der Waals interactions were calculated using a cutoff distance of 10 Å, and long range electrostatic interactions were calculated using the particle mesh Ewald method. The single point charge model was adopted for water molecules as a plausible model for lipid simulations, along with the lipid parameters used for other membrane proteins (155). Simulations were preceded by energy minimization with steepest descent followed by equilibration periods of 200 ps during which the protein backbone atoms were restrained by harmonic potentials so as to allow for the packing of lipid molecules around the protein. The constraints were then removed for the productive runs.

6.15 ANISOTROPIC NETWORK MODEL (ANM) ANALYSIS

ANM analysis is a coarse-grained normal mode analysis, which models the structure as an elastic network with individual nodes corresponding to the α -carbons of the protein. Inter-residue interactions are described by harmonic potentials with uniform spring constant γ . For a protein of

N residues, ANM predicts an ensemble of $3N-6$ modes of motion. The motion along mode k changes the position of residue i as

$$\mathbf{R}_i^{(k)}(\pm s) = \mathbf{R}_i^0 \pm s \lambda_k^{(-1/2)} [\mathbf{u}_k]_i \quad (1)$$

where \mathbf{R}_i^0 is the position vector in the original (*i.e.*, X-ray) structure, s is a parameter that scales the size of the deformation induced by mode k , $[\mathbf{u}_k]_i$ is the i^{th} super element (3-dimensional vector) of the k^{th} eigenvector \mathbf{u}_k (a $3N$ -dimensional normalized vector) of the $3N \times 3N$ Hessian matrix \mathbf{H} , and λ_k is the corresponding eigenvalue (3-4). $[\mathbf{u}_k]_i$ describes the motion of residue i along the k^{th} principal/normal coordinate, and $\lambda_k^{(-1/2)}$ scales with the frequency of the k^{th} mode, such that lower frequency modes make larger contributions to $\mathbf{R}_i^{(k)}$. The lowest frequency modes, also called the softest modes, define the mechanisms of global reconfiguration intrinsically favored by the molecular architecture under physiological conditions. Here we carried out the ANM with default parameters based on the Glt_{ph} outward-facing structure (PDB ID: 1XFH), inward-facing structure (PDB ID: 3KBC), and models constructed for intermediate states (see below).

6.16 MODELING THE STRUCTURE AND DYNAMICS OF INTERMEDIATE STATES

Intermediate structures are constructed by assembling the individual inward-facing or outward-facing subunits upon superimposition of their trimerization domains. The difference between any pair of structures (including the experimentally observed all-outward or all-inward states, and the modeled/assembled intermediate states) is quantitatively described by a $3N$ -dimensional deformation vector \mathbf{d} , evaluated by overlaying the two structures to remove rigid-body

translations and rotations. The correlation between the k^{th} mode of motion predicted by the ANM and the deformation \mathbf{d} is given by $\cos(\mathbf{u}_k, \mathbf{d}) = \mathbf{u}_k \cdot \mathbf{d}/|\mathbf{d}|$ where $|\mathbf{d}|$ is the magnitude of \mathbf{d} , and \mathbf{u}_k is the k^{th} eigenvector calculated for the starting structure. The *cumulative overlap* between a subset of soft modes (m of them) and the observed/modeled structural change \mathbf{d} is given by

$$O_{cum}(m) = [\sum_{k=1}^m \cos^2(\mathbf{u}_k, \mathbf{d})]^{1/2} \quad (2)$$

By definition, $O_{cum}(m)$ sums up to unity for $m = 3N-6$, because the $3N-6$ eigenvectors form an orthonormal basis set that spans the space of conformational changes. In the extreme case of completely random modes, which are uncorrelated with \mathbf{d} , $O_{cum}(m) = (m/3N-6)^{1/2}$. This relationship defines the control curves in panels C and D of Figure 6. High cumulative overlaps achieved by a small subset of low frequency modes indicate the accessibility of the structural changes via soft (energetically favorable) motions.

6.17 DATA ANALYSES

All experiments reported were repeated a minimum of three times with similar results. Data were presented as mean \pm SEM and were analyzed using student's t-test or one-way ANOVA followed by Bonferroni's multiple comparisons test using the software package Prism 4.0 (Graphpad software). $p < 0.05$ was considered to be statistically significant.

APPENDIX A

PUBLISHED PAPERS

Shrivastava IH, **Jiang J**, Amara SG, Bahar I. Time-resolved mechanism of extracellular gate opening and substrate binding in a glutamate transporter. *J Biol Chem*. 2008;283(42):28680-90.

Jiang J, Amara SG. New views of glutamate transporter structure and function: advances and challenges. *Neuropharmacology*. 2011;60(1):172-81.

Jiang J, Shrivastava IH, Watts SD, Bahar I, Amara SG. Large collective motions regulate the functional properties of glutamate transporter trimers. *Proc. Natl. Acad. Sci. U. S. A.* Accepted

BIBLIOGRAPHY

1. Danbolt NC (2001) Glutamate uptake. (Translated from eng) *Prog. Neurobiol.* 65(1):1-105 (in eng).
2. Bergles DE, Diamond JS, & Jahr CE (1999) Clearance of glutamate inside the synapse and beyond. (Translated from eng) *Curr. Opin. Neurobiol.* 9(3):293-298 (in eng).
3. Grewer C & Rauen T (2005) Electrogenic glutamate transporters in the CNS: molecular mechanism, pre-steady-state kinetics, and their impact on synaptic signaling. (Translated from eng) *J. Membr. Biol.* 203(1):1-20 (in eng).
4. Hinoi E, Takarada T, Tsuchihashi Y, & Yoneda Y (2005) Glutamate transporters as drug targets. (Translated from eng) *Curr Drug Targets CNS Neurol Disord* 4(2):211-220 (in eng).
5. Robinson MB, Hunter-Ensor M, & Sinor J (1991) Pharmacologically distinct sodium-dependent L-[3H]glutamate transport processes in rat brain. (Translated from eng) *Brain Res.* 544(2):196-202 (in eng).
6. Fletcher EJ & Johnston GA (1991) Regional heterogeneity of L-glutamate and L-aspartate high-affinity uptake systems in the rat CNS. (Translated from eng) *J. Neurochem.* 57(3):911-914 (in eng).
7. Pines G, *et al.* (1992) Cloning and expression of a rat brain L-glutamate transporter. (Translated from eng) *Nature* 360(6403):464-467 (in eng).
8. Kanai Y & Hediger MA (1992) Primary structure and functional characterization of a high-affinity glutamate transporter. (Translated from eng) *Nature* 360(6403):467-471 (in eng).
9. Storck T, Schulte S, Hofmann K, & Stoffel W (1992) Structure, expression, and functional analysis of a Na(+)-dependent glutamate/aspartate transporter from rat brain. (Translated from eng) *Proc. Natl. Acad. Sci. U. S. A.* 89(22):10955-10959 (in eng).
10. Arriza JL, Eliasof S, Kavanaugh MP, & Amara SG (1997) Excitatory amino acid transporter 5, a retinal glutamate transporter coupled to a chloride conductance. (Translated from eng) *Proc. Natl. Acad. Sci. U. S. A.* 94(8):4155-4160 (in eng).
11. Fairman WA, Vandenberg RJ, Arriza JL, Kavanaugh MP, & Amara SG (1995) An excitatory amino-acid transporter with properties of a ligand-gated chloride channel. (Translated from eng) *Nature* 375(6532):599-603 (in eng).
12. Arriza JL, *et al.* (1994) Functional comparisons of three glutamate transporter subtypes cloned from human motor cortex. (Translated from eng) *J. Neurosci.* 14(9):5559-5569 (in eng).
13. Slotboom DJ, Konings WN, & Lolkema JS (1999) Structural features of the glutamate transporter family. (Translated from eng) *Microbiol. Mol. Biol. Rev.* 63(2):293-307 (in eng).

14. Tolner B, Poolman B, & Konings WN (1992) Characterization and functional expression in *Escherichia coli* of the sodium/proton/glutamate symport proteins of *Bacillus stearothermophilus* and *Bacillus caldotenax*. (Translated from eng) *Mol. Microbiol.* 6(19):2845-2856 (in eng).
15. Engelke T, Jording D, Kapp D, & Puhler A (1989) Identification and sequence analysis of the *Rhizobium meliloti* *dctA* gene encoding the C4-dicarboxylate carrier. (Translated from eng) *J. Bacteriol.* 171(10):5551-5560 (in eng).
16. Tolner B, Poolman B, Wallace B, & Konings WN (1992) Revised nucleotide sequence of the *gltP* gene, which encodes the proton-glutamate-aspartate transport protein of *Escherichia coli* K-12. (Translated from eng) *J. Bacteriol.* 174(7):2391-2393 (in eng).
17. Utsunomiya-Tate N, Endou H, & Kanai Y (1996) Cloning and functional characterization of a system ASC-like Na⁺-dependent neutral amino acid transporter. (Translated from eng) *J. Biol. Chem.* 271(25):14883-14890 (in eng).
18. Arriza JL, *et al.* (1993) Cloning and expression of a human neutral amino acid transporter with structural similarity to the glutamate transporter gene family. (Translated from eng) *J. Biol. Chem.* 268(21):15329-15332 (in eng).
19. Stallcup WB, Bulloch K, & Baetge EE (1979) Coupled transport of glutamate and sodium in a cerebellar nerve cell line. (Translated from eng) *J. Neurochem.* 32(1):57-65 (in eng).
20. Balcar VJ & Johnston GA (1972) Glutamate uptake by brain slices and its relation to the depolarization of neurones by acidic amino acids. (Translated from eng) *J. Neurobiol.* 3(4):295-301 (in eng).
21. Erecinska M, Wantorsky D, & Wilson DF (1983) Aspartate transport in synaptosomes from rat brain. (Translated from eng) *J. Biol. Chem.* 258(15):9069-9077 (in eng).
22. Kanner BI & Sharon I (1978) Active transport of L-glutamate by membrane vesicles isolated from rat brain. (Translated from eng) *Biochemistry (Mosc).* 17(19):3949-3953 (in eng).
23. Zerangue N & Kavanaugh MP (1996) Flux coupling in a neuronal glutamate transporter. (Translated from eng) *Nature* 383(6601):634-637 (in eng).
24. Levy LM, Warr O, & Attwell D (1998) Stoichiometry of the glial glutamate transporter GLT-1 expressed inducibly in a Chinese hamster ovary cell line selected for low endogenous Na⁺-dependent glutamate uptake. (Translated from eng) *J. Neurosci.* 18(23):9620-9628 (in eng).
25. Sarantis M, Everett K, & Attwell D (1988) A presynaptic action of glutamate at the cone output synapse. (Translated from eng) *Nature* 332(6163):451-453 (in eng).
26. Grant GB & Dowling JE (1995) A glutamate-activated chloride current in cone-driven ON bipolar cells of the white perch retina. (Translated from eng) *J. Neurosci.* 15(5 Pt 2):3852-3862 (in eng).
27. Picaud SA, Larsson HP, Grant GB, Lecar H, & Werblin FS (1995) Glutamate-gated chloride channel with glutamate-transporter-like properties in cone photoreceptors of the tiger salamander. (Translated from eng) *J. Neurophysiol.* 74(4):1760-1771 (in eng).
28. Wadiche JI, Amara SG, & Kavanaugh MP (1995) Ion fluxes associated with excitatory amino acid transport. (Translated from eng) *Neuron* 15(3):721-728 (in eng).
29. Wadiche JI & Kavanaugh MP (1998) Macroscopic and microscopic properties of a cloned glutamate transporter/chloride channel. (Translated from eng) *J. Neurosci.* 18(19):7650-7661 (in eng).

30. Zerangue N & Kavanaugh MP (1996) ASCT-1 is a neutral amino acid exchanger with chloride channel activity. (Translated from eng) *J. Biol. Chem.* 271(45):27991-27994 (in eng).
31. Broer A, Wagner C, Lang F, & Broer S (2000) Neutral amino acid transporter ASCT2 displays substrate-induced Na⁺ exchange and a substrate-gated anion conductance. (Translated from eng) *Biochem. J.* 346 Pt 3:705-710 (in eng).
32. Ryan RM & Mindell JA (2007) The uncoupled chloride conductance of a bacterial glutamate transporter homolog. (Translated from eng) *Nat Struct Mol Biol* 14(5):365-371 (in eng).
33. Otis TS & Jahr CE (1998) Anion currents and predicted glutamate flux through a neuronal glutamate transporter. (Translated from eng) *J. Neurosci.* 18(18):7099-7110 (in eng).
34. Grewer C, Watzke N, Wiessner M, & Rauen T (2000) Glutamate translocation of the neuronal glutamate transporter EAAC1 occurs within milliseconds. (Translated from eng) *Proc. Natl. Acad. Sci. U. S. A.* 97(17):9706-9711 (in eng).
35. Grewer C & Grabsch E (2004) New inhibitors for the neutral amino acid transporter ASCT2 reveal its Na⁺-dependent anion leak. (Translated from eng) *J Physiol* 557(Pt 3):747-759 (in eng).
36. Veruki ML, Morkve SH, & Hartveit E (2006) Activation of a presynaptic glutamate transporter regulates synaptic transmission through electrical signaling. (Translated from eng) *Nat. Neurosci.* 9(11):1388-1396 (in eng).
37. Wahle S & Stoffel W (1996) Membrane topology of the high-affinity L-glutamate transporter (GLAST-1) of the central nervous system. (Translated from eng) *J. Cell Biol.* 135(6 Pt 2):1867-1877 (in eng).
38. Conradt M, Storck T, & Stoffel W (1995) Localization of N-glycosylation sites and functional role of the carbohydrate units of GLAST-1, a cloned rat brain L-glutamate/L-aspartate transporter. (Translated from eng) *Eur. J. Biochem.* 229(3):682-687 (in eng).
39. Jording D & Puhler A (1993) The membrane topology of the *Rhizobium meliloti* C4-dicarboxylate permease (DctA) as derived from protein fusions with *Escherichia coli* K12 alkaline phosphatase (PhoA) and beta-galactosidase (LacZ). (Translated from eng) *Mol. Gen. Genet.* 241(1-2):106-114 (in eng).
40. Slotboom DJ, Lolkema JS, & Konings WN (1996) Membrane topology of the C-terminal half of the neuronal, glial, and bacterial glutamate transporter family. (Translated from eng) *J. Biol. Chem.* 271(49):31317-31321 (in eng).
41. Seal RP, Leighton BH, & Amara SG (1998) Transmembrane topology mapping using biotin-containing sulfhydryl reagents. (Translated from eng) *Methods Enzymol.* 296:318-331 (in eng).
42. Seal RP, Leighton BH, & Amara SG (2000) A model for the topology of excitatory amino acid transporters determined by the extracellular accessibility of substituted cysteines. (Translated from eng) *Neuron* 25(3):695-706 (in eng).
43. Seal RP & Amara SG (1998) A reentrant loop domain in the glutamate carrier EAAT1 participates in substrate binding and translocation. (Translated from eng) *Neuron* 21(6):1487-1498 (in eng).
44. Grunewald M & Kanner BI (2000) The accessibility of a novel reentrant loop of the glutamate transporter GLT-1 is restricted by its substrate. (Translated from eng) *J. Biol. Chem.* 275(13):9684-9689 (in eng).

45. Grunewald M, Bendahan A, & Kanner BI (1998) Biotinylation of single cysteine mutants of the glutamate transporter GLT-1 from rat brain reveals its unusual topology. (Translated from eng) *Neuron* 21(3):623-632 (in eng).
46. Slotboom DJ, Konings WN, & Lolkema JS (2001) Cysteine-scanning mutagenesis reveals a highly amphipathic, pore-lining membrane-spanning helix in the glutamate transporter GltT. (Translated from eng) *J. Biol. Chem.* 276(14):10775-10781 (in eng).
47. Slotboom DJ, Sobczak I, Konings WN, & Lolkema JS (1999) A conserved serine-rich stretch in the glutamate transporter family forms a substrate-sensitive reentrant loop. (Translated from eng) *Proc. Natl. Acad. Sci. U. S. A.* 96(25):14282-14287 (in eng).
48. Yernool D, Boudker O, Jin Y, & Gouaux E (2004) Structure of a glutamate transporter homologue from *Pyrococcus horikoshii*. (Translated from eng) *Nature* 431(7010):811-818 (in eng).
49. Boudker O, Ryan RM, Yernool D, Shimamoto K, & Gouaux E (2007) Coupling substrate and ion binding to extracellular gate of a sodium-dependent aspartate transporter. (Translated from eng) *Nature* 445(7126):387-393 (in eng).
50. Reyes N, Ginter C, & Boudker O (2009) Transport mechanism of a bacterial homologue of glutamate transporters. (Translated from eng) *Nature* 462(7275):880-885 (in eng).
51. Brocke L, Bendahan A, Grunewald M, & Kanner BI (2002) Proximity of two oppositely oriented reentrant loops in the glutamate transporter GLT-1 identified by paired cysteine mutagenesis. (Translated from eng) *J. Biol. Chem.* 277(6):3985-3992 (in eng).
52. Leighton BH, Seal RP, Watts SD, Skyba MO, & Amara SG (2006) Structural rearrangements at the translocation pore of the human glutamate transporter, EAAT1. (Translated from eng) *J. Biol. Chem.* 281(40):29788-29796 (in eng).
53. Qu S & Kanner BI (2008) Substrates and non-transportable analogues induce structural rearrangements at the extracellular entrance of the glial glutamate transporter GLT-1/EAAT2. (Translated from eng) *J. Biol. Chem.* 283(39):26391-26400 (in eng).
54. Haugeto O, *et al.* (1996) Brain glutamate transporter proteins form homomultimers. (Translated from eng) *J. Biol. Chem.* 271(44):27715-27722 (in eng).
55. Yernool D, Boudker O, Folta-Stogniew E, & Gouaux E (2003) Trimeric subunit stoichiometry of the glutamate transporters from *Bacillus caldotenax* and *Bacillus stearothermophilus*. (Translated from eng) *Biochemistry (Mosc)*. 42(44):12981-12988 (in eng).
56. Grewer C, *et al.* (2005) Individual subunits of the glutamate transporter EAAC1 homotrimer function independently of each other. (Translated from eng) *Biochemistry (Mosc)*. 44(35):11913-11923 (in eng).
57. Gendreau S, *et al.* (2004) A trimeric quaternary structure is conserved in bacterial and human glutamate transporters. (Translated from eng) *J. Biol. Chem.* 279(38):39505-39512 (in eng).
58. Eskandari S, Kreman M, Kavanaugh MP, Wright EM, & Zampighi GA (2000) Pentameric assembly of a neuronal glutamate transporter. (Translated from eng) *Proc. Natl. Acad. Sci. U. S. A.* 97(15):8641-8646 (in eng).
59. Nothmann D, *et al.* (2010) Hetero-oligomerization of neuronal glutamate transporters. (Translated from Eng) *J. Biol. Chem.* (in Eng).
60. Furuta A, Martin LJ, Lin CL, Dykes-Hoberg M, & Rothstein JD (1997) Cellular and synaptic localization of the neuronal glutamate transporters excitatory amino acid transporter 3 and 4. (Translated from eng) *Neuroscience* 81(4):1031-1042 (in eng).

61. Bar-Peled O, *et al.* (1997) Distribution of glutamate transporter subtypes during human brain development. (Translated from eng) *J. Neurochem.* 69(6):2571-2580 (in eng).
62. Koch HP, Hubbard JM, & Larsson HP (2007) Voltage-independent sodium-binding events reported by the 4B-4C loop in the human glutamate transporter EAAT3. (Translated from Eng) *J. Biol. Chem.* 282:24547-24553 (in Eng).
63. Conradt M & Stoffel W (1995) Functional analysis of the high affinity, Na(+)-dependent glutamate transporter GLAST-1 by site-directed mutagenesis. (Translated from eng) *J. Biol. Chem.* 270(42):25207-25212 (in eng).
64. Bendahan A, Armon A, Madani N, Kavanaugh MP, & Kanner BI (2000) Arginine 447 plays a pivotal role in substrate interactions in a neuronal glutamate transporter. (Translated from eng) *J. Biol. Chem.* 275(48):37436-37442 (in eng).
65. Teichman S & Kanner BI (2007) Aspartate-444 is essential for productive substrate interactions in a neuronal glutamate transporter. (Translated from eng) *J. Gen. Physiol.* 129(6):527-539 (in eng).
66. Zhang Y, Bendahan A, Zarbiv R, Kavanaugh MP, & Kanner BI (1998) Molecular determinant of ion selectivity of a (Na⁺ + K⁺)-coupled rat brain glutamate transporter. (Translated from eng) *Proc. Natl. Acad. Sci. U. S. A.* 95(2):751-755 (in eng).
67. Grunewald M & Kanner B (1995) Conformational changes monitored on the glutamate transporter GLT-1 indicate the existence of two neurotransmitter-bound states. (Translated from eng) *J. Biol. Chem.* 270(28):17017-17024 (in eng).
68. Borre L & Kanner BI (2001) Coupled, but not uncoupled, fluxes in a neuronal glutamate transporter can be activated by lithium ions. (Translated from eng) *J. Biol. Chem.* 276(44):40396-40401 (in eng).
69. Zhang Y & Kanner BI (1999) Two serine residues of the glutamate transporter GLT-1 are crucial for coupling the fluxes of sodium and the neurotransmitter. (Translated from eng) *Proc. Natl. Acad. Sci. U. S. A.* 96(4):1710-1715 (in eng).
70. Tao Z, Zhang Z, & Grewer C (2006) Neutralization of the aspartic acid residue Asp-367, but not Asp-454, inhibits binding of Na⁺ to the glutamate-free form and cycling of the glutamate transporter EAAC1. (Translated from eng) *J. Biol. Chem.* 281(15):10263-10272 (in eng).
71. Tao Z, *et al.* (2010) Mechanism of cation binding to the glutamate transporter EAAC1 probed with mutation of the conserved amino acid residue T101. (Translated from Eng) *J. Biol. Chem.* (in Eng).
72. Tao Z & Grewer C (2007) Cooperation of the conserved aspartate 439 and bound amino acid substrate is important for high-affinity Na⁺ binding to the glutamate transporter EAAC1. (Translated from eng) *J. Gen. Physiol.* 129(4):331-344 (in eng).
73. Holley DC & Kavanaugh MP (2009) Interactions of alkali cations with glutamate transporters. (Translated from eng) *Philos. Trans. R. Soc. Lond. B. Biol. Sci.* 364(1514):155-161 (in eng).
74. Shrivastava IH, Jiang J, Amara SG, & Bahar I (2008) Time-resolved mechanism of extracellular gate opening and substrate binding in a glutamate transporter. (Translated from eng) *J. Biol. Chem.* 283(42):28680-28690 (in eng).
75. Larsson HP, *et al.* (2010) Evidence for a third sodium-binding site in glutamate transporters suggests an ion/substrate coupling model. (Translated from eng) *Proc. Natl. Acad. Sci. U. S. A.* 107(31):13912-13917 (in eng).

76. Huang Z & Tajkhorshid E (2010) Identification of the third Na⁺ site and the sequence of extracellular binding events in the glutamate transporter. (Translated from eng) *Biophys. J.* 99(5):1416-1425 (in eng).
77. Rosental N, Bendahan A, & Kanner BI (2006) Multiple consequences of mutating two conserved beta-bridge forming residues in the translocation cycle of a neuronal glutamate transporter. (Translated from eng) *J. Biol. Chem.* 281(38):27905-27915 (in eng).
78. Tao Z, *et al.* (2010) Mechanism of cation binding to the glutamate transporter EAAC1 probed with mutation of the conserved amino acid residue Thr101. (Translated from eng) *J. Biol. Chem.* 285(23):17725-17733 (in eng).
79. Kavanaugh MP, Bendahan A, Zerangue N, Zhang Y, & Kanner BI (1997) Mutation of an amino acid residue influencing potassium coupling in the glutamate transporter GLT-1 induces obligate exchange. (Translated from eng) *J. Biol. Chem.* 272(3):1703-1708 (in eng).
80. Raunser S, *et al.* (2006) Structure and function of prokaryotic glutamate transporters from *Escherichia coli* and *Pyrococcus horikoshii*. (Translated from eng) *Biochemistry (Mosc.)* 45(42):12796-12805 (in eng).
81. Tao Z, Gameiro A, & Grewer C (2008) Thallium ions can replace both sodium and potassium ions in the glutamate transporter excitatory amino acid carrier 1. (Translated from eng) *Biochemistry (Mosc.)* 47(48):12923-12930 (in eng).
82. Teichman S, Qu S, & Kanner BI (2009) The equivalent of a thallium binding residue from an archeal homolog controls cation interactions in brain glutamate transporters. (Translated from eng) *Proc. Natl. Acad. Sci. U. S. A.* 106(34):14297-14302 (in eng).
83. Fontana AC, *et al.* (2007) Enhancing glutamate transport: mechanism of action of Parawixin1, a neuroprotective compound from *Parawixia bistriata* spider venom. (Translated from eng) *Mol. Pharmacol.* 72(5):1228-1237 (in eng).
84. Watzke N, Rauen T, Bamberg E, & Grewer C (2000) On the mechanism of proton transport by the neuronal excitatory amino acid carrier 1. (Translated from eng) *J. Gen. Physiol.* 116(5):609-622 (in eng).
85. Grewer C, Watzke N, Rauen T, & Bicho A (2003) Is the glutamate residue Glu-373 the proton acceptor of the excitatory amino acid carrier 1? (Translated from eng) *J. Biol. Chem.* 278(4):2585-2592 (in eng).
86. Jardetzky O (1966) Simple allosteric model for membrane pumps. (Translated from eng) *Nature* 211(5052):969-970 (in eng).
87. Larsson HP, Tzingounis AV, Koch HP, & Kavanaugh MP (2004) Fluorometric measurements of conformational changes in glutamate transporters. (Translated from eng) *Proc. Natl. Acad. Sci. U. S. A.* 101(11):3951-3956 (in eng).
88. Mim C, Tao Z, & Grewer C (2007) Two conformational changes are associated with glutamate translocation by the glutamate transporter EAAC1. (Translated from eng) *Biochemistry (Mosc.)* 46(31):9007-9018 (in eng).
89. Huang Z & Tajkhorshid E (2008) Dynamics of the Extracellular Gate and Ion-Substrate Coupling in the Glutamate Transporter. (Translated from Eng) *Biophys. J.* (in Eng).
90. Leighton BH, Seal RP, Shimamoto K, & Amara SG (2002) A hydrophobic domain in glutamate transporters forms an extracellular helix associated with the permeation pathway for substrates. (Translated from eng) *J. Biol. Chem.* 277(33):29847-29855 (in eng).

91. Grunewald M, Menaker D, & Kanner BI (2002) Cysteine-scanning mutagenesis reveals a conformationally sensitive reentrant pore-loop in the glutamate transporter GLT-1. (Translated from eng) *J. Biol. Chem.* 277(29):26074-26080 (in eng).
92. Shlaifer I & Kanner BI (2007) Conformationally Sensitive Reactivity to Permeant Sulfhydryl Reagents of Cysteine Residues Engineered into Helical Hairpin 1 of the Glutamate Transporter GLT-1. (Translated from eng) *Mol. Pharmacol.* 71(5):1341-1348 (in eng).
93. Koch HP & Larsson HP (2005) Small-scale molecular motions accomplish glutamate uptake in human glutamate transporters. (Translated from eng) *J. Neurosci.* 25(7):1730-1736 (in eng).
94. Crisman TJ, Qu S, Kanner BI, & Forrest LR (2009) Inward-facing conformation of glutamate transporters as revealed by their inverted-topology structural repeats. (Translated from Eng) *Proc. Natl. Acad. Sci. U. S. A.* 106(49):20752-20757 (in Eng).
95. Ryan RM, Mitrovic AD, & Vandenberg RJ (2004) The chloride permeation pathway of a glutamate transporter and its proximity to the glutamate translocation pathway. (Translated from eng) *J. Biol. Chem.* 279(20):20742-20751 (in eng).
96. Seal RP, Shigeri Y, Eliasof S, Leighton BH, & Amara SG (2001) Sulfhydryl modification of V449C in the glutamate transporter EAAT1 abolishes substrate transport but not the substrate-gated anion conductance. (Translated from eng) *Proc. Natl. Acad. Sci. U. S. A.* 98(26):15324-15329 (in eng).
97. Borre L, Kavanaugh MP, & Kanner BI (2002) Dynamic equilibrium between coupled and uncoupled modes of a neuronal glutamate transporter. (Translated from eng) *J. Biol. Chem.* 277(16):13501-13507 (in eng).
98. Ryan RM & Vandenberg RJ (2002) Distinct conformational states mediate the transport and anion channel properties of the glutamate transporter EAAT-1. (Translated from eng) *J. Biol. Chem.* 277(16):13494-13500 (in eng).
99. Huang S & Vandenberg RJ (2007) Mutations in Transmembrane Domains 5 and 7 of the Human Excitatory Amino Acid Transporter 1 Affect the Substrate-Activated Anion Channel. (Translated from Eng) *Biochemistry (Mosc).* 46:9685-9692 (in Eng).
100. Chen TY & Hwang TC (2008) CLC-0 and CFTR: chloride channels evolved from transporters. (Translated from eng) *Physiol. Rev.* 88(2):351-387 (in eng).
101. Dutzler R, Campbell EB, Cadene M, Chait BT, & MacKinnon R (2002) X-ray structure of a ClC chloride channel at 3.0 Å reveals the molecular basis of anion selectivity. (Translated from eng) *Nature* 415(6869):287-294 (in eng).
102. Vandenberg RJ, Huang S, & Ryan RM (2008) Slips, leaks and channels in glutamate transporters. (Translated from eng) *Channels (Austin)* 2(1):51-58 (in eng).
103. Henzler-Wildman K & Kern D (2007) Dynamic personalities of proteins. (Translated from eng) *Nature* 450(7172):964-972 (in eng).
104. Vandenberg RJ (2006) Mutational analysis of glutamate transporters. (Translated from eng) *Handb Exp Pharmacol* (175):113-135 (in eng).
105. Kobilka BK (1990) The role of cytosolic and membrane factors in processing of the human beta-2 adrenergic receptor following translocation and glycosylation in a cell-free system. (Translated from eng) *J. Biol. Chem.* 265(13):7610-7618 (in eng).
106. Raunser S, *et al.* (2006) Heterologously expressed GLT-1 associates in approximately 200-nm protein-lipid islands. (Translated from eng) *Biophys. J.* 91(10):3718-3726 (in eng).

107. Katz BA & Kossiakoff A (1986) The crystallographically determined structures of atypical strained disulfides engineered into subtilisin. (Translated from eng) *J. Biol. Chem.* 261(33):15480-15485 (in eng).
108. Falke JJ, *et al.* (1988) Structure of a bacterial sensory receptor. A site-directed sulfhydryl study. (Translated from eng) *J. Biol. Chem.* 263(29):14850-14858 (in eng).
109. Jiang J & Amara SG (2011) New views of glutamate transporter structure and function: advances and challenges. (Translated from eng) *Neuropharmacology* 60(1):172-181 (in eng).
110. Salsbury FR, Jr. (2010) Molecular dynamics simulations of protein dynamics and their relevance to drug discovery. (Translated from eng) *Curr Opin Pharmacol* 10(6):738-744 (in eng).
111. Atilgan AR, *et al.* (2001) Anisotropy of fluctuation dynamics of proteins with an elastic network model. (Translated from eng) *Biophys. J.* 80(1):505-515 (in eng).
112. Eyal E, Yang LW, & Bahar I (2006) Anisotropic network model: systematic evaluation and a new web interface. (Translated from eng) *Bioinformatics* 22(21):2619-2627 (in eng).
113. Bahar I, Lezon TR, Bakan A, & Shrivastava IH (2010) Normal mode analysis of biomolecular structures: functional mechanisms of membrane proteins. (Translated from eng) *Chem. Rev.* 110(3):1463-1497 (in eng).
114. Bahar I, Lezon TR, Yang LW, & Eyal E (2010) Global dynamics of proteins: bridging between structure and function. (Translated from eng) *Annu Rev Biophys* 39:23-42 (in eng).
115. Koch HP, Brown RL, & Larsson HP (2007) The glutamate-activated anion conductance in excitatory amino acid transporters is gated independently by the individual subunits. (Translated from eng) *J. Neurosci.* 27(11):2943-2947 (in eng).
116. Cui Q & Bahar I (2006) *Normal Mode Analysis: Theory and Applications to Biological and Chemical Systems*, by Chapman & Hall/CRC.
117. Bahar I (2010) On the functional significance of soft modes predicted by coarse-grained models for membrane proteins. (Translated from eng) *J. Gen. Physiol.* 135(6):563-573 (in eng).
118. Gordon SE, Varnum MD, & Zagotta WN (1997) Direct interaction between amino- and carboxyl-terminal domains of cyclic nucleotide-gated channels. (Translated from eng) *Neuron* 19(2):431-441 (in eng).
119. Groeneveld M & Slotboom DJ (2007) Rigidity of the subunit interfaces of the trimeric glutamate transporter GltT during translocation. (Translated from eng) *J. Mol. Biol.* 372(3):565-570 (in eng).
120. Bahar I, Chennubhotla C, & Tobi D (2007) Intrinsic dynamics of enzymes in the unbound state and relation to allosteric regulation. (Translated from eng) *Curr. Opin. Struct. Biol.* 17(6):633-640 (in eng).
121. Tobi D & Bahar I (2005) Structural changes involved in protein binding correlate with intrinsic motions of proteins in the unbound state. (Translated from eng) *Proc. Natl. Acad. Sci. U. S. A.* 102(52):18908-18913 (in eng).
122. Leary GP, Stone EF, Holley DC, & Kavanaugh MP (2007) The glutamate and chloride permeation pathways are colocalized in individual neuronal glutamate transporter subunits. (Translated from eng) *J. Neurosci.* 27(11):2938-2942 (in eng).

123. Torres-Salazar D & Fahlke C (2006) Intersubunit interactions in EAAT4 glutamate transporters. (Translated from eng) *J. Neurosci.* 26(28):7513-7522 (in eng).
124. Otis TS & Kavanaugh MP (2000) Isolation of current components and partial reaction cycles in the glial glutamate transporter EAAT2. (Translated from eng) *J. Neurosci.* 20(8):2749-2757 (in eng).
125. Bergles DE, Tzingounis AV, & Jahr CE (2002) Comparison of coupled and uncoupled currents during glutamate uptake by GLT-1 transporters. (Translated from eng) *J. Neurosci.* 22(23):10153-10162 (in eng).
126. Watzke N, Bamberg E, & Grewer C (2001) Early intermediates in the transport cycle of the neuronal excitatory amino acid carrier EAAC1. (Translated from eng) *J. Gen. Physiol.* 117(6):547-562 (in eng).
127. Melzer N, Biela A, & Fahlke C (2003) Glutamate modifies ion conduction and voltage-dependent gating of excitatory amino acid transporter-associated anion channels. (Translated from eng) *J. Biol. Chem.* 278(50):50112-50119 (in eng).
128. Watzke N & Grewer C (2001) The anion conductance of the glutamate transporter EAAC1 depends on the direction of glutamate transport. (Translated from eng) *FEBS Lett.* 503(2-3):121-125 (in eng).
129. Changeux JP (2010) Allosteric receptors: from electric organ to cognition. (Translated from eng) *Annu. Rev. Pharmacol. Toxicol.* 50:1-38 (in eng).
130. Torres GE & Amara SG (2007) Glutamate and monoamine transporters: new visions of form and function. (Translated from eng) *Curr. Opin. Neurobiol.* 17(3):304-312 (in eng).
131. Accardi A & Picollo A (2010) CLC channels and transporters: proteins with borderline personalities. (Translated from eng) *Biochim. Biophys. Acta* 1798(8):1457-1464 (in eng).
132. DeFelice LJ (2004) Transporter structure and mechanism. (Translated from eng) *Trends Neurosci.* 27(6):352-359 (in eng).
133. Kaback HR, Smirnova I, Kasho V, Nie Y, & Zhou Y (2011) The alternating access transport mechanism in LacY. (Translated from eng) *J. Membr. Biol.* 239(1-2):85-93 (in eng).
134. Gu Y, Shrivastava IH, Amara SG, & Bahar I (2009) Molecular simulations elucidate the substrate translocation pathway in a glutamate transporter. (Translated from eng) *Proc. Natl. Acad. Sci. U. S. A.* 106(8):2589-2594 (in eng).
135. Butchbach ME, Tian G, Guo H, & Lin CL (2004) Association of excitatory amino acid transporters, especially EAAT2, with cholesterol-rich lipid raft microdomains: importance for excitatory amino acid transporter localization and function. (Translated from eng) *J. Biol. Chem.* 279(33):34388-34396 (in eng).
136. Careaga CL & Falke JJ (1992) Thermal motions of surface alpha-helices in the D-galactose chemosensory receptor. Detection by disulfide trapping. (Translated from eng) *J. Mol. Biol.* 226(4):1219-1235 (in eng).
137. Liu Y, Jurman ME, & Yellen G (1996) Dynamic rearrangement of the outer mouth of a K⁺ channel during gating. (Translated from eng) *Neuron* 16(4):859-867 (in eng).
138. Diez M, *et al.* (2004) Proton-powered subunit rotation in single membrane-bound F₀F₁-ATP synthase. (Translated from eng) *Nat Struct Mol Biol* 11(2):135-141 (in eng).
139. Zhao Y, *et al.* (2011) Substrate-modulated gating dynamics in a Na⁺-coupled neurotransmitter transporter homologue. (Translated from eng) *Nature* 474(7349):109-113 (in eng).

140. Zhang X & Qu S (2011) Proximity of transmembrane segments 5 and 8 of the glutamate transporter GLT-1 inferred from paired cysteine mutagenesis. (Translated from eng) *PLoS One* 6(6):e21288 (in eng).
141. Stroud RM (2011) New tools in membrane protein determination. (Translated from eng) *FI000 Biol Rep* 3:8 (in eng).
142. Schmidt-Krey I & Rubinstein JL (2011) Electron cryomicroscopy of membrane proteins: specimen preparation for two-dimensional crystals and single particles. (Translated from eng) *Micron* 42(2):107-116 (in eng).
143. Baldwin AJ & Kay LE (2009) NMR spectroscopy brings invisible protein states into focus. (Translated from eng) *Nat Chem Biol* 5(11):808-814 (in eng).
144. Tong G & Jahr CE (1994) Block of glutamate transporters potentiates postsynaptic excitation. (Translated from eng) *Neuron* 13(5):1195-1203 (in eng).
145. Turecek R & Trussell LO (2000) Control of synaptic depression by glutamate transporters. (Translated from eng) *J. Neurosci.* 20(5):2054-2063 (in eng).
146. Grewer C, Madani Mobarekeh SA, Watzke N, Rauen T, & Schaper K (2001) Substrate translocation kinetics of excitatory amino acid carrier 1 probed with laser-pulse photolysis of a new photolabile precursor of D-aspartic acid. (Translated from eng) *Biochemistry (Mosc)*. 40(1):232-240 (in eng).
147. Diamond JS & Jahr CE (1997) Transporters buffer synaptically released glutamate on a submillisecond time scale. (Translated from eng) *J. Neurosci.* 17(12):4672-4687 (in eng).
148. Kavanaugh M, *et al.* (2008) Kinetic behavior of a high-affinity glutamate transporter blocker reveals a diffusion barrier in the trimer central cavity *Poster presented as part of the Society for Neuroscience Annual Meeting, Washington DC, 15-19 Nov 2008.*
149. Zhou Y, Guan L, Freitas JA, & Kaback HR (2008) Opening and closing of the periplasmic gate in lactose permease. (Translated from eng) *Proc. Natl. Acad. Sci. U. S. A.* 105(10):3774-3778 (in eng).
150. Takeuchi A, Reyes N, Artigas P, & Gadsby DC (2008) The ion pathway through the opened Na(+),K(+)-ATPase pump. (Translated from eng) *Nature* 456(7220):413-416 (in eng).
151. Sobolevsky AI, Beck C, & Wollmuth LP (2002) Molecular rearrangements of the extracellular vestibule in NMDAR channels during gating. (Translated from eng) *Neuron* 33(1):75-85 (in eng).
152. Daniels GM & Amara SG (1998) Selective labeling of neurotransmitter transporters at the cell surface. (Translated from eng) *Methods Enzymol.* 296:307-318 (in eng).
153. Wittig I, Braun HP, & Schagger H (2006) Blue native PAGE. (Translated from eng) *Nat Protoc* 1(1):418-428 (in eng).
154. Schwieters CD, Kuszewski JJ, Tjandra N, & Clore GM (2003) The Xplor-NIH NMR molecular structure determination package. (Translated from eng) *J. Magn. Reson.* 160(1):65-73 (in eng).
155. Shrivastava IH & Sansom MS (2000) Simulations of ion permeation through a potassium channel: molecular dynamics of KcsA in a phospholipid bilayer. (Translated from eng) *Biophys. J.* 78(2):557-570 (in eng).